ASSESSMENT OF LAND USE AND LAND COVER CHANGE IMPACT ON LAND SURFACE TEMPERATURE IN METEHARA CITY, ETHIOPIA

Mikru Wegma Tereda

A Thesis Submitted to The Department of Geomatics Engineering

School of Civil Engineering and Architecture

Presented in Partial Fulfillment of the Requirement for the Degree of Master's in Geomatics Engineering

Office of Graduate Studies

Adama Science and Technology University

Jun, 2024

Adama, Ethiopia

Assessment of Land Use and Land Cover Change Impact on Land Surface Temperature In Metehara City, Ethiopia

MIKRU WEGMA TEREDA

Advisor: DejeneTesema Bulti (PhD)

A Thesis Submitted to

The Department of Geomatics Engineering

School of Civil Engineering and Architecture

Presented in Partial Fulfillment of the Requirement for the Degree of Master's in Geomatics Engineering

Office of Graduate Studies

Adama Science and Technology University

June, 2024

Adama, Ethiopia

Declaration

I hereby declare that this Master Thesis entitled "Assessment of Land Use and Land Cover Change Impact on Land Surface Temperature In Metehara City, Ethiopia" is my original work. That is, it has not been submitted for the award of any academic degree, diploma or certificate in any other university. All sources of materials that are used for this thesis have been duly acknowledged through citation.

__________________________ _______________________ ________________

Name of the student	Signature	Date

Recommendation of advisor

The major advisor of this research, hereby certifies that I have closely advice the student while developing this research and read the draft thesis entitled “assessment of land use and land cover change impact on land surface temperature in Metehara city, Ethiopia” prepared by Mikru Wegma submitted in partial fulfillment of the requirements for the degree of Mater’s of Science in Geomatics Engineering. Therefore, I recommend the submission of revised version of the thesis to the department following the applicable procedures.

__________________________ _______________________ ________________

Major Advisor Signature Date

Approval

I, the advisors of the thesis entitled **"assessment of land use and land cover change impact on land surface temperature in Metehara city, Ethiopia" prepared by Mikru Wegma Tereda**, hereby certify that the recommendation and suggestions made by the board of examiners are appropriately incorporated into the final version of the thesis.

Dejene Tesema (PhD)	______________________	_______________
Major Advisor	Signature	Date

We, the undersigned, members of the Board of Examiners of the thesis by Mikru Wegma have read and evaluated the thesis entitled assessment of land use and land cover change impact on land surface temperature in Metehara city, Ethiopia and examined the candidate during the open defense. This is, therefore, to certify that the thesis is accepted for partial fulfillment of the requirement of the degree of Master of Science in Geoinformatices Engineering.

________________________	______________________	_______________
Chairperson	Signature	Date
________________________	______________________	_______________
Internal Examiner	Signature	Date
________________________	______________________	_______________
External Examiner	Signature	Date

Finally, approval and acceptance of the thesis is contingent upon submission of its final Copy to the Office of Postgraduate Studies (OPGS) through the Department Graduate Council (DGC) and School Graduate Committee (SGC).

________________________	______________________	_______________
Department Head	Signature	Date
________________________	______________________	_______________
School Dean	Signature	Date
________________________	______________________	_______________
Office of Postgraduate Studies, Dean	Signature	Date

ACKNOWLEDGEMENT

First of all, I express my greatest gratitude to God; no success would have been achieved without his grace and mercy.

I would like to express my sincerest gratitude to my great advisor Dr. Dejene Tesema for his valuable guidance, help and encouragement during the progress of this thesis. And also thanks to my department Geomatics Engineering by writing any letter which useful to get data collection in other institution.

Last, but definitely not least, I would like to heartily and deeply thank my greatest parents, my mom, my brother and sister for their greatest help.

TABLE OF CONTENTS

Declaration iii

Approval v

ACKNOWLEDGEMENT vi

LIST OF TABLE xi

LIST OF FIGURE xii

LIST OF ACRONYMS xiv

ABSTRACT xvi

Chapter One 1

1. Introduction 1

1.1 Background of the Study 1

1.2 Statement of the Problem 3

1.3. Objectives of the Study 4

1.3.1. General objective 4

1.3.2. Specific objectives 4

1.4. Research Questions 4

1.5. Significance of the Study 4

1.6 Scope of the Study 5

1.7 Limitation of the study 6

1.8 Organization of thesis 6

Chapter Two 7

2. Review of Related Literature 7

2.1 Concept of urbanization 7

2.1.1 Effects of Urbanization 8

2.2. Concept of LULC 9

2.2.1 Effects of LULC change 10

2.2.2 Driving Forces of LULC change 11
2.3 Concept of Land Surface Temperature (LST) 12
2.3.1 Importance of Land Surface Temperature (LST) 13
2.4 Remote Sensing in LULC 13
2.5 Land surface temperature and elevation 13
2.4.1 Role of Remote Sensing in LST Analysis 14
2.6 NDVI, NDWI, and NDBI indices 15
2.6.1 Normalized difference vegetation index (NDVI) 15
2.6.3 Normalized Difference Built-up Index (NDBI) 16
2.8 Empirical literature review 16
Chapter Three 18
3. Material and Method 18
3.1. Description of Study Area 19
3.1.1. Location and area 19
3.1.2. The topography of the study area 20
3.2. Climate 21
3.2.1. Temperature 21
3.3. Datasets and Sources 23
3.3.1. Remotely Sensed Data 23
3.3.2. Meteorology Data 26
3.3.3. Ground Truth Data and Google Earth Data 26
3.4. Software 26
3.5. Methods of analysis 27
3.5.1. Digital Image Preprocessing 29
3.5.2. Multispectral Radiometric Correction 29
3.6. Land surface temperature retrieval 29

3.7 Extraction of LULC and accuracy assessment 32
3.7.1 Supervised Classification Top of Form 32
3.7.2 Accuracy assessment 33
3.8 Urban Land use and Land cover Thematic Layer 35
3.9 Change Detection Analysis 36
3.9.3 Normalized Difference Water Index (NDWI) 37
3.10 Zonal statics 37
3.10.1 Zonation for spatial coverage of LST 38
3.11 Correlational Analysis 38
Chapter Four 39
4. Result and Discussion 39
4.1 LULC classification and area coverage in 1999, 2010 and 2020 39
4.3 LULC change from 1999 to 2020 43
4.4 LULC Transformation matrix 45
4.4.1 LULC transformation matrix from 1999 to 2010 45
4.3.2 Change detection from 2010 to 2020 48
4.4.3 Change detection from 1999 to 2020 50
4.4 Accuracy assessment 52
4.5 The sptio-temporal distribution of NDVI 55
4.6. The Spatio-temporal Distribution of NDBI 57
4.7 The sptio temporal variation of NDWI 58
4.8 The LST Spatial and Temporal Distribution from 1999 to 2020 59
4.9. LST zone and influence of LULC on LST in 1999, 2010, and 2020 61
4.10 Correlation between LST AND LULC induces and elevation 66
4. 10.1 Correlation between LST AND NDVI, NDBI and NDWI in 1999, 2010 and 2020 66

4.11 correlation between LST and elevation in 1999, 2010, 2020 70

Chapter Five 73

5. Conclusion and Recommendation...73

5.1 Conclusion 73

5.2 Recommendation 74

REFERENCE 75

APPENDICES 89

Ground points were used for accuracy assessment of LULC classification. 89

LIST OF TABLE

Table 3.1: Remote sensing datasets were used for the study and its descriptions 24
Table 3. 2: Remote sensing datasets were used for the study and its descriptions 24
Table 3.3 : Landsat 8 OLI and TIRS bands description.. 25
Table 3.4 : LULC class type and description.. 35
Table 4. 1: LULC level in 1999, 2010 and 2020 in study area…………………………….....40
Table 4.2 : each LULC area coverage and net change 1999 to 2020 in study area 44
Table 4. 3 : transformation matrix from 2010 to 2020.. 46
Table 4. 4 : LULC change detection matrix from 2010 to 2020 in Metehara city other. 48
Table 4.5: Error matrix of 1999 LULC 53
Table 4. 6 : Error matrix of 2010 LULC 54
Table 4. 7 : Error matrix of 2020 LULC 55
Table 4. 8 : the NDVI maximum, minimum and mean value in 1999, 2010 and 2020 57
Table 4. 9 : maximum, minimum and mean value of LST in Metehara city 60
Table 4.10 : The LST zone and area coverage in each LULC class in 1999 62
Table 4. 11 : LST zone and area coverage in each LULC class in 2010 63
Table 4. 12 : LST zone and area coverage in each LULC class in 2020 64

LIST OF FIGURE

Figure 3.1: Location map of study Area 20
Figure 3.2 : elevation map of Metehara city 21
Figure 3.3 : maximum mean monthly temperature in study area 22
Figure 3. 4 : maximum and minimum monthly temperature 22
Figure 3. 5 : maximum and minimum monthly temperature 23
Figure 3. 6 : general work flow. 29
Figure 4. 1 : land use land cover map of study area in 1999, 2010 and 2020………………...41
Figure 4. 2 : LULC area change from 1999 to 2020 42
Figure 4. 3 : land sat image shows water body appeared in 2010 and 2020 43
Figure 4.4: LULC change from 1999 to 2020 45
Figure 4. 5: LULC change detection from 1999 to 2010 47
Figure 4. 6 : LULC change transformation from one LULC to other in 2010 to 2020 49
Figure 4. 7 : LULC transformation matrix from each LULC 1999 to 2020 51
Figure 4. 8 : LULC change transformation matrix from 1999 to 2020.................................. 52
Figure 4. 9 : The NDVI map of study area in 1999, 2010 and 2020...................................... 56
Figure 4. 10 : The NDBI value in study area in 1999, 2010 and 2020 58
Figure 4. 11 : NDWI value in study area 1999, 2010 and 2020 59
Figure 4. 12 : LST value in study area 61
Figure 4. 13 : LST zone in each LULC in 1999 in Metehara city 64
Figure 4. 14 LST zone in each LULC in 2010 in Metehara city 65
Figure 4. 15: LST zone in each LULC in 2020 in Metehara city 65
Figure 4. 16 : correlation between LST and NDVI in 1999.. 67
Figure 4. 17 correlation between LST and NDBI in 1999... 67
Figure 4. 18 correlation between LST and NDWI in 1999.. 68
Figure 4.19 correlation between LST and NDVI in 2010... 68
Figure 4.20: Correlation between LST and NDBI in 2010... 68
Figure 4. 21 correlation between LST and NDWI in 2010... 69
Figure 4. 22 : correlation between LST and NDVI in 2020.. 69
Figure 4. 23: correlation between LST and NDBI IN 2020.. 70
Figure 4. 24 : correlation between LST and NDWI in 2020.. 70

Figure 4. 25: correlation between LST and DEM IN 1999 71
Figure 4. 26 : correlation between LST and elevation in 2010 72
Figure 4. 27: correlation between LST and DEM in 2020 72

LIST OF ACRONYMS

ASTER	Advanced Space borne Thermal Emission and Reflection Radiometer
CSA	Central Statistical Agency
DEM	Digital Elevation Model
EDW	Elevation-Dependent Warming
ENVI	Environment for Visualizing Images
ESSAP	Economic and Social Sector Adjustment Program
ETM+	Enhanced Thematic Mapper Plus
GDEM	Global Digital Elevation Model
GIS	Geographic Information System
GPS	Global Positioning System
IPCC	Intergovernmental Panel on Climate Change
LSE	Land Surface Emissivity
LST	Land Surface Temperature
LULC	Land Use and Land Cover
MODIS	Moderate Resolution Imaging Spectroradiometer
MS Excel	Microsoft Excel
NASA	National Aeronautics and Space Administration
NDVI	Normalized Difference Vegetation Index
NMA	National Meteorological Agency
NSTGE	Near-Surface Temperature Gradient with Elevation
OLI	Operational Land Imager
QGIS	Quantum GIS
RS	Remote Sensing

SDGs	Sustainable Development Goals
SUHI	Surface Urban Heat Island
TM	Thematic Mapper
UHI	Urban Heat Island
UN	United Nations
UN DESA	United Nations Department of Economic and Social Affairs
USGS	United States Geological Survey

ABSTRACT

This study investigates the Land Use Land Cover change (LULC) patterns and their consequences for local climate dynamics in Metehara City, Ethiopia, from 1999 to 2020. Using multi-temporal Landsat satellite images and advanced remote sensing and GIS techniques, the study reveals significant shifts in land cover classes and their impacts on land surface temperature (LST).

Key findings indicate that the built-up area expanded significantly, growing from 35.97 hectares in 1999 to 149.7 hectares in 2010, and further to 202.21 hectares by 2020. Conversely, other land classes, including agricultural areas, exhibited varied trends, with notable expansions and contractions over the study period. The study recorded LST ranges of 24.24°C to 32.95°C in 1999, 30.01°C to 38.387°C in 2010, and 22.4049°C to 39.39°C in 2020. A progressive increase in mean temperatures was observed, with a mean difference of 0.77°C between 1999 and 2010, 0.75°C between 2010 and 2020, and an overall increase of 1.52°C from 1999 to 2020. Maximum temperatures recorded were 32.95°C, 38.887°C, and 39.4049°C for the respective years.

Detailed analysis of agricultural zones highlighted significant temperature fluctuations: from 128.16 hectares with a mean temperature of 31.35°C in 1999, to 144.66 hectares with 36.53°C in 2010, and reducing to 113.85 hectares with 36.12°C in 2020. These changes underscore the influence of active land surface heating from agricultural activities on regional temperatures. The study also found a negative correlation between LST and both the Normalized Difference Vegetation Index (NDVI) and Normalized Difference Water Index (NDWI), and a positive correlation between LST and the Normalized Difference Built-up Index (NDBI).

Keywords: GIS, Remote sensing, LULCC, Land surface temperature, Cross Tabulation.

Chapter One

1. Introduction

1.1 Background of the Study

Since its discovery by Luke Howard in 1818, the phenomenon known as Urban Heat Island (UHI) has gained significant attention in light of the current acceleration of urbanization worldwide. Forecasts for urbanization show a global trend of increasing urban growth, especially in developing nations driven by economic expansion (ESSAP, 1993). By 2050, it is predicted that 68% of people would live in cities, a significant increase from the current 55% (United Nations, 2018). In this dynamic urban environment, Ethiopia's Metehara City stands out as a microcosm, illustrating the various ways that urbanization has affected regional climates.

By 2050, Ethiopia is expected to have the most urbanized population in the world, with an estimated 814 million people living there (current urban population rate stated). The country has an urbanization rate of 1.1%. Beyond the bounds of traditional cities, this unheard-of urban expansion is displacing marshes, vegetation, and agricultural regions and exerting pressure on the surrounding natural resources. The implications of this rapid urbanization include altered precipitation patterns, heatwaves, urban heat islands and climate change (Bai et al., 2018; Estoque & Murayama, 2013; Malik et al., 2020; Mohammad et al., 2019).

Alongside rising greenhouse gas concentrations in the atmosphere, urbanization characterized by the expansion of built-up regions and infrastructure has emerged as a major human caused driver to climate change (IPCC, 2007, 2013). At both the local and regional levels, changes in land use/cover (LULC), particularly the quick switch from pervious to impervious surfaces, pose environmental issues (Rousta et al., 2018; Zhou et al., 1998). Two notable effects of LULC changes in urban environments include variations in Land Surface Temperature (LST) and the creation of urban heat islands (Mohammad & Goswami, 2018).

Temperature fluctuations across distinct land cover categories are caused by surface reflectance and roughness, which are influenced by land surface temperature (LST), a crucial parameter in studies of surface energy balance and climate change (Tomlinson et al., 2011; Li et al., 2017; Hu & Jia, 2009). For smart cities to be designed and spatially planned effectively in the context of mitigating climate change, it is essential to comprehend how LULC changes affect urban LST (Wang et al., 2008; Carter et al., 2015; Xie et al., 2013). Several studies underline how LULC has a significant impact on surface temperature, especially in urban areas (Pal and Ziaul, 2017; Weng et al., 2004).

In the Eastern African context, the main cause of LULC changes is the increase in human and livestock populations, which results in the overuse of land for agricultural purposes. As a result of this change, naturally vegetated land is transformed into built-up areas, pasture grounds, farmlands, and urban regions. Soil erosion, deforestation, land degradation, biodiversity loss, and major contributions to climate change-related global warming are among the repercussions (Pomeroy et al., 2003; Maitima et al., 2009).

Ethiopia is a country in East Africa that is seeing a rapid increase in land use and land cover change, which is mainly caused by population expansion and changing local community views on sustainable land management (Hurni et al., 2005; Belay et al., 2014). Complicating the dynamic state of the nation's landscapes are additional difficulties such surface flooding, runoff, and sedimentation. Particularly in the Amhara National Regional State, population pressure causes marked land degradation, resulting in the loss of forest, shrubland, bushland, and grasslands to make room for farming, grazing land development, and habitation (Bekele, 2005).

Researchers are now better equipped to explore the complex link between UHI and landscape dynamics thanks to developments in thermal remote sensing, Geographic Information Systems (GIS), and statistical techniques. Several studies have produced insights that help policymakers understand the dynamics of UHI and help create strategies that work (Quattrochi and Luvall, 1999; Yuan and Bauer, 2007; Rizwan et al., 2008; Junxiang et al., 2011; Kumar et al., 2012; Radhi et al., 2013; Myint et al., 2013; Zhou et al., 2014; Adams and Smith, 2014; Coseo and Larsen, 2014; Song et al., 2014; Chun and Guldmann, 2014; Rotem-Mindali et al., 2015). Remote sensing and GIS technology integration have become essential for detecting LULC changes and retrieving LST data (Choudhury et al., 2019).

This study attempts to evaluate the complex relationship between urban LULC changes and LST in the Metehara City using thermal bands of Landsat imageries. This study aims to offer significant insights into forecasting future land warming trends through the utilization of remote sensing and GIS methods. In light of continued urbanization and climate change, the results are expected to provide useful information for environmental specialists, natural resource managers, and urban planners, encouraging the management of natural landscapes for sustainability and health.

1.2 Statement of the Problem

Methara City's urban conditions are mainly dictated by the necessities of the city, the facilities which are available, and the ongoing development movement. Additionally, there has been an enormous increase in migration from rural to urban as an outcome of the city's quicker population growth and growing economy. The shift of population puts an extensive amount of demand on the infrastructure, reduces natural resources, and facilitates the spread of uncontrolled growth in cities and slums. Problems associated with environmental change are made worse by the shifts of land use as well as land cover patterns generated by multiple human activities and population growth. The result leads to essential urban growth.A number of noticeable fluctuations in LST as an outcome of the shifting land use and land cover trends in Methara City, which are mostly driven by human beings. It becomes important to study urban climates, especially the impact of the urban heat islands (UHI)., Knowing that land surface temperature influences the air temperature within the boundary layer of the atmosphere. The surrounding environment and climate are seriously affected by the changes in urban LST (Claus and Mushtaq, 2011). An understanding of the particular relationship between terrain features and LST is required to effective resource management to become feasible.

Despite the existing study on the spatial distribution of surface temperature in the Main Ethiopian Rift, specifically focusing on volcano-tectonic activity (Reda et al., 2022), there has been no comprehensive study addressing the impact of Land Use and Land Cover (LULC) changes on Land Surface Temperature (LST) in Metehara City. In addition to the existing challenges posed by urbanization and population growth in Methara City, there is a critical need to address the specific impacts of Land Use and Land Cover (LULC) changes on Land Surface Temperature (LST). These changes, driven predominantly by human activities and urban development, significantly alter the thermal characteristics of the cityscape, exacerbating the Urban Heat Island (UHI) effect. The absence of a comprehensive study focusing on LULC-LST dynamics in Methara City underscores the urgency for such research. Understanding these dynamics is crucial for effective urban planning, resource management, and climate adaptation strategies tailored to mitigate the adverse effects of urbanization on local climate and environment.

1.3. Objectives of the Study

1.3.1. General objective

The general objective of this study is to investigate the impact of changes in land Use and land cover (LULC) on land surface temperature (LST) in Metehara City, Ethiopia, in the years 1999, 2010, and 2020.

1.3.2. Specific objectives

The specific objectives of the study to:

1. Examine changes in Land Use and Land Cover (LULC) within Metehara City across the years 1999, 2010, and 2020.
2. Investigate the Land Surface Temperature (LST) patterns in Metehara City for the research periods 1999, 2010, and 2020.
3. Explore the effects of changes in Land Use and Land Cover (LULC) on land surface temperature variations in Metehara City in the years 1999, 2010, and 2020.
4. Investigate how land use, land cover indices, terrain features, and Land Surface Temperature (LST) are interrelated across the research years 1999, 2010, and 2020.

1.4. Research Questions

1. How has the Land Use and Land Cover (LULC) evolved within Metehara City during the research years of 1999, 2010, and 2020?

2. What are the patterns of Land Surface Temperature (LST) in Metehara City for the research periods 1999, 2010, and 2020?

3. What are the effects of changes in Land Use and Land Cover (LULC) on variations in local land surface temperature in Metehara City during the years 1999, 2010, and 2020?

4. How are land use land cover indices and elevation related to Land Surface Temperature (LST) within Metehara City during the research years of 1999, 2010, and 2020?

1.5. Significance of the Study

For academic and practical purposes, the MSc thesis "Assessment of Land Use and Land Cover (LULC) Change Impact on Land Surface Temperature in Metehara City, Ethiopia" is of utmost importance. Through an examination of the intricate connections among Land Surface Temperature (LST), LULC fluctuations, and urban development, this study advances the field of urban climatology. It provides a sophisticated understanding of how local climatic dynamics are impacted by the fast urbanization seen in Metehara City. The study's conclusions directly relate to Metehara City's environmental management and urban development in terms of practical ramifications. Using cutting-edge remote sensing and Geographic Information System (GIS) techniques, the thesis achieves a high degree of methodological rigor that serves as a useful model for future research. The research findings can provide guidance for making decisions on land-use management, climate-resilient infrastructure planning, and sustainable urban development. Additionally, by providing evidence-based insights that might direct policymakers in the region, the study adds to the larger conversation about policy. As a teaching tool, the MSc thesis expands on the body of knowledge in urban climatology by laying the groundwork for future studies and giving scholars, researchers, and educational institutions insightful information. All things considered, this research fills in a significant knowledge vacuum regarding the dynamics of urban climates and provides a thorough and useful manual for overcoming the difficulties brought about by LULC fluctuations and their effects on Land Surface Temperature in Metehara City.

1.6 Scope of the Study

The study's precise physical border is Metehara City, which is located in Ethiopia's East African Rift Valley. This guarantees a targeted analysis of the dynamics of the urban climate inside a particular metropolitan center. The boundary encompasses the area most directly impacted by land-use changes and urbanization, which includes the administrative limits of Metehara City and its near surrounds.

The study's content covers a wide range of topics, with a focus on the unique impact that LULC changes have on land surface temperature. In order to identify various land cover types, measure changes over time, and correlate these changes with variations in LST, the research entails the collection and analysis of satellite imagery. Furthermore, in order to better understand the subtleties of the microclimate in Metehara City, the study investigates how elevation affects the way that LULC changes affect LST. In order to better understand how particular urban features, such built-up areas, vegetation cover, and water bodies, affect temperature changes, the content also contains a comparative examination of various land use categories.

1.7 Limitation of the study

Although Metehara is one of Ethiopia's fastest-growing cities, its impact on land surface temperature has not been thoroughly examined, nor has it been fully examined in terms of the dynamics of the urban landscape and how it affects urban heat islands. To make matters worse, important documents for accurate assessment in digital format, such as aerial photos, are unavailable to urban researchers from the federal urban development office as well as regional offices. It is quite challenging to obtain Landsat data collected in any weather condition because the sensor is optical. Thus, taking into account the lack of cloud cover, the Landsat LST data is acquired at a highly specific time.

1.8 Organization of thesis

The introduction includes the problem statement, background information, objectives, significance, scope, and constraints of the investigation. The concept of urbanization, the effect of LULC on LST, LST retrieval, LCI, and the function of remote sensing on LST are all covered in the second chapter's literature review sections. The third chapter includes information on the study area, data, and software utilized, as well as image categorization, LST retrieval, and LCI. The findings and discussion of the study, including the relationship between LCI and LST, the spatial distribution of LST, and the change of LULC, are presented in Chapter 4. The study's recommendation and conclusion are presented in Chapter 5.

Chapter Two

2. Review of Related Literature

2.1 Concept of urbanization

Improved job, healthcare, and educational possibilities are major drivers of urbanization, a dynamic global phenomena that is driving more people to migrate to cities and adjacent areas (UN DESA, 2019). It is estimated that by 2050, the percentage of people living in cities worldwide would have increased to 68% from 55% in 2018. Increased artificial impervious surfaces at the expense of natural surfaces and a noticeable migration of people from rural to urban regions are two outcomes of this fast urbanization, which is inextricably tied to socioeconomic development.

Urbanization encompasses various aspects such as demographic shifts, land use changes, environmental impacts, and socio-economic transformations. According to UN-Habitat (2013), urbanization is a global phenomenon driven by factors like rural-urban migration, natural population growth, and economic opportunities in urban centers. As people move from rural to urban areas, cities experience population growth, which in turn spurs the demand for housing, services, and infrastructure. This process often leads to land use changes, including the conversion of agricultural land to residential or commercial use, impacting natural ecosystems and landscapes.

The concept of urbanization is intertwined with several socio-economic dynamics. As urban areas expand, they become centers of economic activity, innovation, and employment opportunities. This concentration of resources and activities attracts people seeking better livelihoods and access to amenities such as education, healthcare, and transportation. However, rapid urbanization can also lead to challenges such as overcrowding, informal settlements, inadequate infrastructure, and environmental degradation. Research by Seto et al. (2014) emphasizes the complex interplay between urbanization and environmental sustainability. They highlight how urban expansion affects ecosystems, biodiversity, and natural resources, emphasizing the need for sustainable urban development practices to mitigate negative environmental impacts. Urbanization's effects on climate, air quality, water resources, and land use patterns are also significant areas of research within the context of urban sustainability and resilience. Urbanization is a multifaceted and complex process that encompasses various dimensions of human settlement and development. It involves not only the physical expansion of cities but also profound socio-economic and environmental changes. The concept of urbanization has evolved over time, reflecting shifts in population distribution, land use patterns, infrastructure development, and societal structures.

At its core, urbanization signifies the shift of people from rural to urban areas, driven by factors such as economic opportunities, improved living standards, access to education and healthcare, and the allure of urban amenities and lifestyle. This migration of people results in the concentration of population and activities in urban centers, leading to the growth of cities and towns. From a socio-economic perspective, urbanization is associated with increased economic productivity, job creation, technological innovation, and cultural diversity. Cities become hubs of industry, commerce, finance, education, and cultural exchange, driving regional and national development. However, rapid urbanization can also give rise to social inequalities, urban poverty, housing challenges, and strains on public services and infrastructure.

Environmental implications are also significant in the context of urbanization. The conversion of natural landscapes into built-up areas, industrial zones, and transportation networks can lead to habitat loss, fragmentation, and biodiversity decline. Urban areas contribute to environmental issues such as air pollution, water pollution, waste generation, energy consumption, and greenhouse gas emissions. Managing these environmental impacts becomes crucial for sustainable urban development and mitigating climate change effects. Research by Angel et al. (2011) highlights the spatial patterns and dynamics of global urbanization, emphasizing the need for efficient urban planning, infrastructure investment, and governance mechanisms to address urban challenges. Similarly, Seto et al. (2014) discuss the environmental consequences of urban expansion, including changes in land cover, ecosystem services, and carbon emissions, underscoring the importance of sustainable land use and resource management strategies in urban areas.

2.1.1 Effects of Urbanization

Urban environments are multifaceted due to the intricate framework that includes human organizations, biodiversity, and infrastructure. Comprehending the impact of land use and land cover changes in megacities and their implications on Land Surface Temperature (LST) becomes imperative in order to support sensible planning (Weng and Schubring, 2004; 2010; 2014). Understanding these effects is also necessary. The rise in Surface Urban Heat Island

(SUHI) impacts, which have an adverse influence on human health, air quality, and climate change, is one of the negative environmental implications of this urbanization boom, though (Estoque et al., 2017).

The rapidly changing urban landscape brought about by the world's population expansion has made a rigorous reevaluation of sustainable development imperative. The importance of establishing inclusive, safe, resilient, and sustainable cities is emphasized by the 17 Sustainable Development Goals (SDGs) of the United Nations, especially Goal 11 (Souch & Grimmond, 2006). The need to acknowledge the extensive ecological impact of urban growth has reignited conversations over the layout and composition of cities.

Urbanization has a significant impact on Land Use/Land Cover (LULC) change and Land Surface Temperature (LST), as evidenced by numerous research studies. Bai et al. (2018) and Mohammad and Goswami (2018) highlight the transformation of natural landscapes into urban infrastructure, leading to increased impervious surfaces and reduced vegetation cover. This alteration in LULC patterns contributes to elevated LSTs, particularly in densely developed urban areas, exacerbating the Urban Heat Island (UHI) effect. The spatial and temporal variability of LST within urban areas is emphasized by Quattrochi and Luvall (1999) and Muhammad et al. (2019), noting higher daytime temperatures in central urban zones compared to peripheral areas with more vegetation. Mitigation strategies proposed by Estoque and Murayama (2013) and Eng et al. (2016) focus on integrating green spaces, cool roofing materials, and sustainable urban planning practices to mitigate LST increases and reduce the adverse effects of urbanization on local climates. Understanding these dynamics is crucial for developing resilient and sustainable cities in the face of rapid urban growth.

2.2. Concept of LULC

Key elements in the complex interaction between human activity and the surface of the Earth are land use and land cover (LULC). "Land cover" encompasses the natural condition of the surface, including solid surfaces, creatures, water bodies, and soil, whereas "land use" refers to human activities and their frequently undetectable effects (Lo, 1986; Jansen & Di Gregorio, 2003). LULC research explore how these characteristics change globally, highlighting the phenomenon's unparalleled scope, effects on Earth's systems, and need for a better comprehension of its underlying causes (Lambin et al., 2001; Foley et al., 2005). Land

Use/Land Cover (LULC) is a fundamental concept in environmental science and land management, encompassing the physical and biological characteristics of the Earth's surface as influenced by both natural processes and human activities. This concept is extensively discussed and researched in the literature, with numerous studies highlighting its importance in understanding landscape dynamics and their implications for various environmental processes. For example, Estoque and Murayama (2013) emphasize the significance of LULC in studying the impact of urbanization on regional climates, particularly focusing on Land Surface Temperature (LST). Their research delves into how changes in land use, such as urban expansion and vegetation loss, can lead to alterations in surface temperature patterns, contributing to phenomena like the Urban Heat Island (UHI) effect.

Similarly, Bai et al. (2018) discuss the effects of LULC change on environmental factors such as surface runoff, groundwater recharge, and pollution levels, particularly in the context of urban expansion and its associated increase in impervious surfaces. Their study highlights the role of LULC in shaping hydrological processes and urban environmental quality. Muhammad et al. (2019) explore the relationship between LULC changes and Land Surface Temperature (LST), linking transformations in land cover, such as deforestation or urbanization, to changes in surface temperature regimes. They emphasize the importance of considering LULC dynamics in understanding local climate variations and their impacts on ecosystems and human populations.

Remote sensing technologies, geographic information systems (GIS), and spatial analysis techniques are commonly employed in LULC research to map, monitor, and analyze land cover types, land use patterns, and their changes over time. This interdisciplinary approach integrates ecological, hydrological, and socio-economic perspectives, providing valuable insights for land management, environmental planning, and sustainable development strategies.

2.2.1 Effects of LULC change

LULC modifications have substantial environmental effects, especially in metropolitan areas. Urban Heat Islands (UHIs) are the product of LULC adjustments in urban environments, which also affect Land Surface Temperature (LST) (Mohammad & Goswami, 2018). Changes in LULC distribution have an impact on LST, and this complex link between LULC and LST is crucial to comprehending UHI impacts (Walawender et al., 2014; Song et al., 2014). According to Zhang et al. (2013), LULC changes also work in tandem with greenhouse gas concentrations as key anthropogenic drivers of climate change. The effects of Land Use/Land Cover (LULC) change are extensively studied and documented in research literature, highlighting the diverse and often profound impacts of alterations in land use and land cover patterns on various environmental processes, ecosystems, and human well-being.

For instance, Estoque and Murayama (2013) emphasize the effects of LULC change, particularly urbanization, on Land Surface Temperature (LST) and regional climates. Their research illustrates how urban expansion and the conversion of natural landscapes to impervious surfaces can lead to higher LSTs, contributing to phenomena like the Urban Heat Island (UHI) effect and altering local and regional climate dynamics. Bai et al. (2018) delve into the environmental consequences of LULC change, such as changes in surface runoff, groundwater recharge, and pollution levels, especially in the context of urban growth and increased impervious surfaces. Their study underscores the interconnectedness of land use patterns with hydrological processes and urban environmental quality.

Muhammad et al. (2019) investigate the impacts of LULC changes on Land Surface Temperature (LST) and local climate variations, linking shifts in land cover types, such as deforestation or agricultural expansion, to changes in surface temperature regimes. They highlight the implications of these changes for ecosystems, water resources, and human populations, particularly in terms of heat stress, water availability, and habitat quality. Remote sensing technologies, geographic information systems (GIS), and spatial analysis techniques are instrumental in studying the effects of LULC change, enabling researchers to map, quantify, and analyze land cover transitions, their spatial patterns, and associated environmental impacts. These methods facilitate the assessment of ecosystem services, biodiversity conservation, land degradation, and resilience to climate change, providing valuable insights for land management, environmental planning, and sustainable development strategies.

2.2.2 Driving Forces of LULC change

It's essential to comprehend the motivations for LULC revisions. Research examines how changes in LULC and population growth affect the development of Urban Heat Islands (Zhang et al., 2013). Furthermore, it is clear how LULC changes are entwined with land-use change and urbanization, affecting the Normalized Difference Vegetation Index (NDVI) and Land Surface Temperature (LST) in urban regions (Li et al., 2011).

One important environmental factor affecting the local microclimate, especially the modification of LST, is Land Use and Land Cover Change (LULCC). This phenomenon is a reflection of socioeconomic changes associated with human activity and arises from a confluence of anthropogenic and natural elements in globalized land systems (Popp et al., 2017). Urban LST estimation becomes more difficult in areas where natural and semi-natural land coverings are being replaced by impermeable surfaces due to surface heterogeneity (Akinbobola, 2019). Understanding the environmental dynamics of a place requires accurate identification, with LULC emerging as a crucial characteristic. The quick transition from pervious to impermeable surfaces caused by LULC changes has a significant impact on the local and regional environments, highlighting the significant impact of LULC on surface temperature, especially in metropolitan areas (Rousta et al., 2018; Zhou et al., 1998; Weng et al., 2004).

Basically, answering important issues concerning the changing land cover, the types of changes, and the speeds at which these changes happen requires an understanding of the notion, consequences, and causes behind LULC. Understanding the dynamic relationships between land use and land cover changes over time and forecasting future change patterns depend on simulation modeling (Brown et al., 2000; Loveland and Acevedo, 2006). Finding and evaluating LULC changes are essential techniques for evaluating ecological and environmental degradation (Beevi et al., 2015; Hadeel et al., 2011).

2.3 Concept of Land Surface Temperature (LST)

The result of all surface-atmosphere interactions and energy fluxes between the atmosphere and the ground are combined to form the land surface temperature (LST), a complete measurement. According to Duan et al. (2019), it is essential to comprehend the dynamics of the urban thermal environment. Numerous surface characteristics, including as building materials, the composition of urban vegetation, land cover, elevation, and climate, all have an impact on LST. An important area of urban climatology is the relationship between rising land surface temperatures and increased heat-transmitting anthropogenic emissions, reduced water-pervious surfaces, and increased land surface covering with high heat conductivities (Sara Afrasiabi Gorgani, 2016).

2.3.1 Importance of Land Surface Temperature (LST)

According to Sobrino and Raissouni (2000), land surface temperature is a function of surface qualities and is greatly influenced by the structure of urban vegetation and the materials used in construction. The relationship between vegetation quality and LST, which is influenced by soil types, land use, and urbanization, complicates our understanding of urban heat islands. The inverse connection highlights the complex dynamics affecting LST.

2.4 Remote Sensing in LULC

For a thorough grasp of the dynamics of the Earth's surface, remote sensing techniques are essential for evaluating changes in land use and cover (Chao et al., 2020). The Land Surface Temperature (LST) is a fundamental indication that allows different elements of land usage and land cover changes to be measured by satellite-based thermal remote sensing. Tracking spectrally sensitive changes on the surface of the Earth is made possible by remote sensing's wide coverage, equivalent geographic scales, and temporal consistency (Jensen, 2007).

2.5 Land surface temperature and elevation

When elevation differences were taken into account, Gallo et al. (1993) discovered better connections between recorded fluctuations in minimum temperatures and differences in NDVI between urban and rural areas. ASTER data is useful for many applications, such as vegetation dynamics and land cover change, because to its wide spectrum coverage and excellent spatial resolution (Land Processes Distributed Active Archive Center, 2009). Elevation data was gathered using the Global Digital Elevation Model version 3 (GDEM v3) of the Advanced Spaceborne Thermal Emission and Reflection Radiometer (ASTER) from the USGS website (Abrams et al., 2020). It is essential to look into changes in LST caused by elevation differences between spatially distant points with similar surface characteristics in larger studies of LST, which frequently cover huge areas with significant height variations. While counteracting the impacts of elevation change, an understanding of such variations might aid in attributing LST changes to particular characteristics.

In the context of elevation-dependent warming (EDW), the literature acknowledges the importance of the link between LST and elevation.. Numerous studies highlight the accelerated warming rates at higher elevations, such as those by Rangwala et al. (2012) and Giorgi et al. (1997). Snow-albedo feedback was highlighted by Minder et al.'s (2018) detailed elevation-dependent warming patterns in the Rocky Mountains. Higher elevations were found to have greater warming rates by Palazzi et al. (2017), who concentrated on the Tibetan Plateau–Himalayas. The direct effect of elevation on LST has not been as well investigated as the effects of land use/cover and NDVI on LST (Yanev & Filchev, 2016).

2.4.1 Role of Remote Sensing in LST Analysis

Renowned for their worldwide reach since 1972, NASA's Landsat missions play a significant role in the detection of changes in land cover and use. They provide freely accessible, moderate-to-high resolution data (Helmer et al., 2000; Lu and Weng, 2004; Gao and Zhang, 2009; Kumar and Acharya, 2016). In order to analyze LULC changes and LST, remote sensing (RS) and geographic information systems (GIS) are essential tools (Ayele et al., 2018; Hc et al., 2020). Using synoptic LULC data from satellite-based RS, one may map and identify changes in land surface temperature as well as land use (Chew et al., 2016; Malik et al., 2020). The thermal sensor on Landsat makes it easier to calculate LST, a crucial statistic that represents ground temperature and is primarily used to identify Urban Heat Islands (UHI) (Rajeshwari and Mani, 2014; Choudhury & Das Arijit Das, 2019).

According to Ullah et al. (2019), remote sensing indices like the NDVI and NDBI are essential for determining how land use change would affect LST. Using LST from remote sensing data made possible by satellite sensors such as MODIS, ASTER, and Landsat is essential for UHI research because it provides extensive spatial coverage over a range of temporal scales (Imhoff et al., 2010). Geographical technology and remote sensing are key tools in contemporary environmental analysis for locating land use change (LULC) and extracting subtle variations in land surface temperature (Choudhury et al., 2019). The quick computation of LST is made possible by the use of satellite imagery from Landsat, NOAA-AVHRR, and MODIS (Frey et al., 2012).

In order to ensure accurate LST determination, atmospheric correction procedures particularly the split-window method frequently employed for Landsat-8 LST retrieval address atmospheric influences (Honnerová et al., 2016).Many agree that Land Surface Temperature (LST) is important for evaluating temperature changes in urban areas, and that this has consequences for regional climate and human-environment interactions (Zhang et al., 2017). A wealth of research on the temporal dynamics of vegetation and climate indices in different places is reflected in the Scopus database. Knowing LST trends becomes essential to understanding climate change effects (Sadiq Khan et al., 2020). The distribution and change of LST are significantly influenced by natural vegetation, and one commonly used metric for calculating LST is the normalized difference vegetation index, or NDVI (Guha et al., 2018). Understanding the effects of climate change requires in-depth research using remote sensing datasets, as the conversion of natural vegetation to impermeable surfaces in urban land cover drastically changes the microclimate (Sadiq Khan et al., 2020). Determining local solar radiation, atmospheric parameters, and surface features, the surface thermal environment (LST) is a manifestation of the heat exchange equilibrium between the ground and the atmosphere. According to Yang et al. (2017), LST changes significantly as a result of the growing urbanization of areas. Natural surfaces such as vegetation and water bodies are replaced by impermeable artificial surfaces, which causes geographic variations in energy exchange.

According to Dewan & Yamaguchi (2009) and Gogoi et al. (2019), land surface temperature (LST) is a critical indication of the energy balance at the ground surface and varies greatly depending on changes in land use and cover. Because urban surface alterations alter local thermal conditions, there are health concerns to people (Grimmond, 2007).

2.6 NDVI, NDWI, and NDBI indices

2.6.1 Normalized difference vegetation index (NDVI)

For evaluating vegetation cover worldwide, the Normalized Difference Vegetation Index (NDVI) is a commonly used metric (Jiang et al., 2006; Vani and Mandla, 2017). The index is computed as the reflectance difference between the red band (RED) and the near-infrared band (NIR) of satellite pictures. The Normalized Difference Vegetation Index (NDVI) has a range of -1.0 to +1.0. According to Townshend and Justice (1986), areas with positive values are highly vegetated, whereas areas with negative values are not. The NDVI formula can be found using

$$NDVI = \frac{NIR-RED}{NIR+RED} \quad \text{.........} \quad (2.1)$$

The NDVI for Landsat TM data is computed using bands 3 and 4, and for Landsat OLI data, bands 4 and 5. Values ranging from 0 to +1 represent the amount of vegetation cover, with values near 1 denoting a high leaf density.

2.6.2 Normalized Difference Water Index (NDWI)

The Normalized Difference Water Index (NDWI) uses visible and near-infrared light to identify open water bodies (McFeeters, 1996). The following is the formula for NDWI.

$$NDWI = \frac{NIR - Green}{NIR + Green} \quad \text{...} \quad (2.2)$$

Bands 2 and 4 from Landsat TM data and bands 3 and 5 from Landsat OLI data are used to compute NDWI. The NDWI scale runs from -1 to +1; values larger than 0.5 generally denote the presence of water bodies, whereas lesser values including negative values ignify the presence of vegetation. Water bodies can therefore be distinguished from other types of land cover with the use of NDWI.

2.6.3 Normalized Difference Built-up Index (NDBI)

The Normalized Differen One technique that is frequently used to quantify built-up land in metropolitan settings is the Built-up Index (NDBI) (Kshetri, 2018). The Middle Infrared (MIR) and Near Infrared (NIR) bands are used to calculate the Near Infrared Band Index (NDBI) using the following formula.

$$NDBI = \frac{NIR - MIR}{NIR + MIR} \quad \text{...} \quad (2.3)$$

Landsat TM data uses bands 4 and 5, whereas Landsat OLI data uses bands 5 and 6. A high density of built-up features is indicated by values close to 1, which fall between 0 and 1, which represent built region

2.8 Empirical literature review

1. Estoque and Murayama (2013) examined the impact of urbanization on regional climates, focusing on Land Surface Temperature (LST). They discovered that urban growth contributes to higher LSTs, particularly in central urban areas compared to suburban or peri-urban regions due to denser buildings and reduced green spaces. Their findings emphasized the role of vegetation in mitigating the urban heat island effect, especially during the summer months. As a result, they recommended urban planning strategies that integrate more green spaces and sustainable designs to combat the rising urban temperatures.

2. Bai et al. (2018) investigated the intensification of Urban Heat Islands (UHIs) due to urban expansion, leading to higher temperatures in urban areas compared to rural ones.

They highlighted the role of impervious surfaces in raising temperatures and noted the adverse effects of intensified UHIs on air quality and energy consumption. Their study emphasized the importance of vegetation in reducing UHI effects and proposed incorporating green roofs, urban forests, and reflective materials in urban design as sustainable solutions.

3. Malik et al. (2020) explored the impacts of urbanization on Land Use Land Cover (LULC) changes and Land Surface Temperature (LST). They observed significant alterations in LULC patterns due to urbanization, leading to higher LSTs, particularly in densely developed urban zones. Their findings underscored the exacerbation of the urban heat island effect and recommended the integration of green spaces into urban planning to mitigate rising temperatures and promote sustainable urban development practices.

4. Muhammad et al. (2019) studied the environmental effects of urbanization, focusing on heatwaves and altered precipitation patterns. They highlighted the trapping of heat in urban areas due to dense infrastructure and reduced vegetation, leading to higher temperatures and prolonged heat events. Their study also addressed the impacts of urbanization on rainfall distribution, emphasizing the need for green infrastructure in urban planning to mitigate these effects and promote sustainable urban development.

5. Mohammad and Goswami (2018) investigated the impact of Land Use Land Cover (LULC) changes on Land Surface Temperature (LST), noting the significant increase in surface temperatures in urban and agricultural areas compared to vegetated regions. They emphasized the spatial variability of LST and recommended incorporating more green spaces and sustainable land management practices into urban planning to mitigate these effects.

6. Quattrochi and Luvall (1999) focused on Urban Heat Islands (UHIs), highlighting their formation due to heat-absorbing infrastructure in urban areas. They noted the variability of UHI intensity within cities and recommended incorporating green spaces, water bodies, and reflective materials in urban planning to reduce UHIs.

7. Zhou et al. (1998) examined the environmental impacts of land use and land cover (LULC) changes in metropolitan areas, emphasizing the alteration of natural landscapes

into urban infrastructure and its contribution to higher Land Surface Temperatures (LSTs). They recommended incorporating green infrastructure into urban planning to address these environmental impacts.

8. The study from 2017a emphasized the ecological implications of urban growth, including increased pollution, habitat loss, and elevated Land Surface Temperatures (LST) due to urbanization. It highlighted the importance of green spaces in mitigating these effects and recommended integrating green infrastructure and sustainable practices into urban planning.
9. Peng et al. (2016) investigated changes in the urban surface thermal environment, focusing on the Urban Heat Island (UHI) effect. They emphasized the impact of impervious surfaces and vegetation loss on higher surface temperatures in urban areas and recommended integrating more vegetation into urban areas to mitigate the UHI effect.
10. Souch & Grimmond (2006) stressed the importance of resilient and sustainable cities, addressing challenges like urban heat islands and air pollution. They emphasized the need for green infrastructure and sustainable urban planning but did not specifically explore the relationship between elevation and Land Surface Temperature (LST).

2.9 Research and Knowledge Gaps

Although the literature currently in publication fully discusses the complex interrelationships among LULC changes, LST, and urbanization, there is a significant empirical research gap on the precise impact of altitude on LULC dynamics and the ensuing effects on LST in Metehara City, Ethiopia. The present conversation noticeably lacks the above studies, which concentrate on consequences associated to altitude in the context of Metehara City.

Chapter Three

3. Material and Method

The topography, temperature and precipitation of Metehara City were given. The sources of the data used in this study, as well as the data processing methods like layer stacking, sub-setting, and digital image processing. Procedures for multispectral radiometric correction, image classification, accuracy evaluation, and change detection analysis were all presented in this chapter along with NDVI, NDBI, and LST calculations. The analysis methods used in the study (Zonal statistics and Pearson correlation coefficient) are also covered in this chapter. With the help of these zonal statistics, the value for every LULC class was determined, and the Pearson correlation coefficient was used to look at the relationship between the NDVI and NDBI LULC indices and the LST.

3.1. Description of Study Area

3.1.1. Location and area

The research was carried out in Metehara City, which is situated in the East Shewa Zone of the Oromia Region's Fentale woreda. Metehara is situated 947 meters above sea level and is located between in latitude 08°54′N and longitude 39°55′E. Located on the banks of the Awash River, this city is in the center of Ethiopia, about 200 kilometers east of Addis Ababa, the country's capital. One of the major cities in the area is Metehara.

Metehara is classified as having a hot, semi-arid climate (BSh) by Köppen-Geiger. All year long, the average temperature is between 24 °C (76 °F) and 30 °C (85 °F), with sporadic dips to 10 °C (50 °F) and peaks of 39 °C (103 °F). With 73 wet days each year, measured at the 1 mm (0.04 inch) threshold, the average annual precipitation is approximately 336 mm (13.2 inches). Metehara receives 3982 hours of sunshine on average annually, with daylight ranging from 11 to 12 hours 37 minutes each day. Country city statistics indicates that as of March 31, 2023, there were 23,403 people living in Metehara.

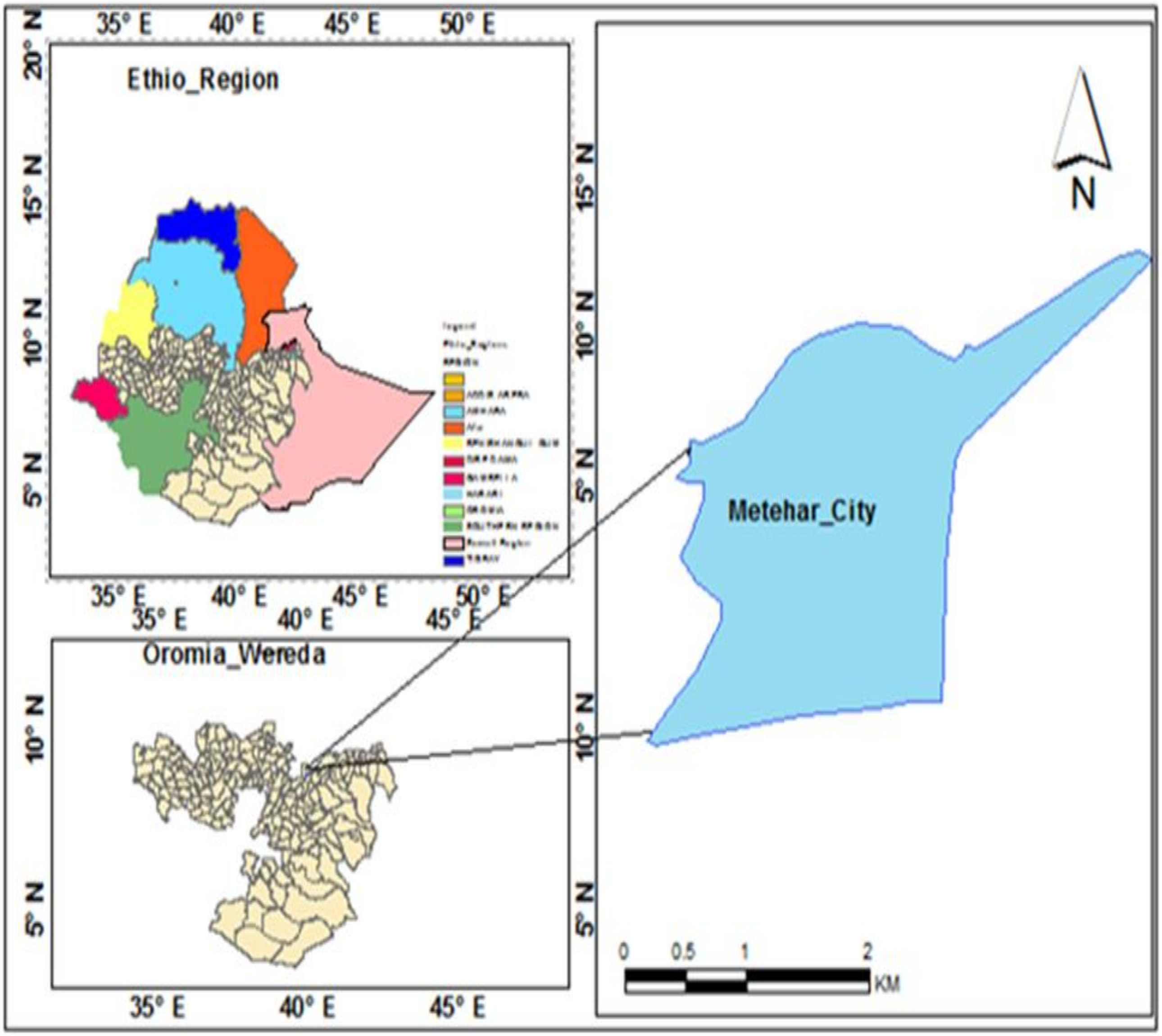

Figure 3.1: Location map of study Area

3.1.2. The topography of the study area

Topography is the natural features and shapes of the earth's surface, as well as other phenomena that are related to it, or it is a fundamental component of the land surface. Topography includes features such as elevation, latitude, longitude, and topographic maps.

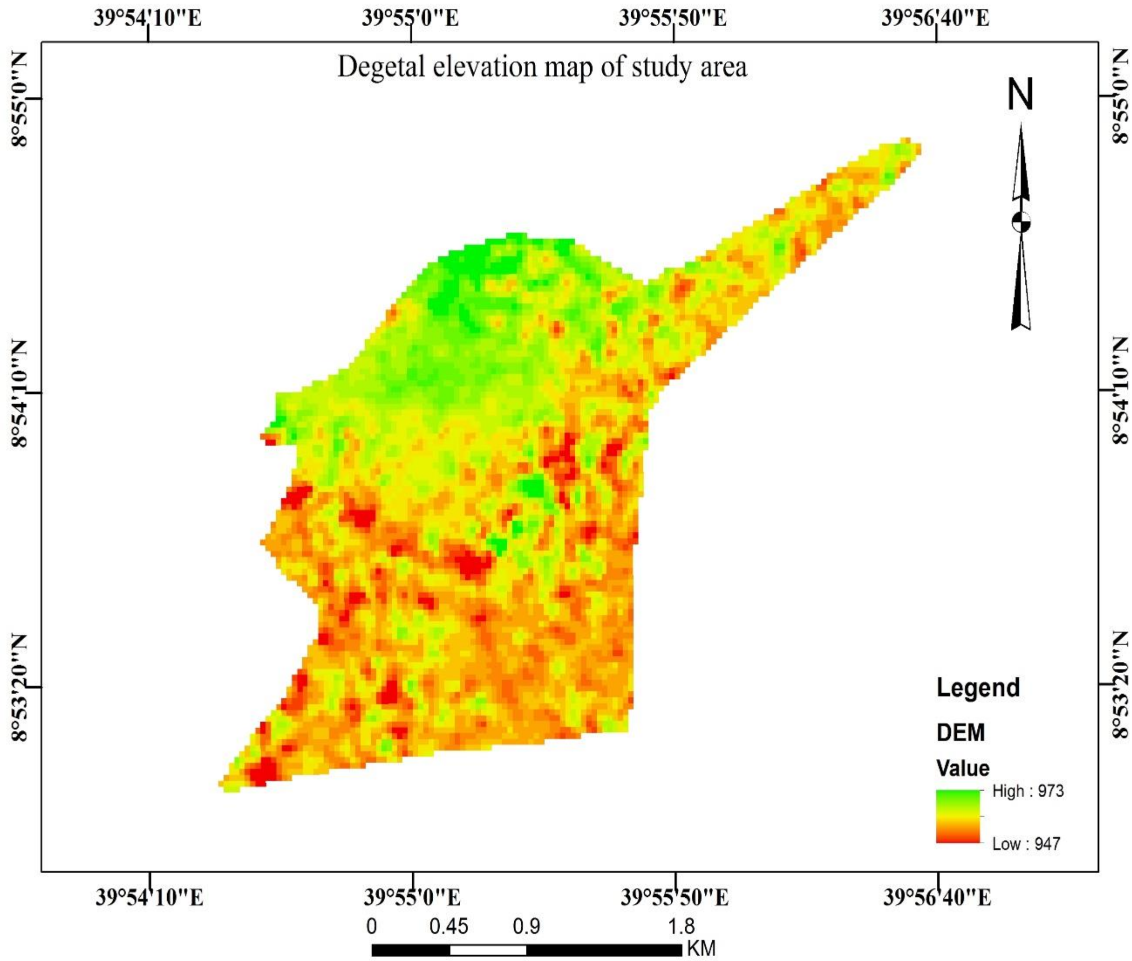

Figure 3.2 : elevation map of Metehara city

3.2. Climate

3.2.1. Temperature

According to data gathered from 1999 to 2020 at the Metehara meteorological station, the highest mean monthly temperature experienced was in February and May. The highest mean monthly temperature recorded over these months was 37.67 °C in March, nevertheless. On the other hand, the lowest maximum mean monthly temperature that was recorded was 13.850c in December, primarily in January, November, and December - September. Further details are displayed in the graph below.

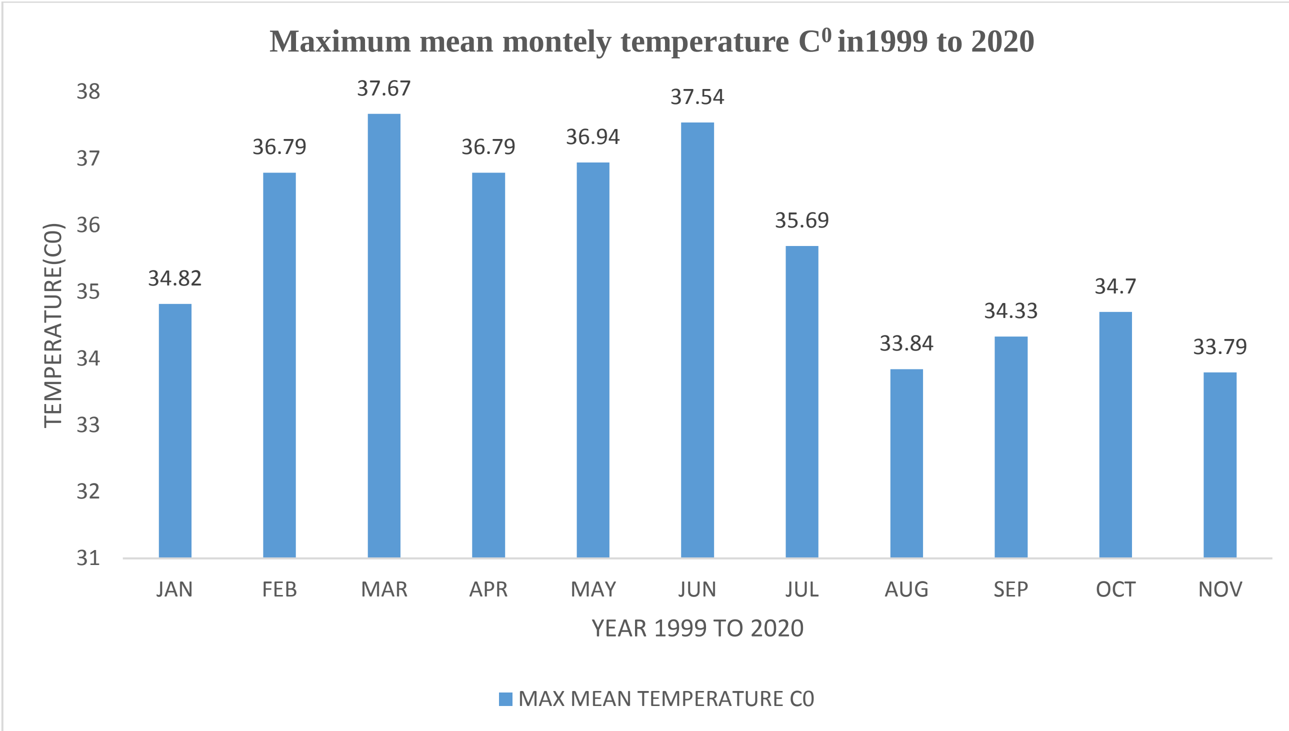

Figure 3.3 : maximum mean monthly temperature in study area

Source: National Meteorological Agency of Ethiopia (Year 1999 to 2020)

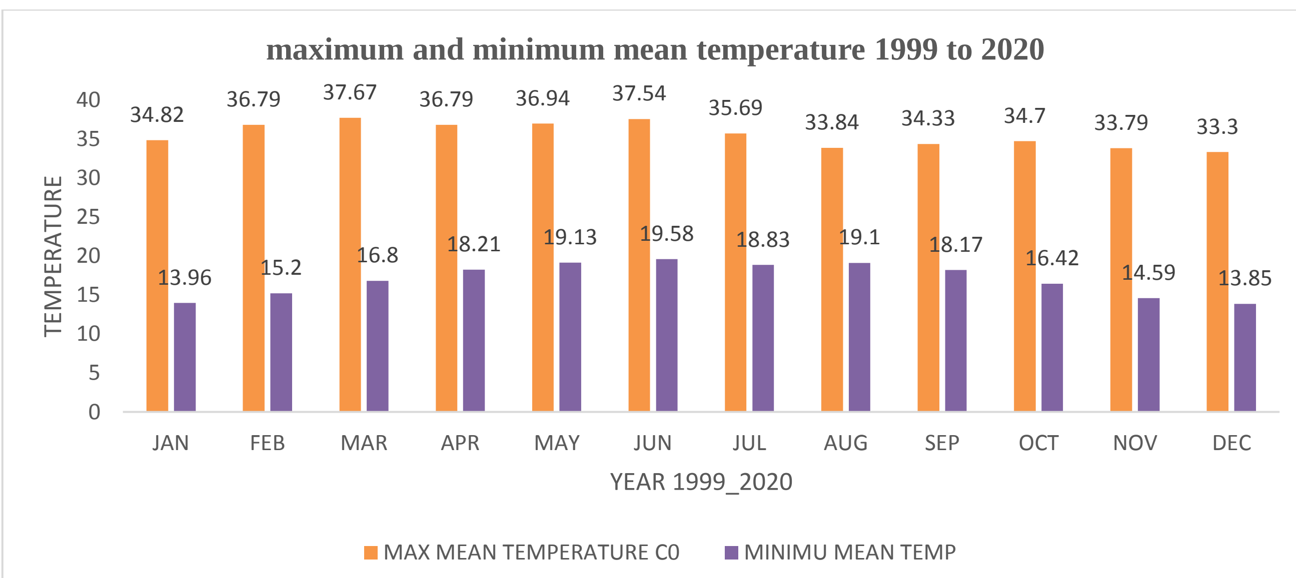

Figure 3. 4 : maximum and minimum monthly temperature

Source: National Meteorological Agency of Ethiopia (1999 to 2020)

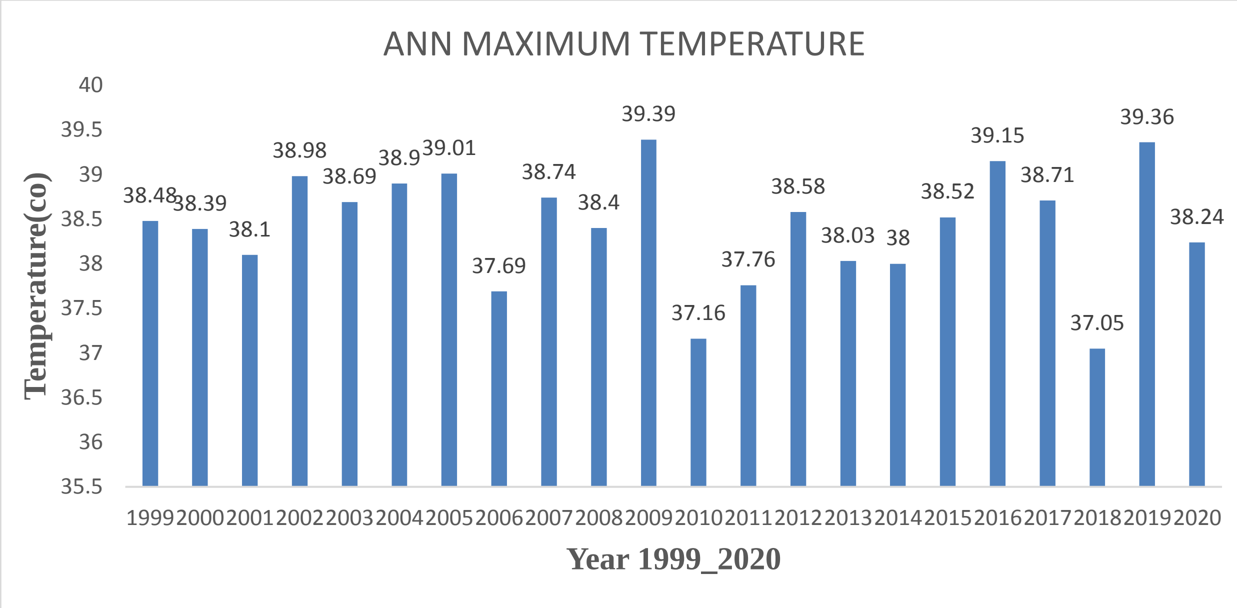

Figure 3. 5 : maximum and minimum monthly temperature

Source: National Meteorological Agency of Ethiopia (1999 to 2020)

3.3. Datasets and Sources

3.3.1. Remotely Sensed Data

Utilizing Landsat data has many benefits, one of which is its broad temporal range (beginning with Landsat-4/5 TM in 1980) in contrast to MODIS (since 1999) and ASTER (since 2000). Seasonal and decadal studies at greater spatial resolutions are made possible by the wider swath coverage of Landsat data (Landsat-5 TM 185 km, Landsat-8 OLI 185 km, ASTER 60 km, and MODIS 2330 km) (Petropoulos et al., 2016; Shimoda and Kimura, 2018). The study opted for Landsat pictures due to their greater spatial resolution, wider breadth, and long-term image availability.

USGS Earth Explorer provided the LANDSAT TM data for 1999 and 2010 as well as the LANDSAT 8 OLI data for 2020 (both with a spatial resolution of 30 m and path/row: 139/44). In order to minimize atmospheric and seasonal impacts, these acquisitions were based on minimal cloud cover measurements made in the same seasons (April and January) (Emran et al., 2018. The study period only included the years 1999 to 2020 due to the MSS sensor's limitations and the lack of data availability; 11 and 10 year intervals were chosen for investigation.

Table 3.1: Remote sensing datasets were used for the study and its descriptions

Path/row	Acquisition date	satellite	sensor	Resolution PAN/MS/TIRS	SOURCE
168/54	02/3/1999	LAND SAT	TM	15/30/120	USGS
168/54	02/15/2010	LAND SAT	TM	15/30/120	USGS
168/54	02/21/2020	LAND SAT	OLI	15/30/100	USGS

Landsat Thematic mapper (TM)

Using the Landsat Thematic Mapper (TM) sensor, remote sensing applications may take pictures of the Earth's surface. From its first debut in 1982, it has provided important data for a range of applications, such as mapping land use and cover, environmental monitoring, agriculture, forestry, and urban planning. It is possible to detect various surface features and attributes thanks to the Landsat TM sensor's operation in the visible, near-infrared, and thermal infrared bands. With a spatial resolution of 30 meters, the TM picture MS (bands 1 through 7 and 7) and 120 m for thermal (band 6). Consequently, in order to detect the LST of the earth's surface, TM Band 6 is particularly sensitive to thermal infrared radiation.

Table 3. 2: Remote sensing datasets were used for the study and its descriptions

LANDSAT 5	Bands numbers	Band names	Wavelength Range (micrometers)	Spatial Resolution (meters)	Temporal resolution per day
Thematic mapper	Band 1	Blue	0.45 - 0.52	30	16
	Band 2	Green	0.52 - 0.60	30	16
	Band 3	Read	0.63 - 0.69	30	16
	Band 4	NIR	0.76 - 0.90	30	16
	Band 5	SWIR_1	1.55 - 1.75	30	16
	Band 6	Thermal	10.40 - 12.50	120	16
	Band 7	SWIR_2	2.08 - 2.35	30	16

NB: NIR-near infrared, SWIR-short wave infrared

Landsat Operational Land Imager (OLI) and Thermal Infrared Sensor (TIRS)

For use in remote sensing and Earth observation, the Landsat Operational Land Imager (OLI) is a satellite instrument. The United States Geological Survey (USGS) and NASA oversee the Landsat program, which includes it. OLI, a multispectral image of the Earth's surface sensor, was launched in 2013 as a component of the Landsat 8 satellite. Its images are useful for a range of commercial, scientific, and environmental applications.

The visible, near-infrared, short-wave infrared, and thermal infrared portions of the electromagnetic spectrum are among the nine spectral bands in which the Landsat OLI sensor functions. The identification and examination of various surface features, including vegetation, water features, cities, and geological formations, are made possible by these bands. Detailed mapping and long-term monitoring of changes in land cover and use are made possible by the spectral band-dependent spatial resolution of Landsat OLI pictures, which spans from 15 to 100 meters. In Table 3.3, OLI/TIRS bands are explained in detail.

Table 3.3 : Landsat 8 OLI and TIRS bands description.

Landsat 8	Bands	Band names	Wavelength Range (micrometers)	Spatial Resolution (meters	Temporal resolution per day
	Band 1	Coastal/Aerosol	0.43 - 0.45	30	16
	Band 2	Blue	0.45 - 0.51	30	16
	Band 3	Green	0.53 - 0.59	30	16
	Band 4	Red	0.64 - 0.67	30	16
	Band 5	NIR	0.85 - 0.88	30	16
OLI /TIRS	Band 6	SWIR 1	1.57 - 1.65	30	16
	Band 7	SWIR 2	2.11 - 2.29	30	16

Band	panchromatic	0.50 - 0.68	15	16
Band 9	Cirrus	1.36 - 1.38	30	16
Band 10	TIRS_1	10.60 - 11.19	100	16
Band 11	TIRS_2	11.50 – 12.11	100	16

3.3.2. Meteorology Data

Meteorological data such as humidity, temperature, and rainfall data were gathered from the National Meteorological Agency of Ethiopia. These data were used to define the climate of the Metehara city through the study periods.

3.3.3. Ground Truth Data and Google Earth Data

Following the creation of stratified sample sites from the Landsat image and their locations from Google Earth, ground truth data were gathered from the field via GPS. By examining the actual LULC of the city, field data were utilized to validate the LULC classified image into distinct classes. Images depicting the various LULC classes in the city were taken in order to reduce categorization errors. Throughout the picture classification procedure, a Google Earth map was used as a visual interpretation.

For maps smaller than 4,000 km2 and with less than 12 classes, Jensen (2015), Lillesand et al. (2008), and Congalton and Green (2009) state that in order to assess accuracy, at least 50 sample points per mapping class must be gathered. Five LULC classes were chosen for this study, and the total area in and around Metehara City is 585.80 hectares.

3.4. Software

Google Earth PRO 2023, ArcGIS 10.8, QGIS 3.10, ERDAS IMAGINE 2014, and Microsoft Word and Excel 2016. The processing of satellite imagery, analysis of urban LULC changes, NDVI, NDBI, LST, and the relationship between LST and LULC indices were all done using ArcGIS 10.8. For picture preprocessing and image classification, ERDASIMAGINE 2014 was utilized. Zonal statistics, categorization, and a layout map of the city were created using Arc GIS10.8. ArcGIS 10.8 was also used for conversion detection analysis, extract LST, and mapping of a town's NDVI, NDBI, NDWI and LULC maps. However, for the sake of visual image interpretation, Google Earth PRO 2023 used as the basis map. Correlation statistics between LST and NDVI, NDBI, NDWI, and DEM were developed using Microsoft Excel 2016.The entirety of this study was assembled using Microsoft Word and Excel 2016.

3.5. Methods of analysis

Remote sensing, GIS, and statistical approaches are the three main methodologies used in this study. The research periods of 1999, 2010, and 2020 are used to examine and analyze historical changes in Land Use and Land Cover (LULC) using multi-temporal satellite imagery. Furthermore, during the same time periods, spatiotemporal patterns in Land Surface Temperature (LST) are examined using data from remote sensing. First, a Landsat 5 and 8 urban land use and land cover change (LULC) analysis is carried out. Subsequently, the second part involves computing LST, NDVI, and NDBI using Landsat images. Zonal and correlation statistics are then used to evaluate how NDVI, NDBI, and NDWI relate to LST. The flow chart that goes with the data processing describes the full methodology.

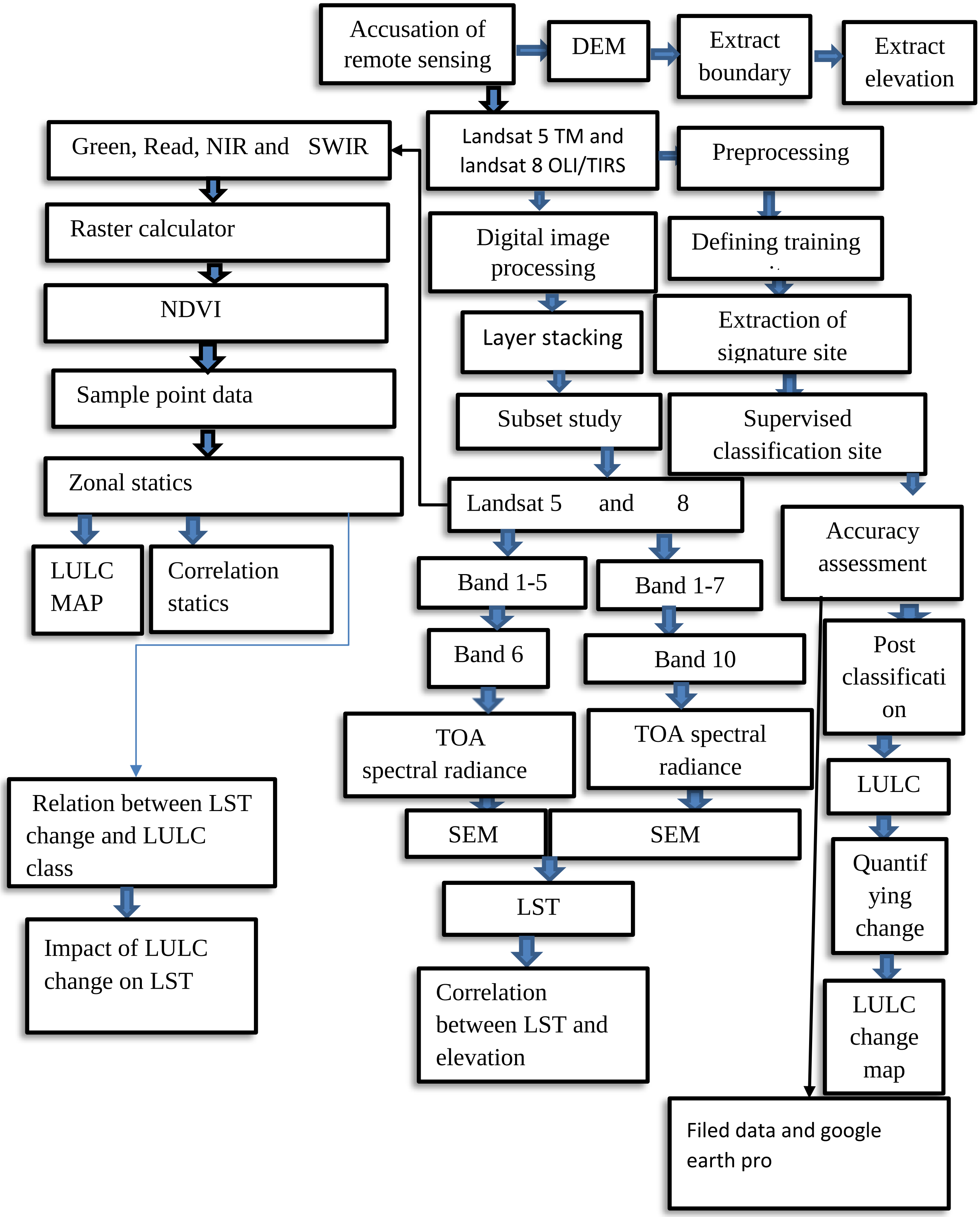
Accusation of remote sensing
DEM
Extract boundary
Extract elevation
Landsat 5 TM and landsat 8 OLI/TIRS
Green, Read, NIR and SWIR
Preprocessing
Raster calculator
Digital image processing
Defining training
NDVI
Layer stacking
Extraction of signature site
Sample point data
Subset study
Supervised classification site
Zonal statics
Landsat 5 and 8
Accuracy assessment
LULC MAP
Correlation statics
Band 1-5
Band 1-7
Band 6
Band 10
Post classificati on
TOA spectral radiance
TOA spectral radiance
LULC
SEM
SEM
Relation between LST change and LULC class
LST
Quantif ying change
Impact of LULC change on LST
Correlation between LST and elevation
LULC change map
Filed data and google earth pro

Figure 3. 6 : general work flow.

Sour*ce (*Congalton and Green, 2*009,* Weng et al., 2004)

3.5.1. Digital Image Preprocessing

A number of factors can impact the quality of satellite imagery, therefore digital processing and correction are required prior to additional study. Utilizing computer software to manipulate and analyze digital photos improves their quality for precise interpretation and categorization. Because digital photographs can be easily maintained on a computer, this technique helps minimize errors during interpretation (Abel, 2018). Typical preprocessing procedures include image registration, geometric correction, atmospheric correction, and normalization. Prior to information extraction for data analysis, certain pre-processing tasks are essential.

3.5.2. Multispectral Radiometric Correction

As radiation from the source interacts with the atmosphere, preprocessing is essential to ensuring the correctness of images (Abel, 2018). For remote sensing applications, the energy reflected from target objects to the sensor is essential. Therefore, the conversion of Digital Numbers (DN) into spectral radiance is required. For example, spectral radiance is converted to radiance in ArcGIS using the formula given by Markham and Barker (1986) after radiometric correction of Landsat 5 TM pictures.

3.6. Land surface temperature retrieval

Utilizing the thermal bands of Landsat pictures, the land surface temperature (LST) was extracted. Landsat 8 was calculated using band 10, and Landsat 5 (TM) and Landsat 7 (ETM+) were calculated using band 6. Digital Numbers (DN), which obliquely depict the spectrum radiances of ground objects, are frequently used to store satellite image data. LST values were extracted from Landsat-8 band 10 and Landsat-5 band 6 photos for this study. Landsat 8 has two thermal bands (bands 10 and 11), however only band 10 was used because of the higher level of uncertainty in LST extraction from band 11 (Landsat 8 calibration notice, 2017, Barsi et al., 2014). Converting ground object DNs is the first stage in the LST retrieval process.

1) Digital number (DN) to radiance conversion/to top of atmosphere (TOA) radiance ($L\lambda$) conversion (Landsat 8 Data Users Handbook, 2019). Band 6 has been designated as a thermal band for Landsat-5 TM imagery, and the spectral radiance ($L\lambda$) can be computed using the following formula.

$$\mathrm{L\lambda} = \frac{\mathrm{L\lambda MAX - L\lambda MIN}}{\mathrm{Qcalmax - Qcalmi}} * (\mathrm{Qcal} - \mathrm{Qcalmin}) + \mathrm{L\lambda min} \ldots\ldots\ldots\ldots\ldots\ldots\ldots\ldots\ldots\ldots\ldots\ldots\ldots \text{(3.1)}$$

The spectral radiances for band 6 at each digital number are represented by LMAXλ and LMINλ, and QCALMIN = 1, QCALMAX = 255, and QCAL = Digital Number of each pixel. LMAXλ = 15.303 and LMINλ = 1.238 are the values. The spectral radiance that is scaled to Qcalmin (W/ (m2 * sr * µm), L\max is the spectral radiance that is scaled to Qcalmax (W/ (m2 * sr * µm), Qcalmin is the minimum quantized calibrated pixel value (corresponding to L\min in DN which is 1), and Qcalmax is the maximum quantized calibrated pixel value (corresponding to L\max in DN which is 255). Following that, level pixel DN values were changed to top of atmospheric (TOA) reflectance using the equation provided below.

Conversion of TOA Radiance to at Sensor Brightness Temperature (TB).

Using the following formula, the brightness temperature was determined from the thermal bands' spectral radiance (Weng et al., 2004, Rajeshwari and Mani, 2014):

$$TB = \left(\frac{K2}{Ln\left(\frac{K1}{L\lambda}+1\right)}\right) - 273.15 \ldots\ldots\ldots\ldots\ldots\ldots\ldots\ldots\ldots\ldots\ldots\ldots\ldots\ldots\ldots\ldots\ldots\ldots\ldots\ldots \text{(3.2)}$$

Where: TB stands for brightness temperature (K), Lλ for TOA spectral radiance, K1 for calibration constant 1, and K2 for calibration constant 2. These values are, respectively, 607.76 and 1260.56. The conversion of Kelvin to Celsius is aided by 273.15.

For Landsat-8 OLI imagery

Step 1. Band 10 is the thermal band, and the following equation has been inferred in order to obtain spectral radiance (Lλ).

$$\mathrm{L\lambda} = \mathrm{ML} * \mathrm{QCAL} + \mathrm{AL} \ldots\ldots\ldots\ldots\ldots\ldots\ldots\ldots\ldots\ldots\ldots\ldots\ldots\ldots\ldots\ldots\ldots\ldots \text{(3.3)}$$

Where Lλ stands for the upper atmosphere's spectral radiation. Furthermore, the band-specific multiplicative rescaling factor (0.0003342) is indicated by ML, while the band-specific additive rescaling factor (0.1) is indicated by AL. Moreover, QCAL, or Quantized and Calibrated Standard Product Pixel value (for the band 10 image particularly), is included in the equation.

The second step involves converting the spectrum radiance to At-satellite brightness temperatures (BT). Following the conversion of the digital number into radiance, the data is now translated using the thermal constant from the metadata file into brightness temperature (BT). The tool's algorithm uses the following equation to convert reflectance to BT.

$$TB = \left(\frac{K2}{Ln\left(\frac{K1}{L\lambda}+1\right)}\right) - 273.15 \quad \text{(3.4)}$$

Where: Lλ, or the top of the atmosphere's spectral radiation measured in W/(m^2 * sr * μm), and TB, or brightness temperature in Kelvin. Furthermore, there exist calibration constants K1 and K2, which have particular values of 1321.0789 and 774.8853, respectively. Using 273.15 as a constant factor makes converting from Kelvin to Celsius easier. Additionally, the values of Mλ and AL represent the band's Radiance multiplicative and additive scaling factors, respectively, and are obtained from metadata like radiance_mult_band_n and radiance_add_band_n. Level one pixel value in DN, or Qcal, is an important input for the conversion process. An equation published by USGS in 2016 is used to convert level 1 pixel DN values to top of atmospheric reflectance. To provide precise and significant pixel value conversion for additional analysis and interpretation in remote sensing applications, this equation takes into account the previously described parameters and factors.

Step-III Vegetable Proportion (PV). To determine the percentage of vegetation, the Normalized Difference Vegetation Index (NDVI) is the primary metric. This is the result of the calculation.

$$PV = \left(\frac{NDVI - NDVImin}{NDVImax - NDVImin}\right)^2 \quad \text{(3.5)}$$

The terms NDVImin and NDVImax in this formula denote the lowest and maximum NDVI values within the dataset or a certain range, respectively. Utilizing NDVI data, which are frequently employed in remote sensing to evaluate vegetation conditions and dynamics, the PV offers an alternate indicator of the health and vitality of the vegetation. For vegetation study, particularly in regions where conventional vegetation indices do not fully represent the range of vegetative responses, the PV computation can be helpful in normalizing the NDVI results.

Step IV: Correction for Emissivity (ε). Now, we may use the following equation to quickly and easily fix the emissivity (ε).

Land surface emissivity $(E) = 0.004 * PV + 0.986$ …………………………………… (3.6)

Step-V Calculation ground surface temperature

$LST = \frac{BT}{1} + W * \frac{BT}{\rho}$*ln*ε .... (3.7)

Where

BT=at satellite temperature, w=wavelength of emitted radiance. $\rho = \frac{h*c}{s}(1.438 * 10^{-2})MK$,h-planks constant, $h = (6.626 * 10^{-34})JS$ s-Boltzmann constant, $s = (1.38 * 10^{-23})J/S$ c-velocity of light, $C = (2.998 * 10^{8}\, m/s)$ and p=14380.

3.7 Extraction of LULC and accuracy assessment

Using the maximum likelihood classification approach, land use land cover (LULC) maps were classified into five different classes in this study. These categories comprise built-up areas, bare land, agricultural land, water bodies, and vegetated land. The technique uses user-defined classes to classify picture cells by utilizing information from multispectral bands. The Bayesian probability distribution is computed over the complete image set using the mean and covariance of the training samples, which are crucial from each class. By comparing each pixel's signature with the signatures of the training samples, this technique uses statistical likelihood to classify each pixel.

According to Gao (2009) and Lillesand et al. (2004), object reflectance values are analyzed to extract information from images, which is the basis for the image classification process. The ensuing classes are arranged into thematic layers that, within the image, symbolize comparable urban LULC patterns. For efficient information extraction, this technique is commonly used in digital remote sensing. When classifying image features, human analysts use visual interpretation components to find homogenous pixel clusters that reflect different land cover classes of interest. A key component of this categorization strategy involves spectral information.

3.7.1 Supervised Classification Top of Form

Using labeled training samples, supervised classification in remote sensing group’s pixels into preset classes. This is accomplished by using a variety of methods, including minimal distance to mean, parallelepiped, and greatest likelihood. Using the maximum likelihood classification technique, Ayanlade and Howard's (2019) work used supervised classification to divide land use land cover (LULC) maps into five classes: built-up areas, bare land, agricultural land, vegetative land, and aquatic bodies. Benefits of this approach include information classes, training sites for self-assessment, and the reusability of these sites. On the other hand, disparities in class homogeneity and uniformity, as well as those between information and spectral classes, could provide difficulties. Supervised classification is still a useful technique for precisely mapping land cover in digital remote sensing applications, despite these difficulties.

3.7.1.1 The Maximum Likelihood Classifier Technique

Statistical techniques such as mean, variance, and covariance are used by the Maximum Likelihood Classifier (MLC) in remote sensing for supervised classification. For every class in the training set, it uses probability theory to define the class centers and the variability of raster values in each input band. Because of this, it can determine the size and form of the class in spectral space as well as the likelihood that a pixel in the input image belongs to a particular class center. It produces more accurate class assignments than other methods, such as minimal distance to means, by calculating all class probabilities for each raster cell and assigning the cell to the class with the highest probability value.

With its ability to define class spectral response pattern variance and covariance statistically, the MLC is useful for spectral response data with varying degrees of variance. When managing different degrees of spectral response data, the MLC method is helpful even though it is less computationally efficient than other methods especially in metropolitan regions where these changes are frequent. But problems like cell mixing can make categorization accuracy difficult, particularly with low-resolution data like Landsat. This was addressed by using more data sources, like field surveys and Google Earth maps, in the study to increase classification accuracy and reduce errors.

Final Land Use Land Cover (LULC) thematic layers were defined and mapped for three different study periods (1999, 2010, and 2020) within Metehara City after the categorization accuracy assessment. Built-up areas, vegetation cover, agricultural land, aquatic bodies, and bare ground are among the LULC classification schemes found for Metehara City.

3.7.2 Accuracy assessment

Analyzing land cover data obtained from remote sensing requires careful consideration of accuracy evaluation, which includes the use of Kappa coefficients, Overall Accuracy (OA), User's Accuracy (UA), and Producer's Accuracy (PA). As far as the map maker is concerned, PA indicates accuracy, and users' perspectives of accuracy are represented by UA. A measure of accuracy in reference site mapping is called OA. Between categorized and reference data, kappa coefficients quantify the degree of agreement.

Error matrices for each time point (1999, 2010 2020 and) were utilized to generate equations that estimated the UA, PA, OA, and Kappa coefficients in order to maximize classification accuracy. To create error matrices for accuracy evaluation, ground truth data gathered with the use of a handheld GPS unit and Google Earth was compared to controlled maps. The aforementioned matrices are useful in evaluating the correlation between reference pixels and land use land cover (LULC) maps. They offer statistical measures such as the accuracy of the producer, user, overall, and kappa coefficient (Congalton and Green, 2009).

Sample points are assigned to each class based on reference data, as shown by the error/confusion matrix arrangement with numbered records and fields. In addition to analyzing overall classification accuracy, this matrix helps in evaluating omission errors (producer accuracy) and commission errors (user accuracy). The user, producer, overall, and Kappa coefficients were all estimated using equations.

Producer's accuracy (i): - Shows the proportion of reference pixels that are correctly classified for a given class out of all reference pixels in that class.

$$PA_i = \left(\frac{\text{Number of correctly classified pixels for class i}}{\text{Total number of reference pixels for class i}}\right) * 100 \ldots\ldots\ldots\ldots (3.8)$$

User's Accuracy (UA) for a class i: Shows the proportion of pixels accurately classified as be

$$\mathrm{UA_i} = \left(\frac{\text{Number of correctly classified pixels for class i}}{\text{Total number of pixels in class i}}\right) * 100 \ldots\ldots\ldots\ldots (3.9)$$

Overall Accuracy (OA): Measures the percentage of correctly classified pixels out of all pixels in the dataset.

$$OA_i = \left(\frac{Number\ of\ correctly\ classified\ pixels}{Total\ number\ of\ pixels}\right) * 100 \ldots\ldots\ldots\ldots (3.10)$$

Kappa Coefficient (Kappa): Computes the predicted agreement using random chance while accounting for the distribution of pixels between classes.

$$K = \frac{N\sum_{I=1}^{r} xii - \sum_{i=1}^{r}(xi+*x+i)}{N^2 - \sum_{i=1}^{r}(xi+*x+i)} \ldots\ldots\ldots\ldots (3.11)$$

Whereas As the Kappa coefficient, or K, has a value between 0 and 1, where 0 denotes no improvement over random chance and 1 denotes complete agreement. The total number of samples (N) in the confusion matrix, the number of observations in each cell (Xii), the total number of observations in each row (Xi+), and the total number of observations in each column (X+i-) are the factors used to compute K. Generally, to represent classification accuracy as a percentage, K is multiplied by 100 (Worku, 2018).

3.8 Urban Land use and Land cover Thematic Layer

Classifying land use and cover (LULC) is a crucial component of geographic information systems (GIS) and remote sensing, offering important insights into the features and spatial distribution of various land surface types. Different classes, each representing unique land uses and ecological qualities, are included in the classification of land cover, including built-up areas, vegetation, aquatic bodies, agricultural, and barren ground. According to Xie et al. (2020), water bodies, which include rivers, lakes, reservoirs, and coastal areas, are essential for hydrological processes, biodiversity, and human activities involving water resources. After determining the correctness of the classification, five LULC thematic layers were identified and mapped for the years 1999, 2010, and 2020. As a result, Metehara City is included in table 3.4 with the following LULC classes.

Table 3.4 : LULC class type and description

NO	LULC classes	Descriptions
1	Built-up	Many different types of structures can be found in the area, including factories, offices, schools, hospitals, schools, homes (both single and mixed-use), roads, warehouses, and places of worship (churches and mosques).
2	Agriculture	The region encompasses both seasonal crops that are planted annually and crops that grow throughout the year (perennial crops).
3	Vegetation	The region includes areas with shrubs, trees, and grasslands.

4	Bare land	A non-vegetated area dominated by rock, eroded and degraded lands; the area covered by day dirt, sand/rock and, dry salt flats, beaches
5	Waterbody	The area covered by river and dams

3.9 Change Detection Analysis

Using techniques like image classification and vegetation indices, particularly the Maximum Likelihood Classification (MLC) algorithm, land use change detection entails assessing changes in land cover and land use using remote sensing. Research shows how useful Landsat imagery is for analyzing urban land use, as shown by the works of Lu and Weng (2004). Widely used for this purpose, the post-classification method uses ArcGIS software to combine LULC change maps, making it easier to calculate area coverage and percentage change for each LULC class for particular years. Making educated decisions about land management and environmental evaluation requires the application of this analytical method.

$$percetage\ change\ detection = \left(\frac{\text{area i year x+1} - \text{Area i yearx}}{\sum_{\text{i=1}}^{\text{r}} \text{Area i year x+1}}\right) * 100 \ \ldots\ldots\ldots\ldots\ldots\ldots\ldots\ldots \ (3.12)$$

Where; Area i year x = area of cover i at the previous year, Area i year x +1 = area of cover i at the next year, $\sum_{\text{i=1}}^{\text{r}} \text{Area i year x} + 1$ the next year

3.9 Determination of the land use land cover indices

3.9.1 Normalized Difference Vegetation Index

For evaluating vegetation cover worldwide, the Normalized Difference Vegetation Index (NDVI) is a commonly used metric (Vani and Mandla, 2017). The index is computed as the reflectance difference between the red band (RED) and the near-infrared band (NIR) of satellite pictures. The Normalized Difference Vegetation Index (NDVI) has a range of -1.0 to +1.0. According to Townshend and Justice (1986), areas with positive values are highly vegetated, whereas areas with negative values are not. The NDVI formula can be found using.

$$NDVI = \frac{NIR-RED}{NIR+RED} \ \ldots\ldots\ldots\ldots\ldots\ldots\ldots\ldots\ldots\ldots\ldots\ldots\ldots\ldots\ldots\ldots\ldots\ldots\ldots\ldots \ (3.13)$$

3.9.2 Normalized Difference Built-up Index (NDBI)

The Normalized Differen One approach frequently used to measure built-up land in metropolitan settings is the Built-up Index (NDBI) (Kshetri, 2018). The Middle Infrared (MIR) and Near Infrared (NIR) bands are used to calculate the Near Infrared Band Index (NDBI) using the following formula.

$$NDBI = \frac{NIR - MIR}{NIR + MIR} \quad \text{.......} \quad (3.13)$$

Landsat TM data uses bands 4 and 5, whereas Landsat OLI data uses bands 5 and 6. A high density of built-up features is indicated by values close to 1, which fall between 0 and 1, which represent built-up regions. The NDVI is computed using band 3 and 4 for Landsat TM data and band 4 and 5 for Landsat OLI data. Values between 0 and +1 represent the amount of plant cover, with values near 1 indicating a high density of vegetation.

3.9.3 Normalized Difference Water Index (NDWI)

The Normalized Difference Water Index (NDWI) uses visible and near-infrared radiation to identify open water bodies (McFeeters, 1996). The following is the formula for NDWI.

$$NDWI = \frac{Green - NIR}{Green + NIR} \quad \text{.......} \quad (3.14)$$

The Landsat TM data bands 2 and 4 and the Landsat OLI data bands 3 and 5 are used to compute NDWI. An area's vegetation is indicated by smaller values, even negative values, while water bodies are often indicated by values greater than 0.5 on the NDWI scale, which runs from -1 to +1. Water bodies and other land cover types can thus be distinguished with the help of NDWI.

3.10 Zonal statics

The method of calculating statistics for specific zones within a dataset using values from a value raster another datasets referred to as zonal statistics. Using this method, the raster data is divided into zones, and the statistics for each zone are computed using the data in that zone. The results are stored in a new raster dataset, and cells in the same zone are given the same values (Abel, 2018). Using ArcGIS 10.8 software, zonal statistics were used to evaluate the differences in each Land Use Land Cover (LULC) type. For the years 1999, 2010, and 2020, maps for Urban LULC, NDVI, and LST were made, and statistical analysis were carried out. This made it possible to examine the temporal and spatial variations in Land Surface Temperature (LST) within each LULC category and to assess how LULC changes affected the LST data, which was then condensed using Microsoft Excel 2016.

3.10.1 Zonation for spatial coverage of LST

Statistical measures like minimum, maximum, mean, and standard deviation were used to divide the surface temperature data into low, medium, and high temperature zones. Based on these statistical values that were computed for the research area, which included all forms of Land Use Land Cover (LULC), the thresholds for each zone were established. A set of criteria based on the minimum and maximum temperature values were used to determine the low and high temperature zones, while the range of the middle temperature zone was calculated by adding and subtracting the standard deviation from the mean temperature. The investigation of the Land Surface Temperature (LST) spatial distribution among several LULC types was made possible by this categorization.

3.11 Correlational Analysis

The Pearson correlation coefficient was used to determine how strongly the NDBI, NDVI, and LST for each pixel were linearly related. This coefficient, which ranges from +1 to -1, measures the degree of linear relationship between two variables, X and Y. Perfect positive relationships are represented by a value of +1, perfect negative relationships by a value of -1, and no relationships are represented by a value of 0. The absolute value of the correlation coefficients was classified as follows in order to determine the degree of correlation between the LST and LULC indices (NDVI and NDBI): weak correlation ($0 < |r| \leq 0.3$), low correlation ($0.3 < |r| \leq 0.5$), moderate correlation ($0.5 < |r| \leq 0.8$), and strong correlation ($0.8 < |r| \leq 1$).

$$r_{xy} = \frac{\sum_{i=1}^{n}(xi - xj) * (yi - yj)}{(\sqrt{[\sum_{i=1}^{n}(xi - xj)^2][\sum_{i1=}^{n}(yi - yj)^2]})} \quad \ldots\ldots\ldots\ldots\ldots\ldots\ldots\ldots\ldots\ldots\ldots\ldots\ldots\ldots\ldots(3.15)$$

Where, rxy is the simple correlation coefficient of variables X and Y, xi is NDBI, and NDVI of the ith year, Yi is LST of the ith year; Xm is the average NDVI and NDBI for all years, Ym is LST for all year

Chapter Four

4. Result and Discussion

4.1 LULC classification and area coverage in 1999, 2010 and 2020

The degree of the linear correlation between NDBI, NDVI, and maximum probability of supervised classification was used in erdas IMAGIN envision 2014, as Table and Figure show, the LULC map was created in 1999, 2010, and 2020 with high accuracy. The total LULC area of the research area is 585.80 hectares.

In 1999 research analysis of land use land cover in Metehara city revealed that agricultural land, covering 128.57 hectares or 22% of the total area, is crucial for the local economy and food production. The remaining 99.60 hectares are barren, indicating potential for future development or habitat restoration. Built-up areas, covering 35.97 hectares or 6% of the total area, represent urban infrastructure, including residential, commercial, and industrial buildings. Vegetation, covering 321.67 hectares or 55%, is the dominant land cover type, encompassing natural vegetation like forests, grasslands, and shrub lands, as well as cultivated vegetation like plantations or gardens.

Since 2010, Metehara City's patterns of urbanization have continued, with 26% of the land under build. Though it still makes up about 20% of the in general area, changes in land use and deforestation are causing the amount of vegetation to gradually decrease. Water such occupy 52.53 hectares, or 9% of the total area. These bodies offer aquatic animals with habitats and provide a vital to the local environment. Between 1999 to 2010, there were significant alterations in the composition of LULC, particularly in built-up areas, bare land, and the amount of vegetation, depending to the analysis.

20% the entire surface, or 119.97 hectares of land are utilized for agricultural. It indicates that agriculture has been steadily present in the area, boosting food production and the economy of the area. The three categories of land that make up Metehara City's total area are built-up, bare ground, and vegetation. Though it has decreased recently, bare ground still makes up 11% of the overall area. The fact that 35% of the land is made up of built-up regions shows that infrastructure and urbanization are still being developed. 19% of the area is covered with vegetation, with a little amount falling out owing to natural vegetation changes or deforestation.

Water bodies, comprising almost 15% of the total area, are crucial for local ecology. The study explores land cover types' changing characteristics and their impact on equitable land use, environmental protection, and urban development. It also provides insights into Metehara city's LULC makeup in 2020.

Between 1999 and 2020, Metehara City's land use and land cover changed significantly due to environmental changes, agriculture methods, and modernization. Agricultural land accounted for 22% of the area, while urban infrastructure was occupied by bare land. Urbanization increased, leading to a 26% increase in densely populated regions and a decrease in vegetation. Water bodies remained vital, accounting for over 15% of the total area. Vegetation covered 113.99 hectares, constituting approximately 19% of the total area. However, vegetation has slightly decreased compared to previous assessments, possibly due to factors like deforestation, land conversion, or natural vegetation changes.

Table 4. 1: LULC level in 1999, 2010 and 2020 in study area

NO		1999		2010		2020	
	LULC class	Area in (Ha)	Area in (%)	Area in (Ha)	Area in (%)	Area in (Ha)	Area in (%)
1	Built up	35.97	6	149.7	26	202.21	35
2	Vegetation	321.67	55	120.31	20	113.99	20
3	Bare land	99.60	17	147.63	25	64.68	11
4	Agriculture	128.57	22	115.59	20	119.97	20
5	Water body	___	___	52.53	9	84.80	15
Total		585.80	100%	585.80	100%	585.80	100%

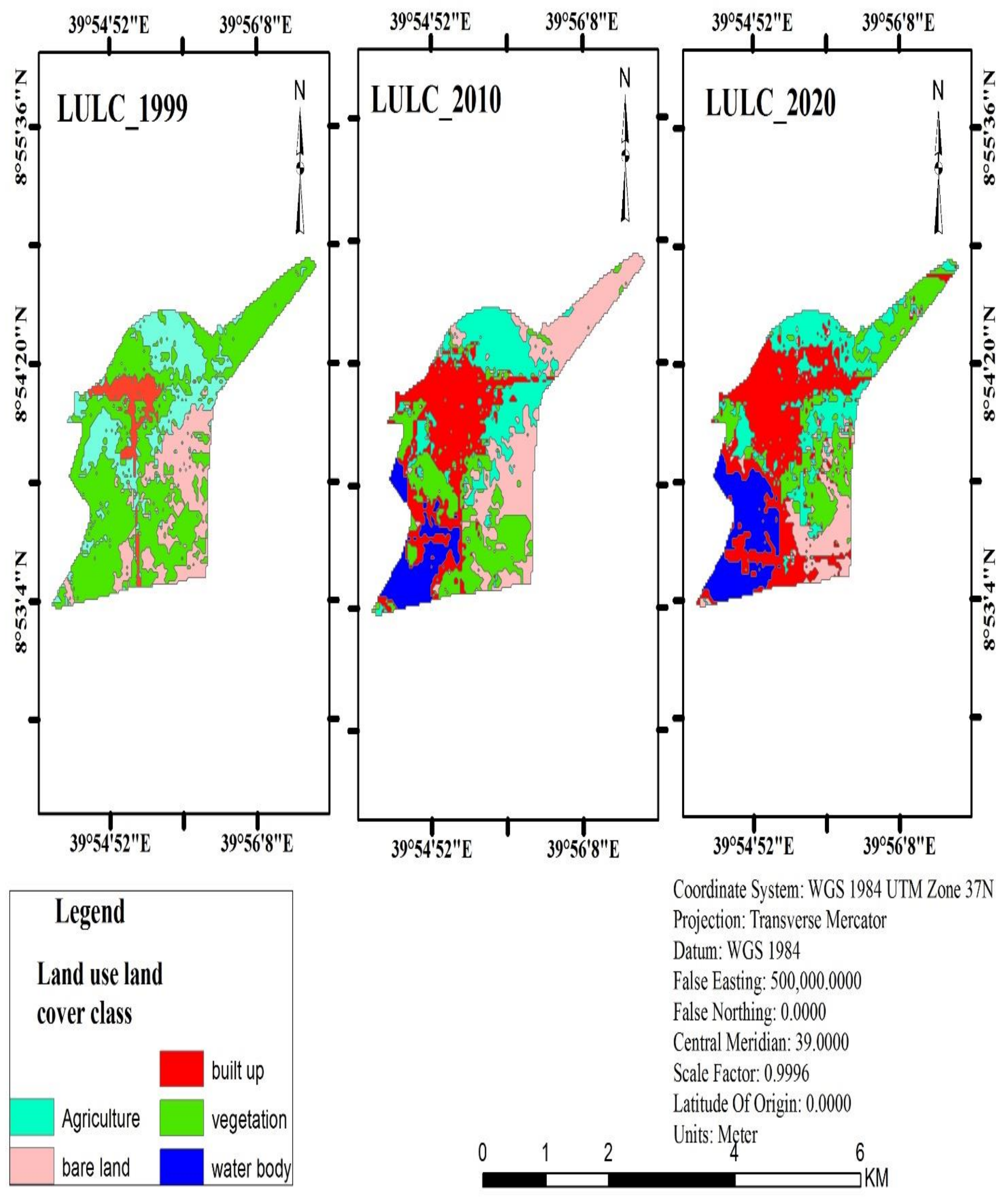

Figure 4. 1 : land use land cover map of study area in 1999, 2010 and 2020

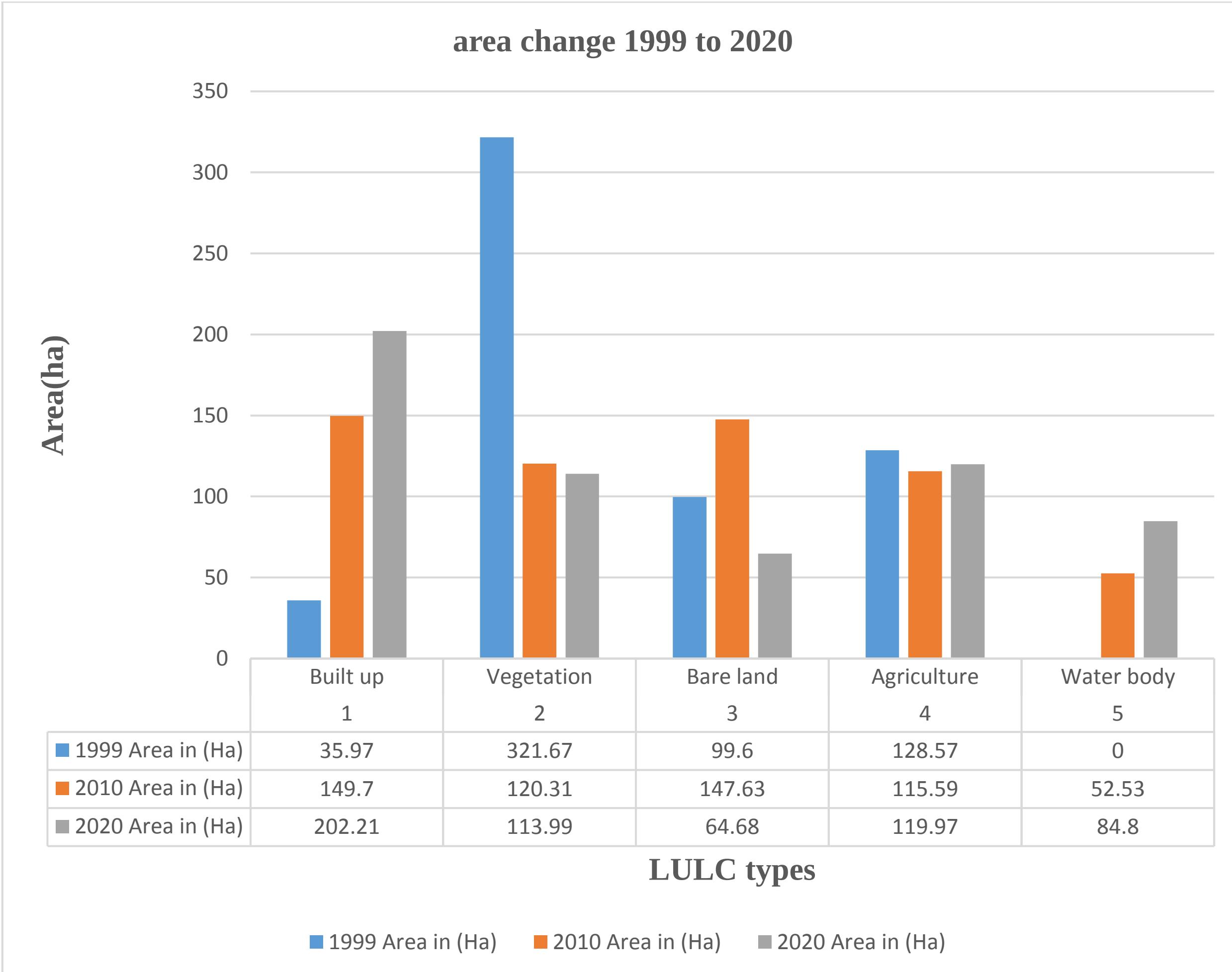

Figure 4. 2 : LULC area change from 1999 to 2020

Water body change in 2010 and 2020

The land use and land cover (LULC) dynamics in Metehara City changed significantly during the course of the study, especially in relation to the existence of water bodies. There were no bodies of water on the terrain in 1999; the main classifications were vegetated areas, bare land, built-up or urban areas, and agricultural. Water bodies, however, saw a significant change between 2010 and 2020, becoming their own separate LULC category. The Basaka Lake's southwestward growth towards Metehara City is responsible for the addition of water bodies to the LULC map. As a result of this geographic shift, new water bodies were created inside the research region, significantly changing the surrounding environment. Specifically, the category of built-up or urban land saw considerable growth, making up a sizeable share of the entire area covered in 2020. The city's urbanization and infrastructure development are reflected in this expansion, signifying a change in land use towards more developed areas. Figure 4.3 below show the satellite image in 1999, 2010 and 2020 how water body increase or emerging in study period 2010 and 2020.

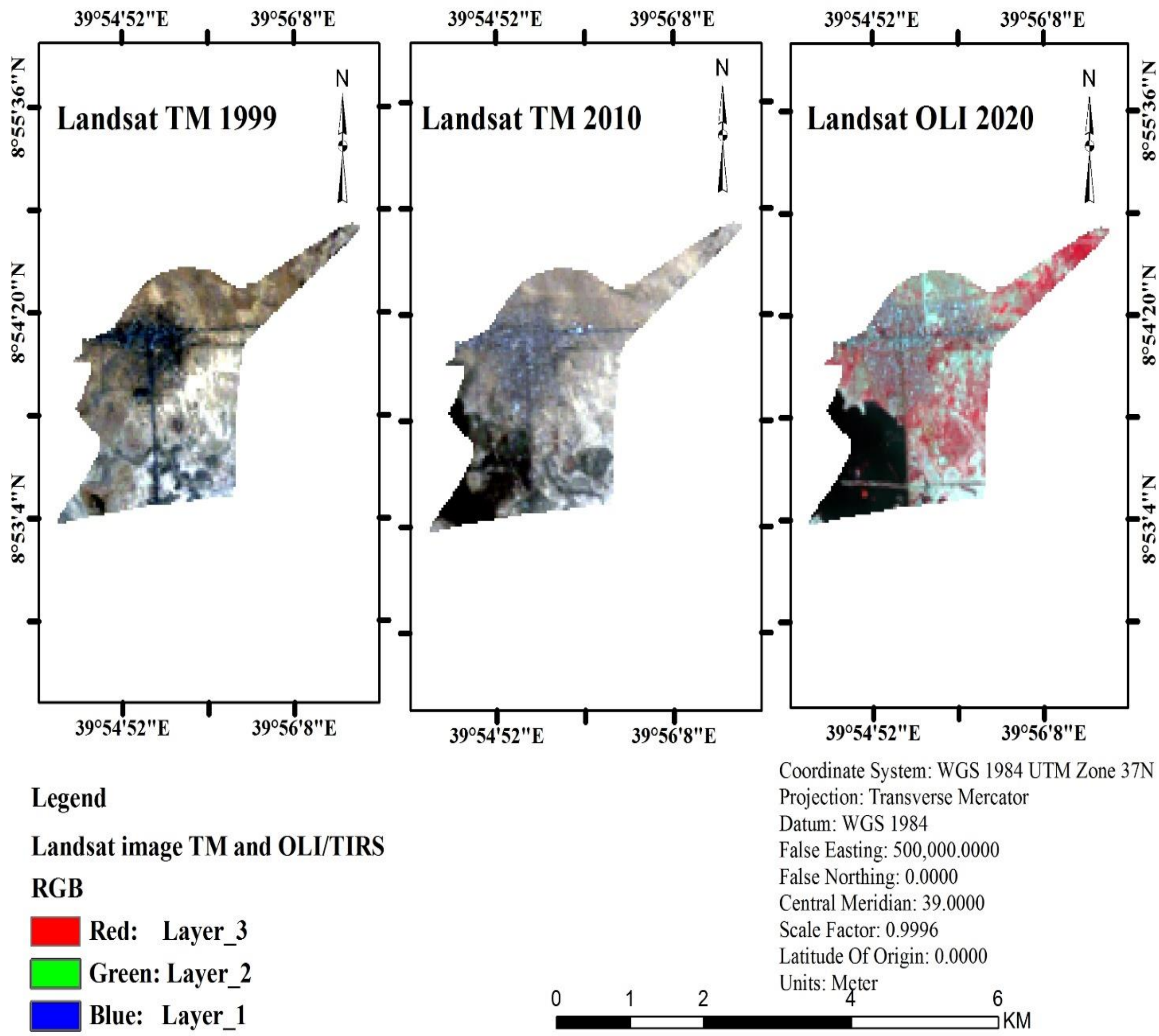

Figure 4. 3 : land sat image shows water body appeared in 2010 and 2020

4.3 LULC change from 1999 to 2020

The Metehara city's Urban Land Use and Landscape Cover (LULC), which assessment between 1999 to 2020 demonstrates continuous differences between various lands cover types. The amount of land examined by vegetation, which amounted to 321.67 hectares in 1999, reduced dramatically to 120.31 hectares by 2010 and then to 113.99 hectares by 2020. Consequently, there was a notable net change of -201.36 hectares coming from 1999 to 2010 and -6.32 hectares about 2010 to 2020, for an overall decrease of -207.67 hectares about 1999 to 2020. Likewise, bare land declined with a period of time between 99.60 hectares in 1999 to 64.68 hectares in 2020, with a net change of -34.92 hectares throughout that period. There had been only slight changes in the amount of agricultural land; it decreased from 128.57 hectares in 1999 to 119.97 hectares by 2020, indicating a total shift of -74.98 hectares. On the reverse hand, water bodies developed, with a total change of 84.40 hectares, from being zero in 1999 to 84.80 hectares in 2020. These modifications emphasize the shifting nature of the land use and land cover (LULC) in Metehara City, which have been characterized over the period of study by relatively constant agricultural zones, declines in vegetation and bare land, and expansion in urban regions and bodies of water.

Table 4.2 : each LULC area coverage and net change 1999 to 2020 in study area

No	LULCClass	1999 Area In ha	2010 Area In ha	2020 Area In ha	Net change 1999to 2010 In ha	Net change 1999 to 2010 in %	Net change 2010 to 2020 In ha	Net change 2010 to 2020 In %	Net change 1999 to 2020 In ha	Net change 1999 to 2020 In %
1	Built up	35.97	149.7	202.21	113.73	20	52.51	9	166.24	29
2	vegetation	321.67	120.31	113.99	201.36	-35	-6.32	-1	-207.67	-35
3	Bare land	99.60	147.63	64.68	48.03	8	-82.5	-14	-34.92	-6
4	Agriculture	128.57	115.59	119.97	12.98	-2	4.38	0	-74.98	-2
5	Water body	0	52.53	84.80	52.53	Infinity	32.27	6	84.40	15

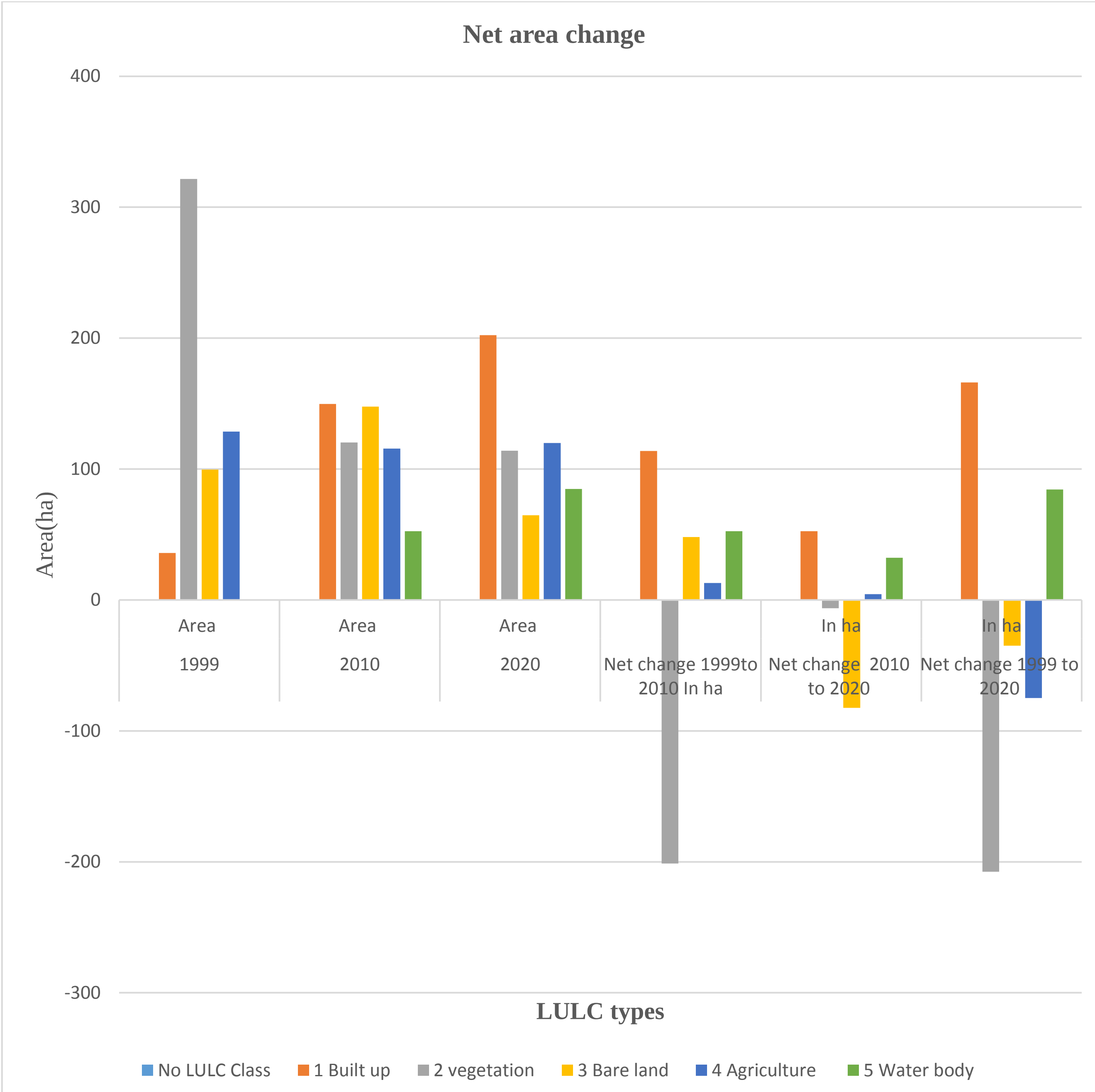

Figure 4.4: LULC change from 1999 to 2020

4.4 LULC Transformation matrix

4.4.1 LULC transformation matrix from 1999 to 2010

Considerable modifications to various kinds of land covering are being noticed in Metehara City during 1999 and 2010, and these changes have had significant impacts on each other. The whole area represented by urban areas increased by 35.12 hectares, primarily due to transformations from related to agriculture, uncultivated vegetation, and water bodies. 33.55

hectares of additional land used for agriculture were added, mostly as a result of conversions from populated areas. 3.90 hectares of bare land have been added, although gradually, as a result of changes in vegetation, agricultural in nature and constructed areas. The total area of vegetation raised by 77.07 hectares, largely due to shifting bare land, agricultural in nature and residential areas. Body of water weren't changed all through that period. In result, the procedure of industrialization significantly affected the transformation of bare and cultivated land into urban area regions, while vegetative areas had significant expansion, demonstrating. Remarkably, Water Bodies did not change, signifying stability during this period. For more detail showed below table and figure.

Table 4. 3 : transformation matrix from 2010 to 2020

LULC class	Area change in hectares from 1999 to 2010				
	Built up(ha)	Agriculture (ha)	Bare land (ha)	Vegetation(ha)	Water body(ha)
Built up	35.12	3.6	0.4	0.51	0.34
Agriculture	33.55	73.54	7.26	11.57	2.62
Bare land	3.90	14.27	54.23	23.49	3.71
Vegetation	77.07	27.77	86.12	84.71	45.79
Water body	0	0	0	0	0

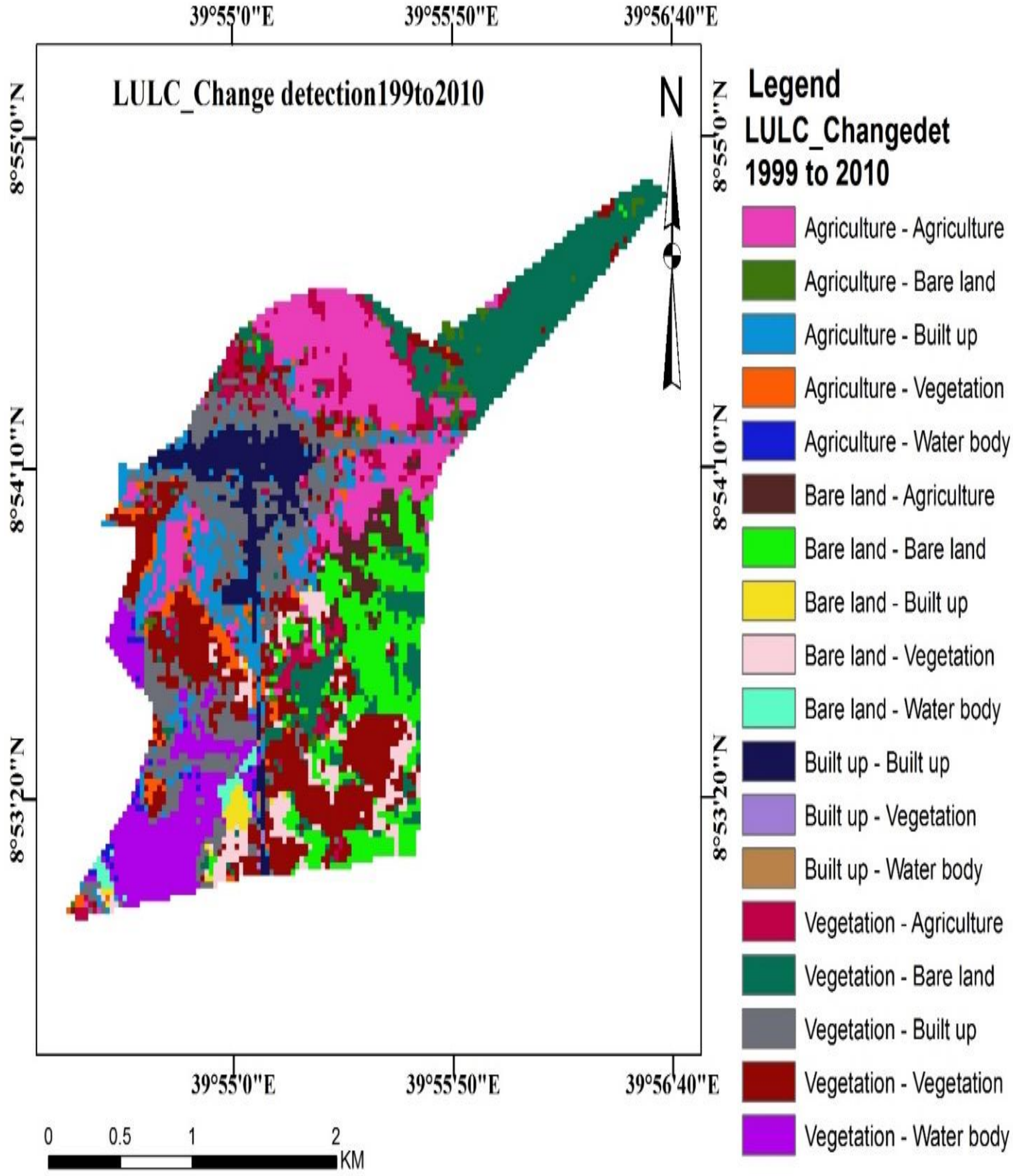

Figure 4. 5: LULC change detection from 1999 to 2010

4.3.2 Change detection from 2010 to 2020

Various significant trends are demonstrated by analyzing the changes in land cover and land use (LULC) in Metehara City during 2010 and 2020. It was an increase of 110.00 hectares in built-up regions, indicating sustained growth in cities and increased infrastructure. Another 69.36 hectare of farmland were included but to a fewer level, proving that agriculture within the city remains going. With an increase of 29.61 hectares, bare land showed slight shifts that could be credited to either organic events or shifting how it is used. Notably, the region occupied by vegetation increased to 40.12 hectares, reflecting shifts in nature such as renewal or reforestation. A rise of 44.85 hectares has been observed in water bodies, indicating possible changes to habitats for fish or management methods. All things looked at, the changes demonstrate the active LULC is in Metehara City, with significant developments in built-up zones, changed agriculture and barren land, substantially raised vegetation, and substantially expanded water bodies inside the study time. As showed below table and figure shows one LULC convert to an

Table 4. 4 : LULC change detection matrix from 2010 to 2020 in Metehara city other.

LULC class	**Area change in hectares from 2010 to 2020**				
	Built up(ha)	Agriculture (ha)	Bare land (ha)	Vegetation(ha)	Water body(ha)
Built up	110.00	8.94	1.07	8.94	20.72
Agriculture	31.41	69.36	4.71	10.09	2.62
Bare land	12.96	33.39	29.61	70.18	1.29
Vegetation	40.12	8.24	29.28	24.69	17.90
Water body	7.61	0	0	0.05	44.85

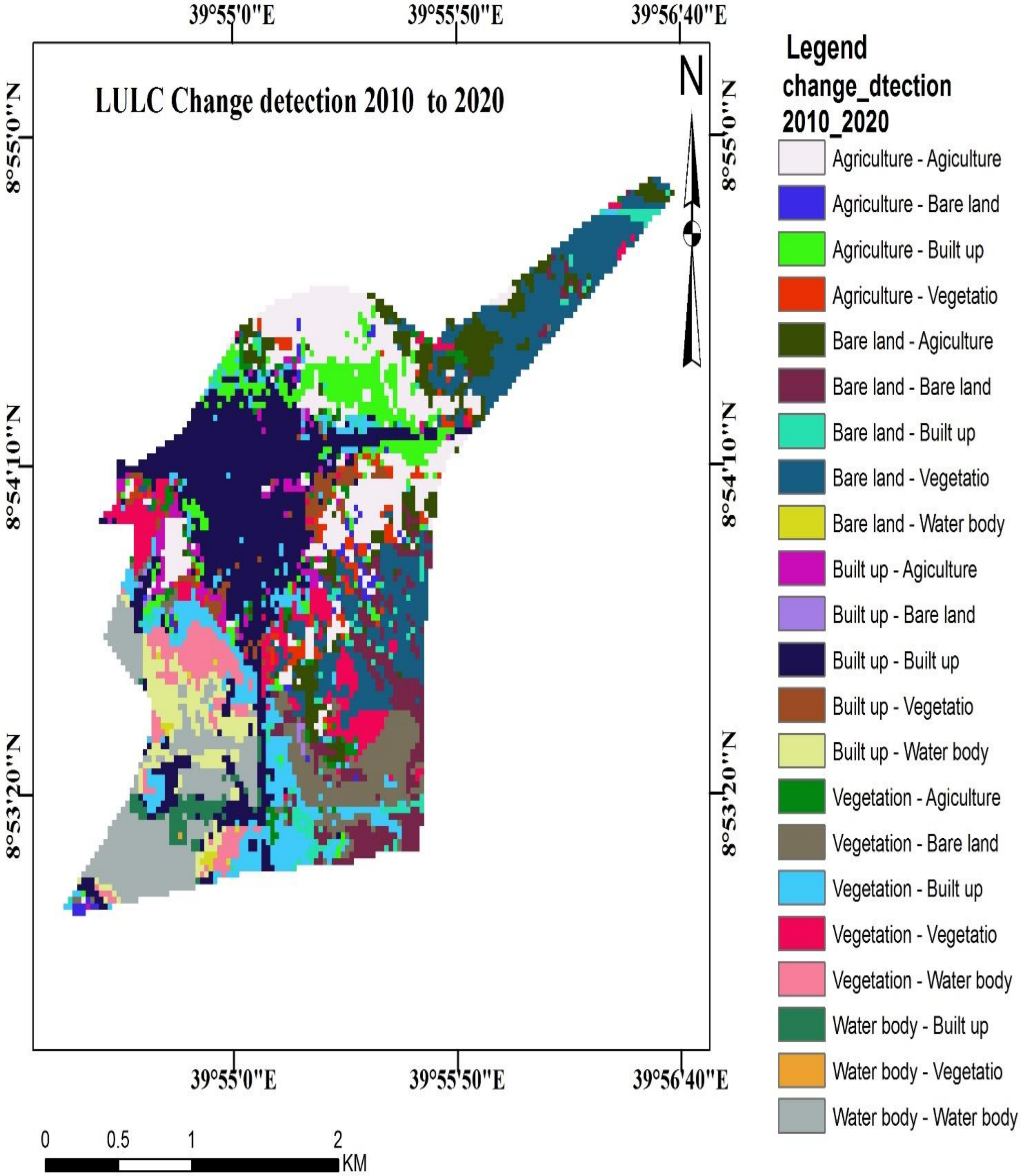

Figure 4. 6 : LULC change transformation from one LULC to other in 2010 to 2020

4.4.3 Change detection from 1999 to 2020

Built-up regions demonstrated an increase of 48.04 hectares during that time, mostly due to increases from constructed areas (60.23 hectares), displaying the transformation of urban places into agricultural property; barren land saw moderately modifications, with a rise of 17.15 hectares caused by transformations from agriculture, built-up regions, and vegetation, and which could indicate changes in how land is used or natural processes; areas with vegetation experienced a notable expansion of 102.33 hectares, with donations from that led to an allocation of 19.90 hectare to Water Bodies and 31.46 hectare to Vegetation. Vegetation Areas undergone shifts in tendency towards urban area. For more detail as shown below table transition matrix with contributions from agriculture, bare land, and built-up areas, highlighting environmental dynamics such as reforestation efforts or natural vegetation regrowth. Water bodies remained unchanged during this period. Overall, these changes demonstrate the dynamic nature of LULC in Metehara city, with significant expansions in built-up areas and agriculture, moderate changes in bare land, substantial growth in vegetation, and stability in water bodies over the analyzed decade.

Table 4.1: Table 4.6 Transformation matrix from 2010 to 2020

	Area change in hectares from 2010 to 2020				
LULC class	Built up(ha)	Agriculture (ha)	Bare land (ha)	Vegetation(ha)	Water body(ha)
Built up	**34.57**	0.59	0.4	0.58	0.34
Agriculture	48.04	**60.23**	3.33	11.62	5.29
Bare land	17.15	14.24	**31.31**	28.08	8.49
Vegetation	102.33	44.87	29.73	**73.43**	70.95
Water body	0	0	0	0	0

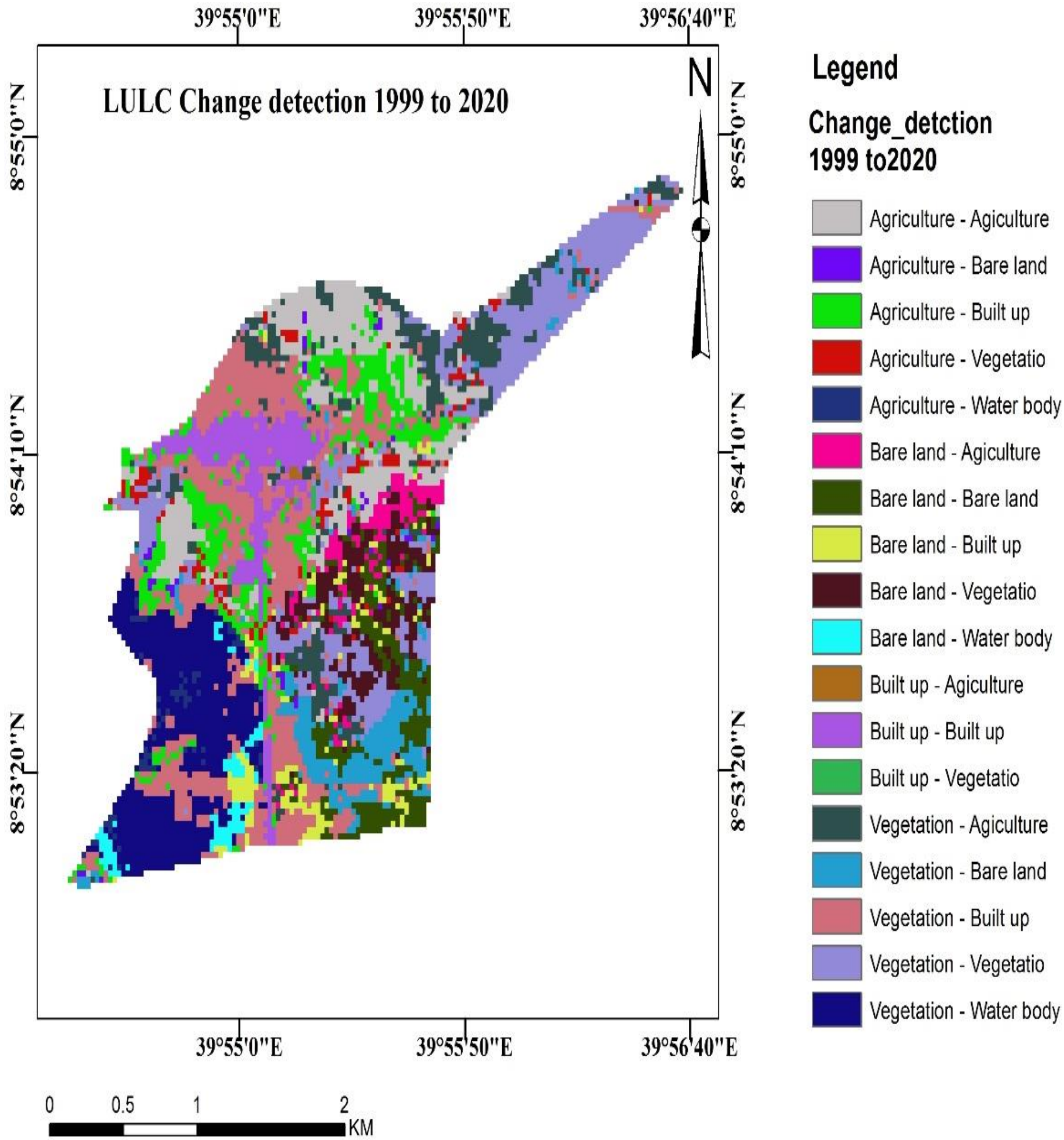

Figure 4. 7 : LULC transformation matrix from each LULC 1999 to 2020

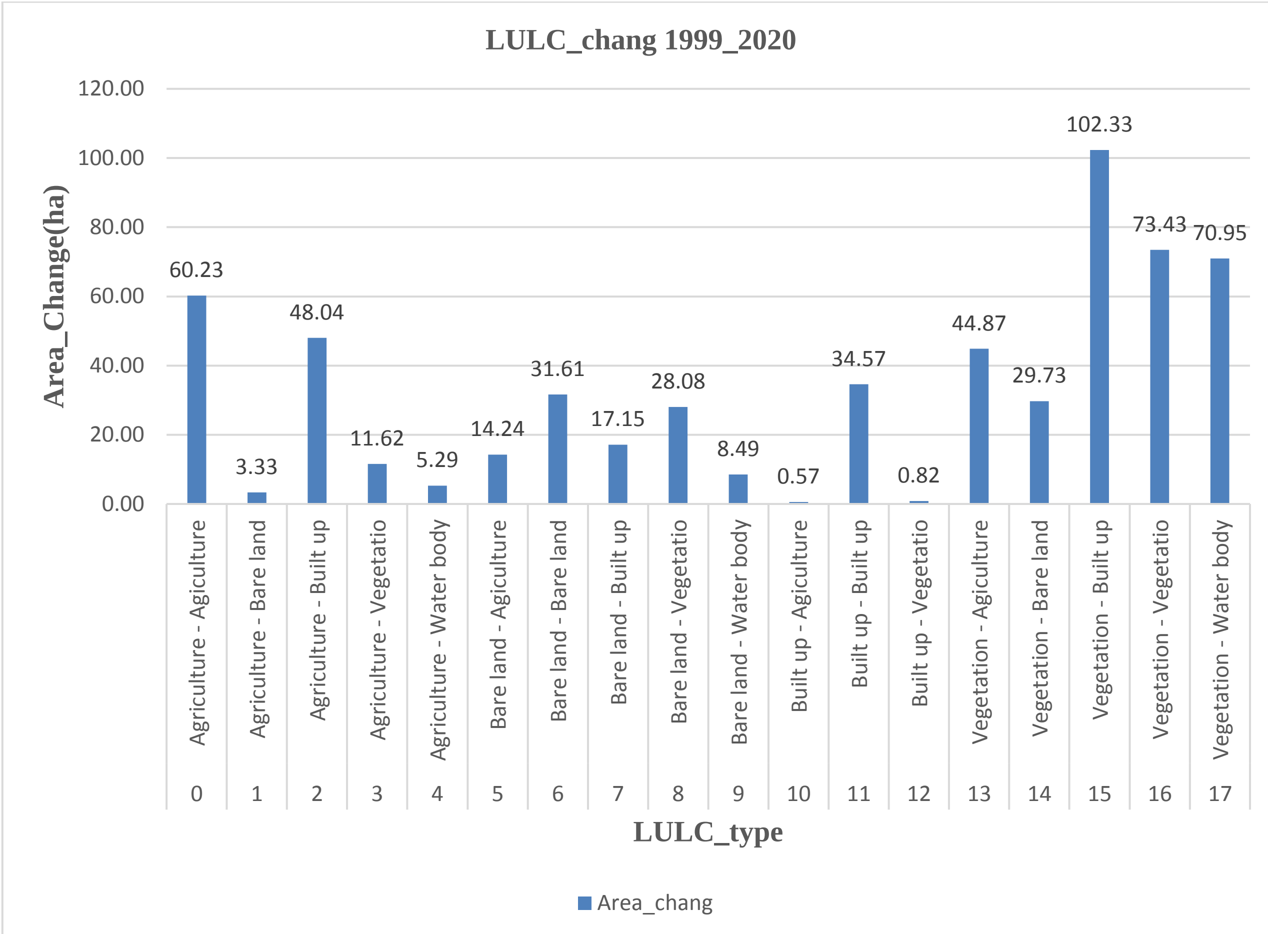

Figure 4. 8 : LULC change transformation matrix from 1999 to 2020

4.4 Accuracy assessment

This investigation assessed the accuracy of land use/land cover designations for 1999, 2010, and 2020 using reference samples collected Google Earth and ground truth data. The classification accuracy was evaluated using user, procedural, and overall correctness criteria.

In 1999 LULC high consistency between the classification and reference information was demonstrated by the assessment of land use, land cover (LULC) assessment in Metehara City, resulting provided a system of classification with an overall accuracy of 92.39%. With a predicted Kappa value of 88.36%, the model was deemed reliable. With a PA and UA of 100%, the "Built-Up" class attained the highest possible correctness metrics. The accuracy rates for different land cover categories, like Vegetation, Agriculture, and Bare land, were equivalent, with commission and omission errors that ranged from 0% to 13.04%.

Table 4.5: Error matrix of 1999 LULC

	Reference data								
Classified data	Bare land	Agriculture	Vegetation	Built up	Total	PA (%)	UA (%)	Cerr%	OE%
Bare land	120	5	5	0	130	88.89	92.31	11.11	7.69
Agriculture	10	100	5	0	115	86.96	86.96	13.04	13.04
Vegetation	5	5	110	0	120	91.97	91.97	8.33	8.33
Built up	0	0	0	95	95	100	100	0	0
Total	135	110	120	95	460				
OA (%)	92.39								
K%	88.36								

Remark: (OA) Overall accuracy, (PA) Producer's accuracy, (UA) User's accuracy, (CE) stands for commission error, (OE) for omission error, and (K) for Kappa statistics.

A classification approach with an overall accuracy of 89.80% had been identified in the 2010 land use and cover (LULC) examination for Metehara City, demonstrating a strong match between the classified information and the reference data. The significant consistency beyond chance was demonstrated by the Kappa value of 81.61%. Any land cover class's effectiveness was assessed using the simulation, and the "Vegetation" class had the highest number of measurement accuracy (100%) of every other class. Other forms of land protect, particularly built-up, water body, bare land, and agriculture, indicated intermediate to exceptional accuracy. Significantly low commissions as well as omissions errors suggest a small percentage of categorization and omission. The Vegetation class demonstrated the most significant degree of accuracy among the studied classes, confirming the model's success in accurately defining the land cover classes in Metehara city.

Table 4. 6 : Error matrix of 2010 LULC

Reference data										
Classified data	Water body	Bare land	Agriculture	vegetation	Built up	Total	PA (%)	UA (%)	CE%	OE%
Water body	85	15	15	0	0	115	100	73.91	0	26.09
Bare land	0	90	22	0	0	112	85.71	80.36	14.29	19.64
Agriculture	0	0	91	0	0	91	71.18	71.18		28.82
vegetation	0	0	0	97	0	97	100	100	0	0
Built up	0	0	0	0	95	95	100	100		0
Total	85	105	128	97	95	510				
OA (%)	89.80%									
Kappa %	81.61									

Remark: (OA) Overall accuracy, (PA) Producer's accuracy, (UA) User's accuracy, (CE) stands for commission error, (OE) for omission error, and (K) for Kappa statistics

The 2020 land use and land cover (LULC) assessment demonstrated an excellent level of agreement between classified data and the reference data, with an overall accuracy of 98.58%. On the different hand, differences in classification were demonstrated by the 81.61% Kappa coefficient. With 100% PA and UA, the Built-Up class had the most outstanding accuracy measurements. High accuracy has been demonstrated by the Water Body class, who’s had a PA of 100% and UA of 85.71%. Similar consistency occurred in other land cover sections, such as Bare Land, Agriculture, and Vegetation, with few commission and omission error.

Table 4. 7 : Error matrix of 2020 LULC

Reference data										
Classified data	Water body	Bare land	Agriculture	vegetation	Built up	Total	PA (%)	UA (%)	CE%	OE%
Water body	18	2	1	0	0	21	100	85.71	0	14.29
Bare land	0	48	5	0	0	53	96.00	90.57	14.29	9.43
Agriculture	0	0	76	0	0	76	96.20	92.68	0	7.32
vegetation	0	0	0	142	0	142	100	100	0	0
Built up	0	0	0	0	258	95	100	100		0
Total	18	50	82	142	258	550				
OA (%)	98.58%									
Kappa %	81.61									

Remark: (OA) Overall accuracy, (PA) Producer's accuracy, (UA) User's accuracy, (CE) stands for commission error, (OE) for omission error, and (K) for Kappa statistics

4.5 The sptio-temporal distribution of NDVI

The NDVI value extracted from the spectral bands of Landsat TM and OLI/TIRS at the region of read and NIR bands. The NDVI results which extracted from the bands of Landsat in each study period which means in 1999, 2010 and 2020 years of period in study area, the NDVI values for the LULC shows different results. The values varies from areas to area based on the amount of vegetation coverage in LULC in each study period of years. The highest vegetation overage area has high amount of NDVI values than the other class.

In 1999, that region surrounds Metehara city had greater temporal extent of vegetation than it did in 2010 and 2020. Since the overall NDVI value in 1999 was larger than the values in 2010 and 2020.in 1999 the maximum and minimum NDVI value was 0.47272 and -0.2222 respectively it is greater than the other study period.

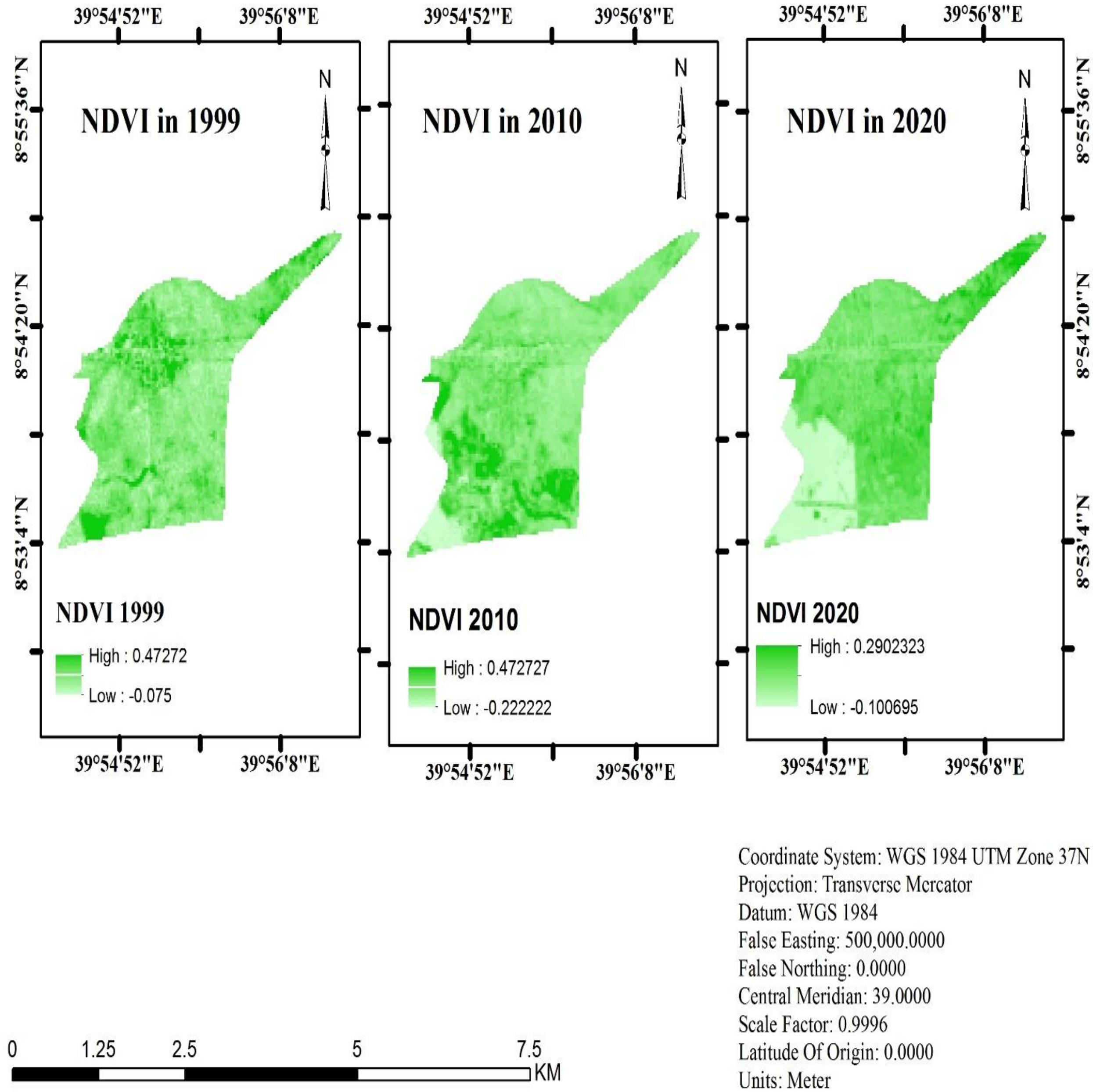

Figure 4. 9 : The NDVI map of study area in 1999, 2010 and 2020

Table 4. 8 : the NDVI maximum, minimum and mean value in 1999, 2010 and 2020

Year	Maximum	mean	Minimum	Standard deviation
1999	0.47272	0.12526	-0.2222	0.26785
2010	0.407321	0.123313	-0.100695	0.1835
2020	0.290323	0.1076615	-0.075	0.1301

4.6. The Spatio-temporal Distribution of NDBI

While greater NDBI value indicate built-up regions including urban or resident communities. As consequence, places with both low and high NDVI values are typically vegetated, whilst low and high NDBI values signify urban or urban area environments. The literature concerning satellite imagery has studied this link in numerous ways. For instance, a study by Jiang et al. (2016) looked at the relationship involving NDVI and NDBI in urban settings and found that, while built-up areas and vegetation cover are inversely correlated, places with high NDVI values typically have lower NDBI values. This relationship becomes crucial for classifying land cover and studying urban expansion because it makes it easier to distinguish between constructed and natural development. During the study period the value of NDBI values difference from each year. Greater NDBI numbers was found to have been connected to built-up urban centers, bare terrain, and agricultural areas, conversely, places with greenery and bodies of water had lower levels. In the year 1999, 2010, and 2020, the city's the NDBI values was 0.09 to 0.35 -0.75 to 0.63, -0.38 to 0.41, and -0.24 to 0.11 respectively as showed below figure.

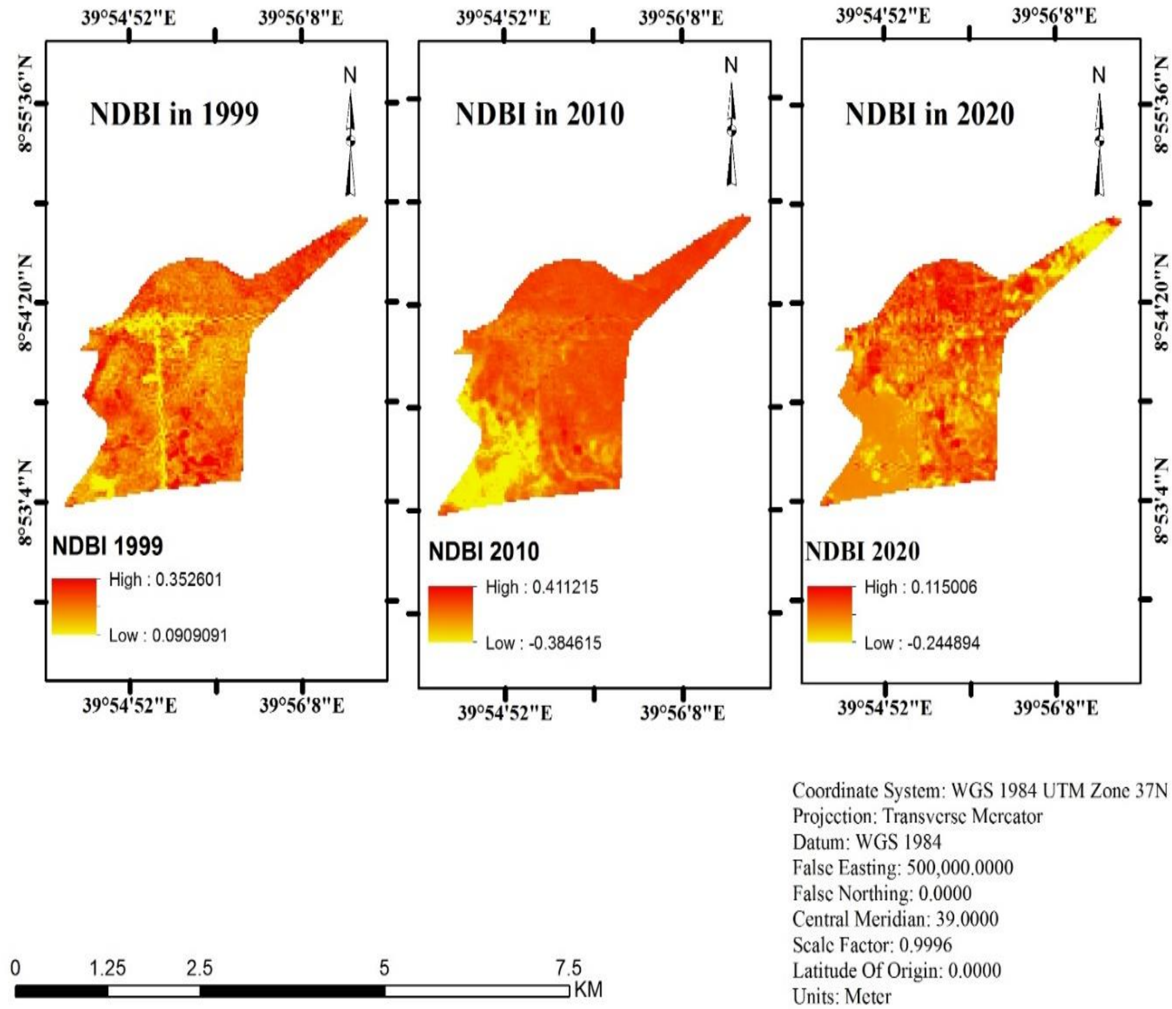

Figure 4. 10 : The NDBI value in study area in 1999, 2010 and 2020

4.7 The sptio temporal variation of NDWI

The use of the normalized difference water index (NDWI) in the delineation of open water features McFeeters, S. K. (1996). By focusing on water bodies only, NDWI improves other imagery indices like NDVI and NDBI. Applications for managing resources and environmental protection can benefit from the way it interacts with other indices, which also improves our understanding of the shifting nature of land cover. During study period the value of NDWI differ from each year.in 1999 the amount of NDWI was less amount compared to 2010 and 2020 because, in 1999 the water body was not available.in 2010 and 2020 increased the value at this time the lakes increased to that area. From the analysis the value of NDWI in1999 was -0.37 to -0.013, in 2010 -0.46 to 0.24 and 2020 -0.37 to 0.12 as showed figure below.

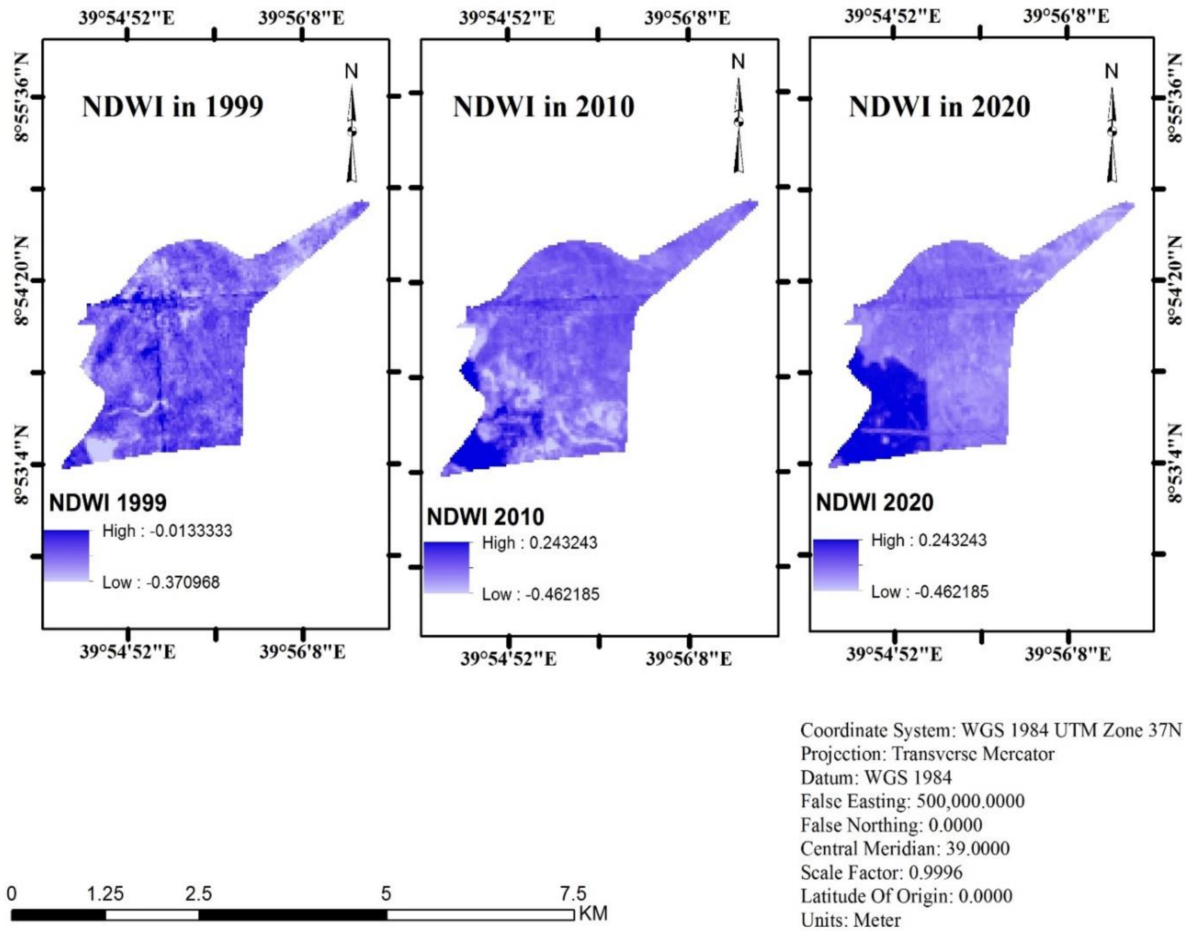

Figure 4. 11 : NDWI value in study area 1999, 2010 and 2020

4.8 The LST Spatial and Temporal Distribution from 1999 to 2020

The LST were calculated for each year of study period in Metehar city in 1999, 2010 and 2020.as described the formula in chapter three the land surface temperature of TM and OLI/TIRS bands of the Landsat image of 1999 and 2010 and 2020 respectively. Therefore, the researcher calculated the LST were 24.24 ^{0}C to 32.95 ^{0}C, 30.01 ^{0}C to 37.22 ^{0}C and 19.73 ^{0}C to 39.39 ^{0}C in 1999, 2010 and 2020 respectively. The mean temperature in 1999 was 29.83 ^{0}C, in 2010 was, 30.60 ^{0}C and in 2020 31.35^{0}C. As the result showed as there was temperature variation in study period from 1999 to 2020 in maximum, minimum and mean temperature.

The mean difference temperature in each study period increase for example, mean temperature difference between 1999 and 2010 was 0.77 ^{0}C, from 2010 to 2020 was 0.75^{0}C and 1999 to 2020 the mean temperature increased by 1.52 ^{0}C.Therefore, the mean temperature also increased in Metehara city as showed below table.

Table 4. 9 : maximum, minimum and mean value of LST in Metehara city

Year	maximum in (^{0}C)	Minimum in (^{0}C)	Mean (^{0}C)	mean difference between each year (^{0}C)
1999	32.95 ^{0}C	24.24 ^{0}C	29.83 ^{0}C	0.77 ^{0}C
2010	37.22 ^{0}C	19.73^{0}C	30.60 ^{0}C	0.75 ^{0}C
2020	39.39 ^{0}C	22.4 ^{0}C	31.35^{0}C	1.52^{0}C

As calculated the LST of each study period in Metehara city in 1999, 2010 and 2020 there were maximum and minimum temperature variation .from those year in 2020 the highest temperature recorded and between 2010 and 1999 2010 was the highest maximum temperature recorded .the maximum temperature were 32.95 ^{0}C, 38.887 ^{0}C and 39.4049 ^{0}C for 1999, 2010 and 2020 respectively.

In 1999, 2010 and 2020 the temperature had high, medium and low temperature value.as showed below figure the temperature zones easily identify in which area is high, medium and low temperature values by using Arc GIS identifier tool. From the figure the rectangle shaped area were high temperature area and the rectangle triangle and ellipse shape showed as low and medium temperature zone.

The spatial area which has high, medium and low temperature zone were identified for example, south west region were low temperature zone because at this region water body area, at south east region high and medium temperature zone because, at this area bare land which high temperature are and some vegetation area for which recorded medium temperature and finally at the center zone which recorded medium temperature at that area were built up and vegetation area and north east zone recorded high temperature because that area were agriculture and bear land area. Figure below showed as the LST temperature for the city in each study period.

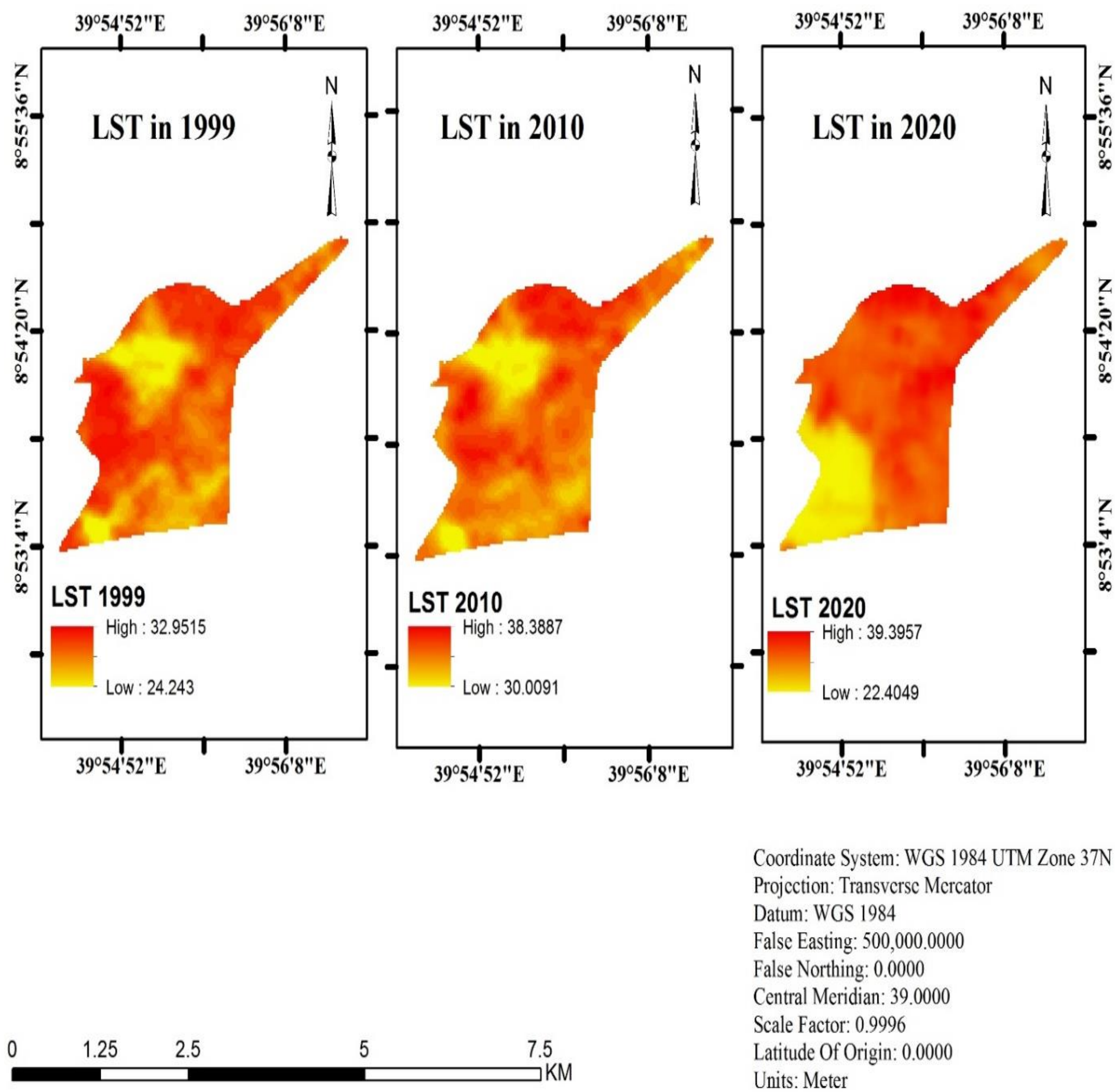

Figure 4. 12 : LST value in study area

4.9. LST zone and influence of LULC on LST in 1999, 2010, and 2020

There were noticeable differences in the land surface temperature (LST) and land use land cover (LULC) zones in Metehara City in 1999. Reflecting active land surface heating, agricultural regions spanning 128.16 hectares had an average temperature of 31.35°C. There was little vegetation or exposed soil on the 92.61 hectares of bare land, as evidenced by the somewhat lower mean temperature of 30.30°C. Because of their developed environments and sparser vegetation, built-up zones, which cover 35.61 hectares, had the lowest mean temperature, 27.88°C. A mean temperature of 30.26°C was recorded in the largest vegetation zone, which spanned 307.44 hectares and demonstrated the cooling impact of forest cover. Emphasizing the importance of vegetation in moderating surface temperatures, these temperature changes are consistent with projected land cover influences, with implications for environmental research, agricultural management, and urban development.

Table 4.10 : The LST zone and area coverage in each LULC class in 1999

CLASS_NAME	**ZONE_CODE**	**AREA (ha)**	**MIN(^{0}C)**	**MAX(^{0}C)**	**MEAN(^{0}C)**
Agriculture	1	128.16	26.79	32.95	31.35
Bare land	2	92.61	28.05	32.55	30.30
Built up	3	35.61	25.95	31.74	27.88
vegetation	4	307.44	24.24	32.55	30.26

Land Surface Temperature (LST) zones and various land cover types showed differing temperature patterns in Metehara City in 2010. The mean temperature of the 144.66 hectare Agriculture zone was 36.53°C, which is higher than average and suggests that agricultural operations are actively heating the land surface. In a similar vein, the 135.18 hectare bare land zone recorded somewhat lower mean temperatures (35.67°C) but remained relatively warm, indicating greater ground surface heating and little vegetation cover. This is in contrast to the 146.88 hectare Built Up zone, which had a mean temperature of 34.76°C but fluctuated temperatures due to the diversity of land cover and urban structures. At an average temperature of 35.42°C. Over 117.18 hectares, the plant zone demonstrated cooling effects, underscoring the function of vegetation in regulating temperature.

Table 4. 11 : LST zone and area coverage in each LULC class in 2010

Table LST zone in 2010					
CLASS_NAME	ZONE_CODE	AREA (ha)	MIN(^{0}C)	MAX(^{0}C)	MEAN(^{0}C)
Agriculture	1	144.66	32.86	38.39	36.53
Bare land	2	135.18	33.26	38.00	35.67
Built up	3	146.88	31.65	38.00	34.76
vegetation	4	117.18	32.86	38.00	35.42
Water body	5	49.95	30.01	37.22	34.62

Varying land cover types and Land Surface Temperature (LST) zones in Metehara City demonstrated varying temperature characteristics in 2020. The average temperature of the 113.85 hectare Agriculture zone was 36.12°C, with a wide range of temperatures from 28.16°C to 39.40°C. This suggests that agricultural activity-related land surface heating is ongoing. There was little vegetation cover and more land surface heating in the 64.65-hectare bare land zone, where temperatures ranged from 28.66°C to 38.65°C, with a mean temperature of 33.42°C. Urban structures and a diversity of land cover types influenced the mean temperature of the 179.82 hectare Built-up zone, which ranged from 22.41°C to 38.45°C. A mean temperature of 31.66°C was recorded in the 109.80 hectare Vegetation zone, with temperatures ranging from 23.36°C to 38.85°C. Whose average temperature was 31.66°C, emphasizing how cold plant cover is. The lowest temperatures, ranging from 22.40°C to 28.51°C with a mean temperature of 23.18°C, were seen in the 81-hectare Water body zone, which contributed to the local cooling effects. In 2020, these results will be essential for comprehending environmental changes and putting into practice sensible land use plans in Metehara City, as they show the intricate temperature dynamics impacted by different forms of land cover. For each study period LST temperature zone shown below table.

Table 4. 12 : LST zone and area coverage in each LULC class in 2020

CLASS_NAME	ZONE_CODE	AREA (ha)	MIN(^{0}C)	MAX(^{0}C)	MEAN(^{0}C)
Agriculture	1	113.85	28.16	39.40	36.12
Bare land	2	64.65	28.66	38.65	33.42
Built up	3	179.82	22.41	38.45	31.42
vegetation	4	109.80	23.36	38.85	31.66
Water body	5	81	22.40	28.51	23.18

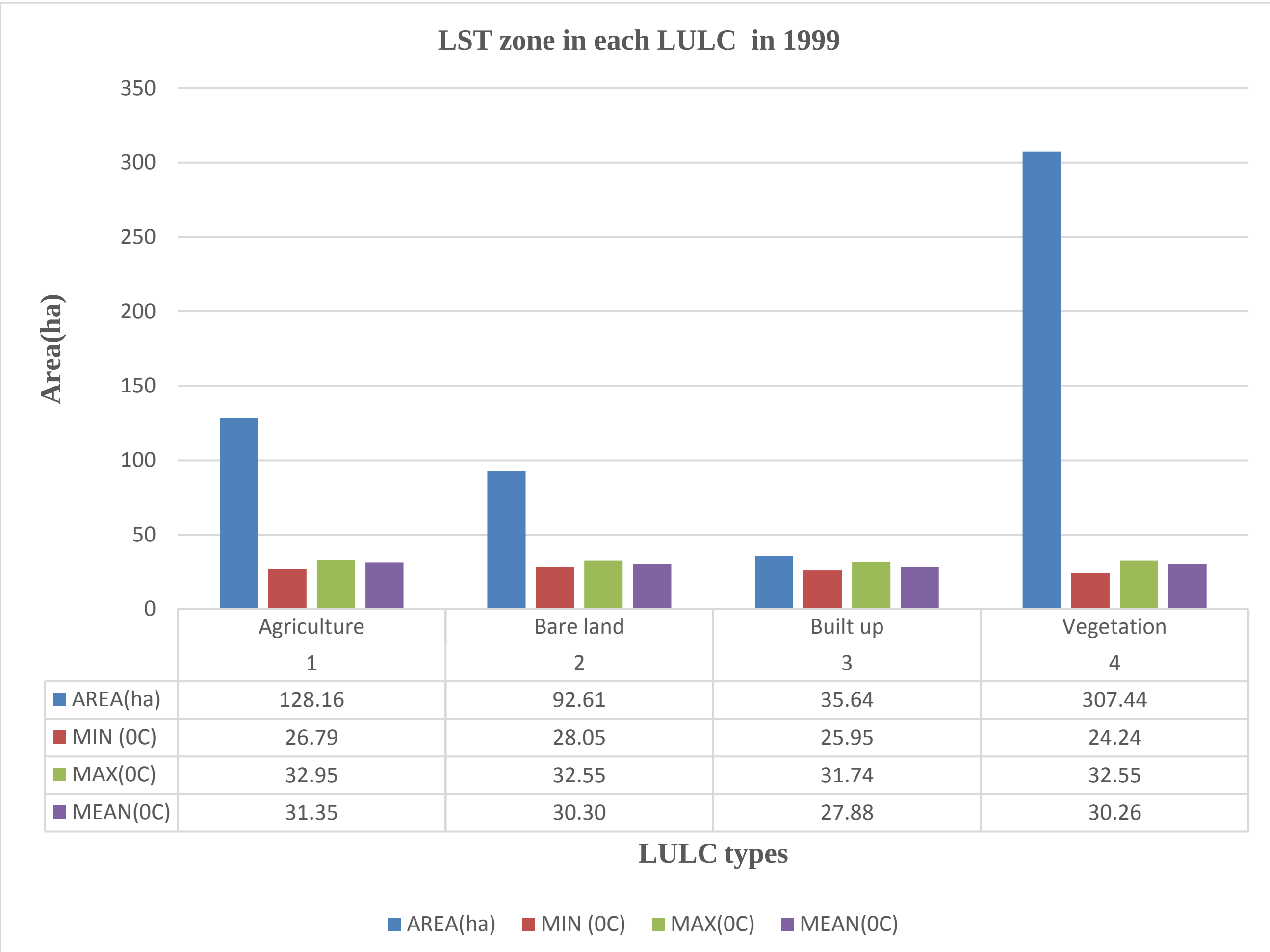

	Agriculture 1	Bare land 2	Built up 3	Vegetation 4
AREA(ha)	128.16	92.61	35.64	307.44
MIN (0C)	26.79	28.05	25.95	24.24
MAX(0C)	32.95	32.55	31.74	32.55
MEAN(0C)	31.35	30.30	27.88	30.26

Figure 4. 13 : LST zone in each LULC in 1999 in Metehara city

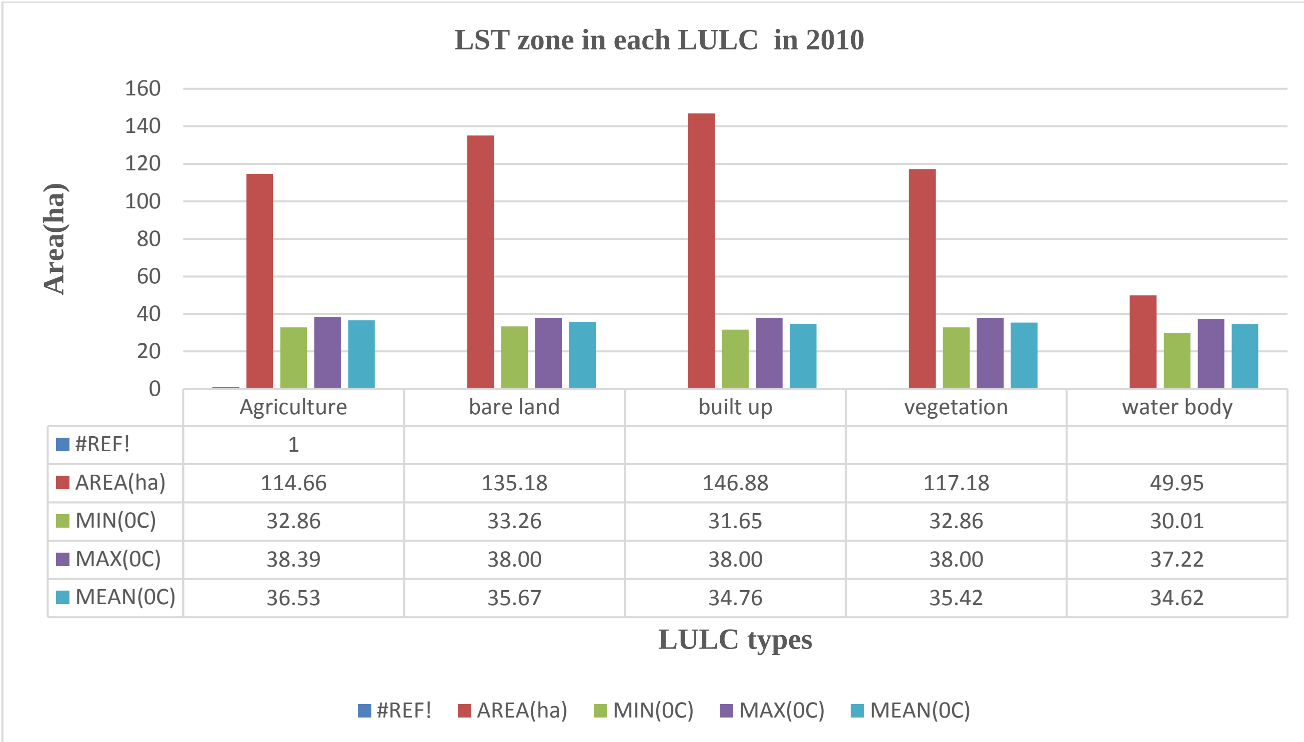

	Agriculture	bare land	built up	vegetation	water body
#REF!	1				
AREA(ha)	114.66	135.18	146.88	117.18	49.95
MIN(0C)	32.86	33.26	31.65	32.86	30.01
MAX(0C)	38.39	38.00	38.00	38.00	37.22
MEAN(0C)	36.53	35.67	34.76	35.42	34.62

Figure 4. 14 LST zone in each LULC in 2010 in Metehara city

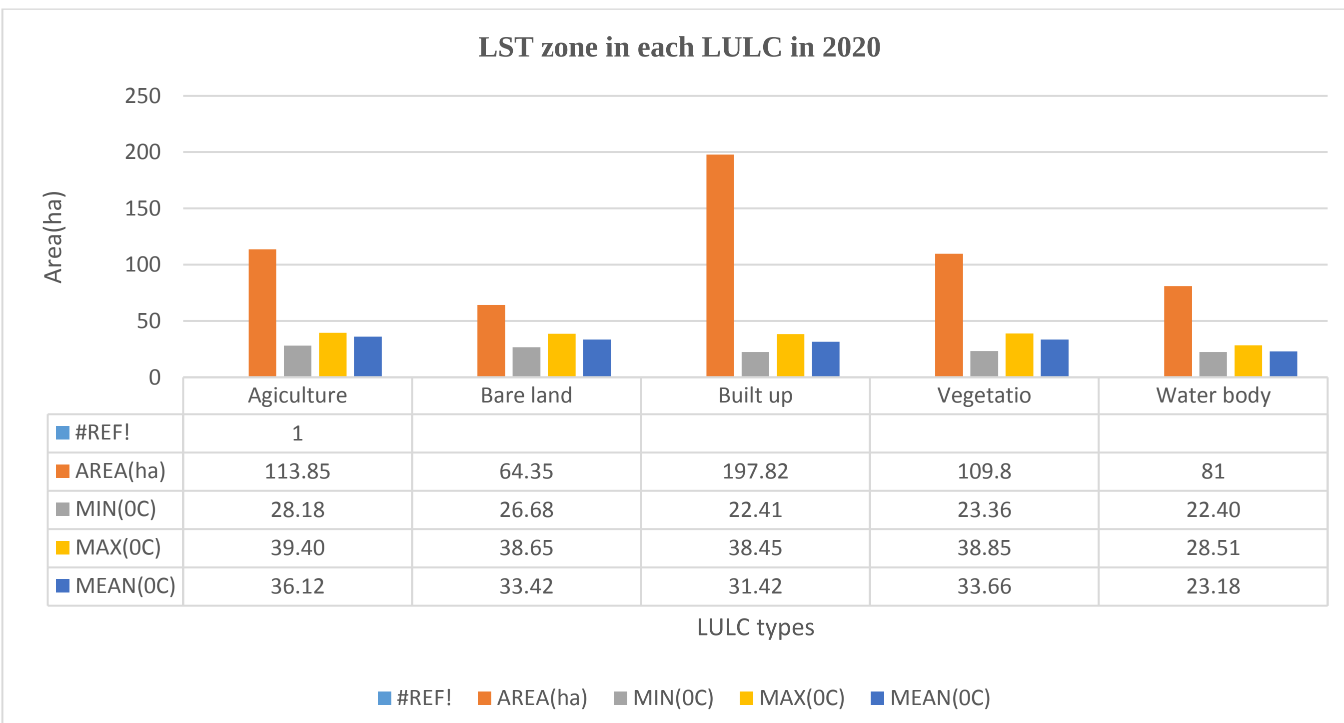

	Agiculture	Bare land	Built up	Vegetatio	Water body
#REF!	1				
AREA(ha)	113.85	64.35	197.82	109.8	81
MIN(0C)	28.18	26.68	22.41	23.36	22.40
MAX(0C)	39.40	38.65	38.45	38.85	28.51
MEAN(0C)	36.12	33.42	31.42	33.66	23.18

Figure 4. 15: LST zone in each LULC in 2020 in Metehara city

4.10 Correlation between LST AND LULC induces and elevation

4. 10.1 Correlation between LST AND NDVI, NDBI and NDWI in 1999, 2010 and 2020

Lower surface temperatures are associated with denser vegetation cover, as seen by the negative correlation observed in 1999 between LST1 and NDVI in Metehara City. The NDVI values range from -0.0427 to 0.2167, whereas the LST values span from 24.24°C to 32.95°C.

Tentative connections between LST1 and NDVI1 are seen in 2010, indicating that lower surface temperatures are associated with more robust vegetation. The range of LST values is 19.73°C to 37.22°C, while the range of NDVI values is -0.033 to 0.311. Furthermore, possible negative connections between the 2010 LST and NDWI show how surface temperatures were impacted by water content at that time. The range of LST values is 19.73°C to 36.44°C, whereas the range of NDWI values is -0.368 to 0.210.

For Metehara City in 2020, the Land Surface Temperature (LST) and Normalized Difference Vegetation Index (NDVI) datasets offer vital information on environmental changes. Higher NDVI values (ranging from 0.105 to 0.397), which represent denser and healthier vegetation cover, are correlated with lower LST levels (ranging from 22.40°C to 39.10°C), according to the study's moderately negative correlation between LST and NDVI (Jiang et al., 2019; Sobrino et al., 2020). Figures from statistics show this inverse link, highlighting the significance of NDVI as a vegetation health indicator and how it affects the regulation of surface temperature.

A substantial positive association between NDBI and LST is shown in the study, which analyzes Land Surface Temperature (LST1) and Normalized Difference Built-up Index (NDBI) data for Metehara City in 2020. Between 22.40°C and 39.39°C are the LST levels, while between 0 and 0.35 are the NDBI values. This emphasizes the consequences of urbanization and the effects of urban heat islands (Wu et al., 2019; Li et al., 2020). More urbanization and heat retention in some locations are indicated by the statistics, which show a clear correlation between higher NDBI values and higher LST levels.

The cooling effect of water bodies on land surface temperatures is demonstrated by an inverse connection found while examining the Normalized Difference Water Index (NDWI) and LST data for Metehara City in 2020. LST values range from 22.40°C to 39.39°C, while NDWI values range from -0.267 to 0.109 (Garcia et al., 2023). Where there are water bodies, the NDWI values are higher and the LST values are lower, indicating colder surface temperatures.

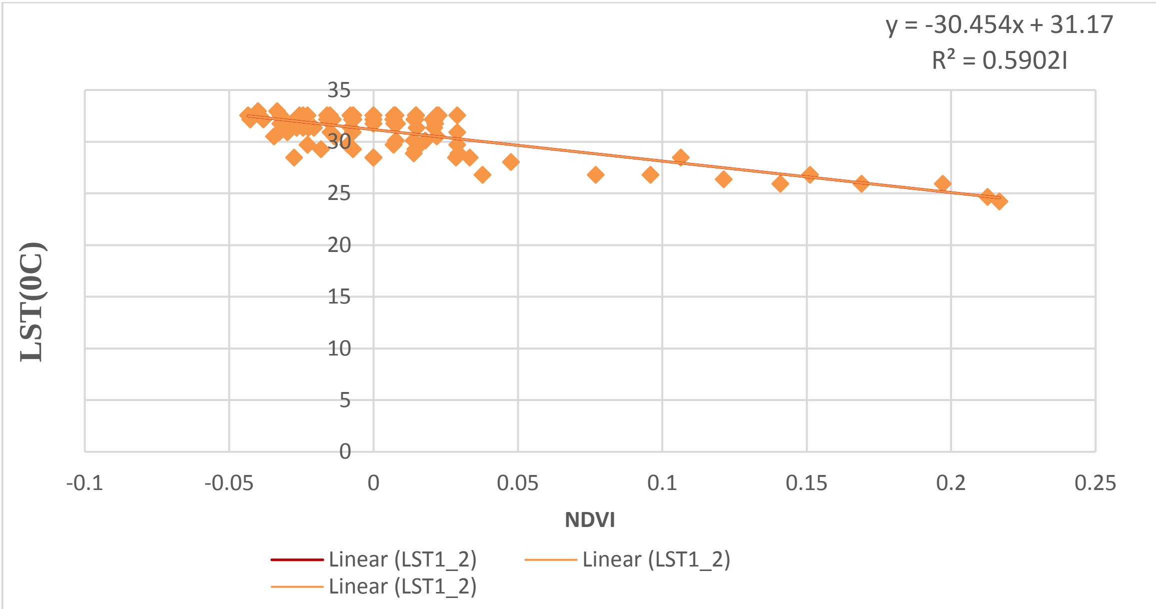

Figure 4. 16 : correlation between LST and NDVI in 1999

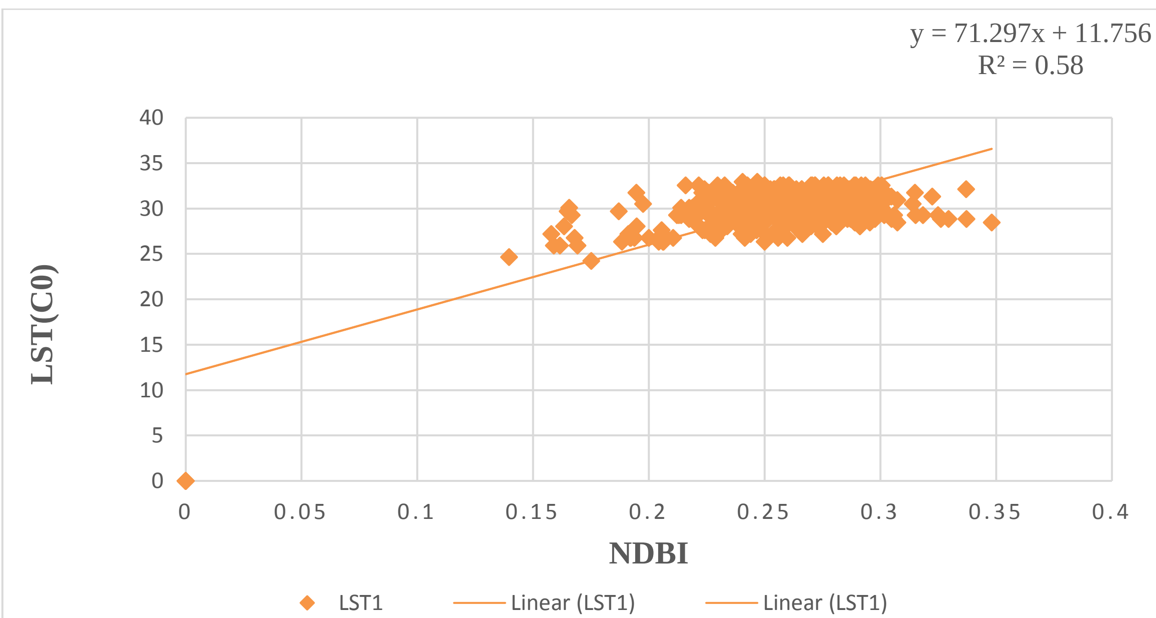

Figure 4. 17 correlation between LST and NDBI in 1999

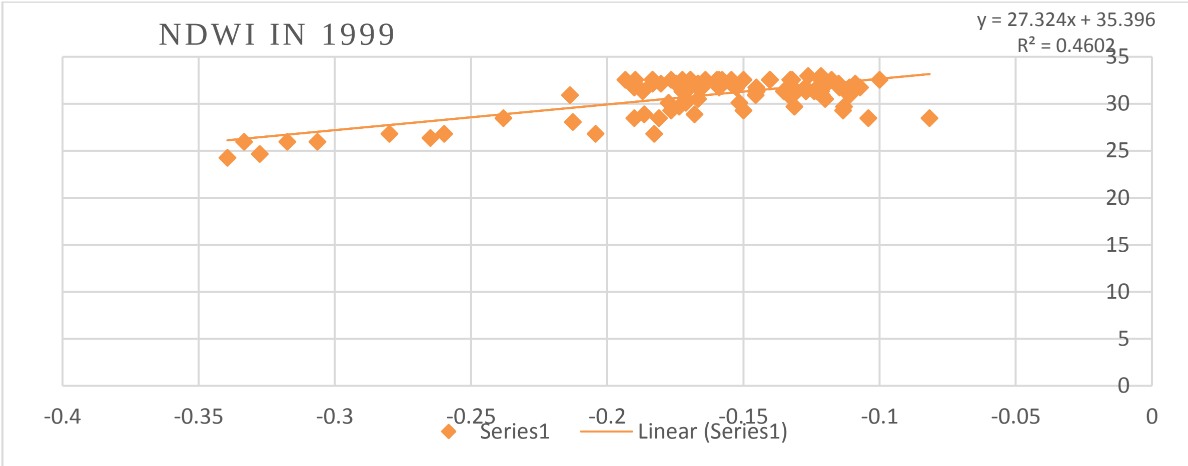

Figure 4. 18 correlation between LST and NDWI in 1999

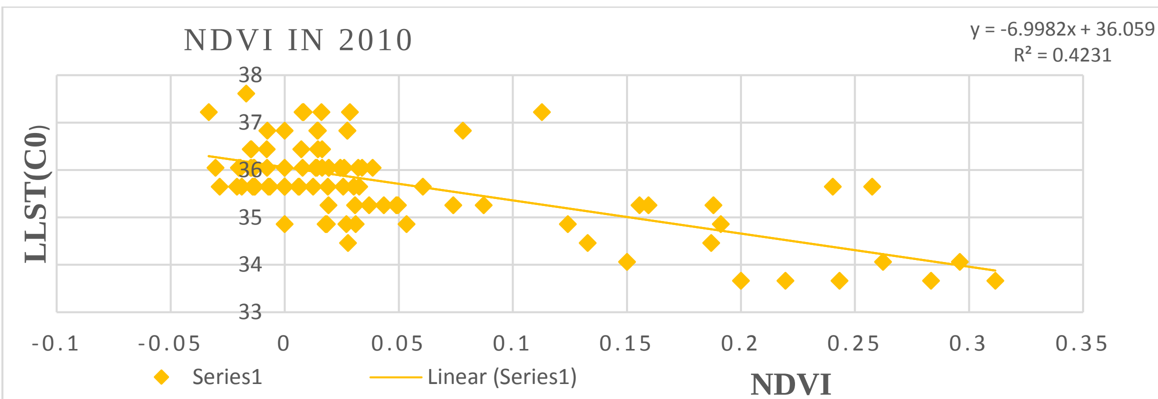

Figure 4.19 correlation between LST and NDVI in 2010

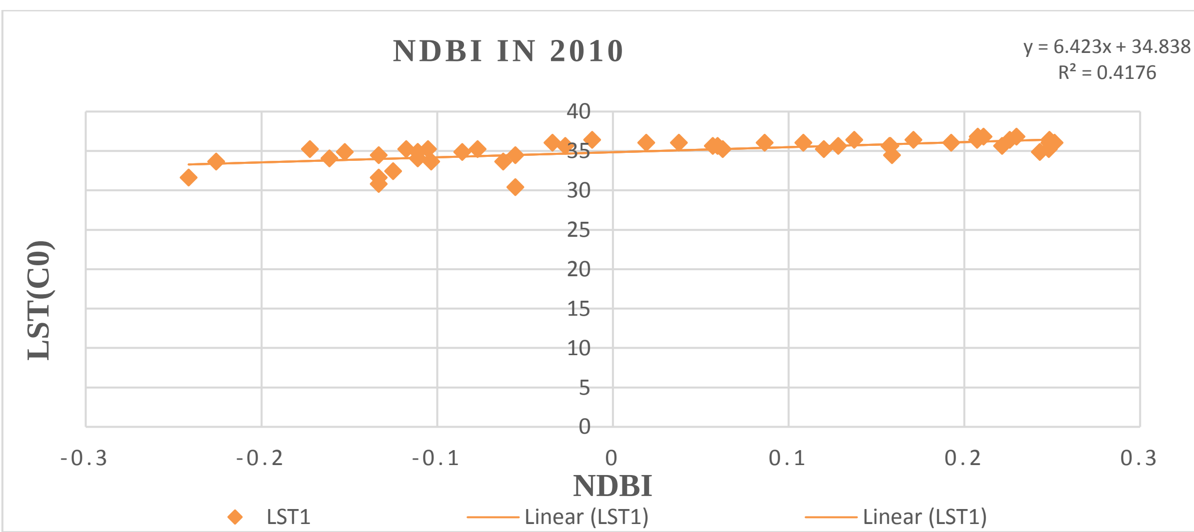

Figure 4.20: Correlation between LST and NDBI in 2010

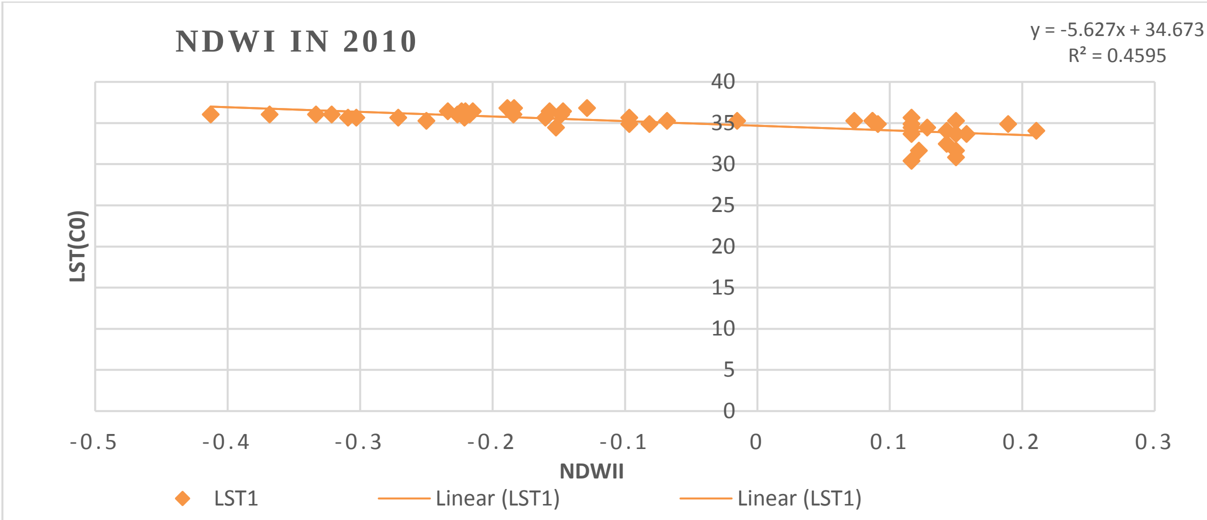

Figure 4. 21 correlation between LST and NDWI in 2010

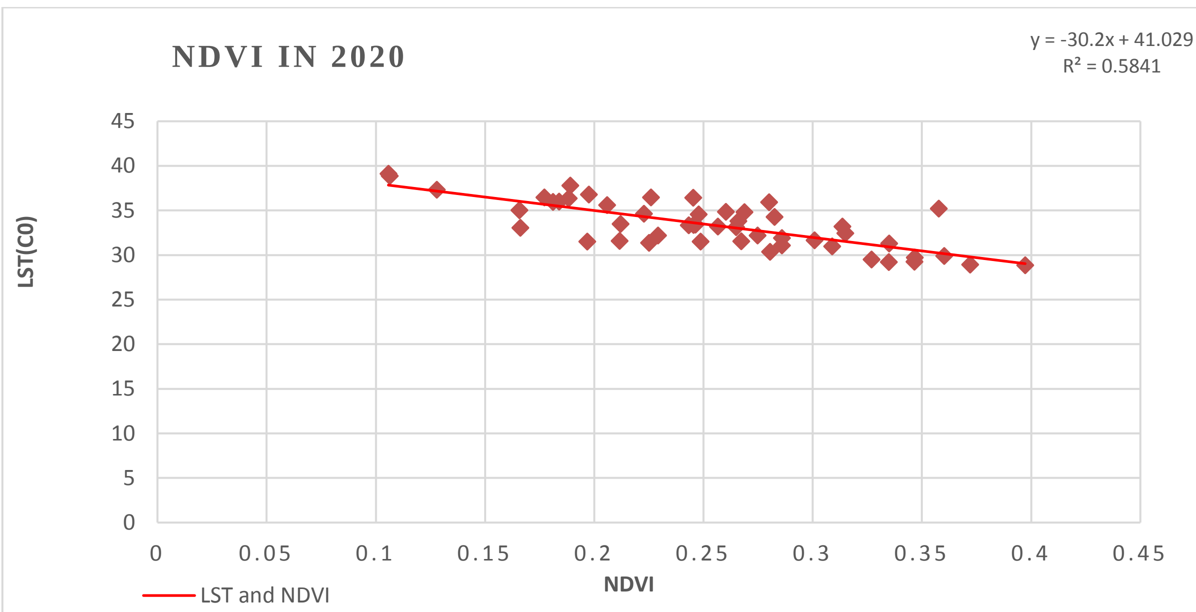

Figure 4. 22 : correlation between LST and NDVI in 2020

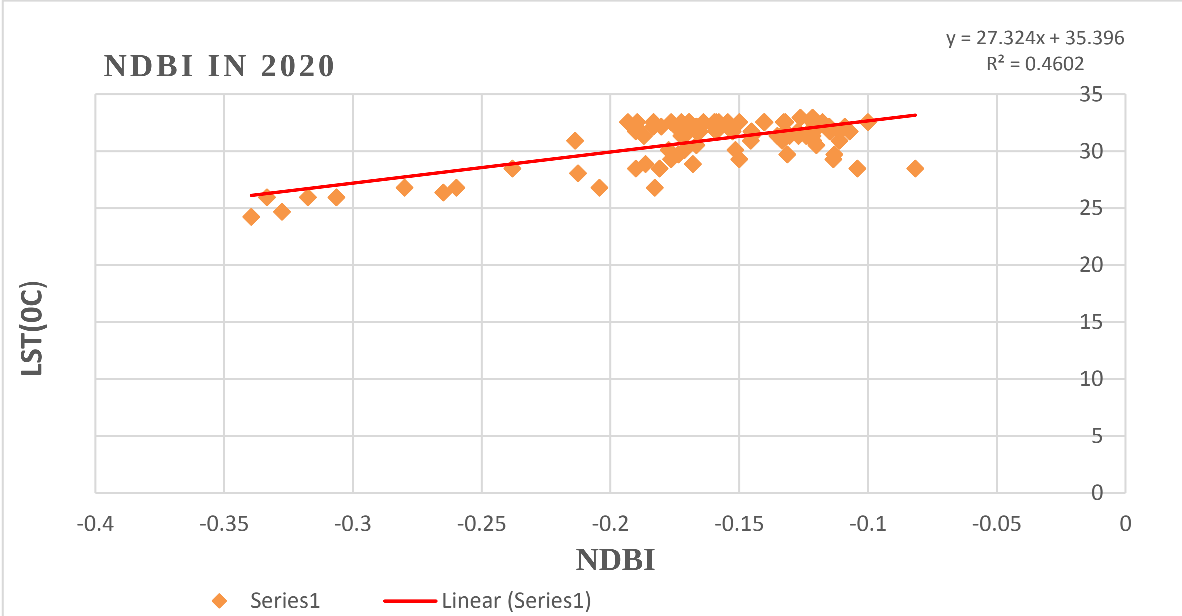

Figure 4. 23: correlation between LST and NDBI IN 2020

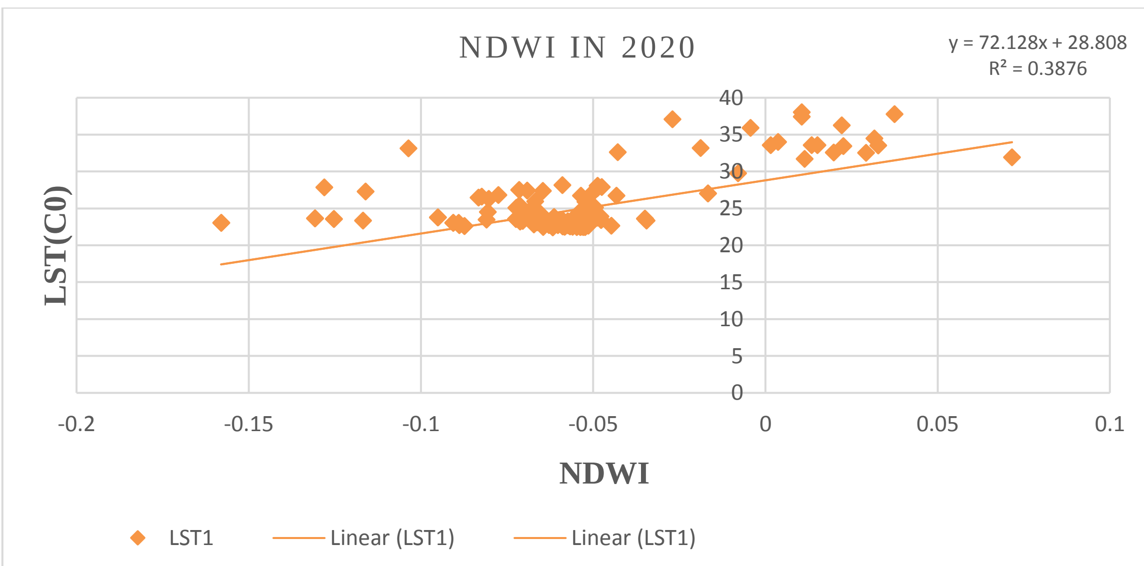

Figure 4. 24 : correlation between LST and NDWI in 2020

4.11 correlation between LST and elevation in 1999, 2010, 2020

As seen from the data of the Digital Elevation Model (DEM), Metehara City's Land Surface Temperature (LST) varied in 1999 across different elevations. Lower temperatures are typically correlated with higher elevations and vice versa; the LST ranged from 24.24°C to 32.95°C. In contrast, the LST dropped noticeably to around 24.67°C at 967m, but the temperature remained continuously high at elevations around 950m at about 32.55°C. In the research area throughout that time, this tendency points to a possible inverse link between elevation and temperature." In Metehara City saw fluctuating elevations in 2010, ranging from 950 meters to 971 meters. The Land Surface Temperature (LST) readings in degrees Celsius corresponding to this elevation range were provided.

The collection contains LST values for several elevation sites ranging from 19.73°C to 37.22°C. The examination of this data sheds light on the region's 2010 thermal characteristics. In general, LST values were lower at higher elevations, signifying lower temperatures, and higher at lower elevations, signifying hotter temperatures. Understanding local climatic dynamics and thermal gradients within a geographical area is made possible by the link between elevation and temperature, which is a core component of environmental research.

A study looking at the connection between land surface temperature (LST) and elevation was carried out in Metehara City in 2020. Between 950 and 971 meters in elevation and their corresponding LST values in degrees Celsius made up the dataset. The results of statistical analysis showed that elevation and LST had a strong negative association, with lower LST values seen at higher elevations. A regression equation showing an LST reduction of 0.05°C per meter increase in elevation and scatter plots with fitted trend lines supported this inverse link. The correlation coefficient was -0.87. These results indicate that, over the given period, height had a significant impact on local temperature changes in Metehara city.

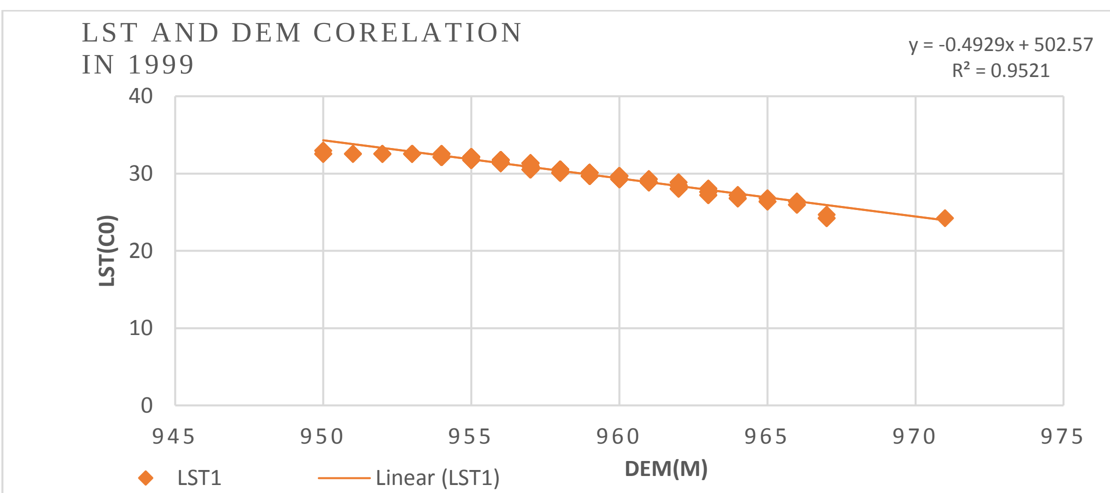

Figure 4. 25: correlation between LST and DEM IN 1999

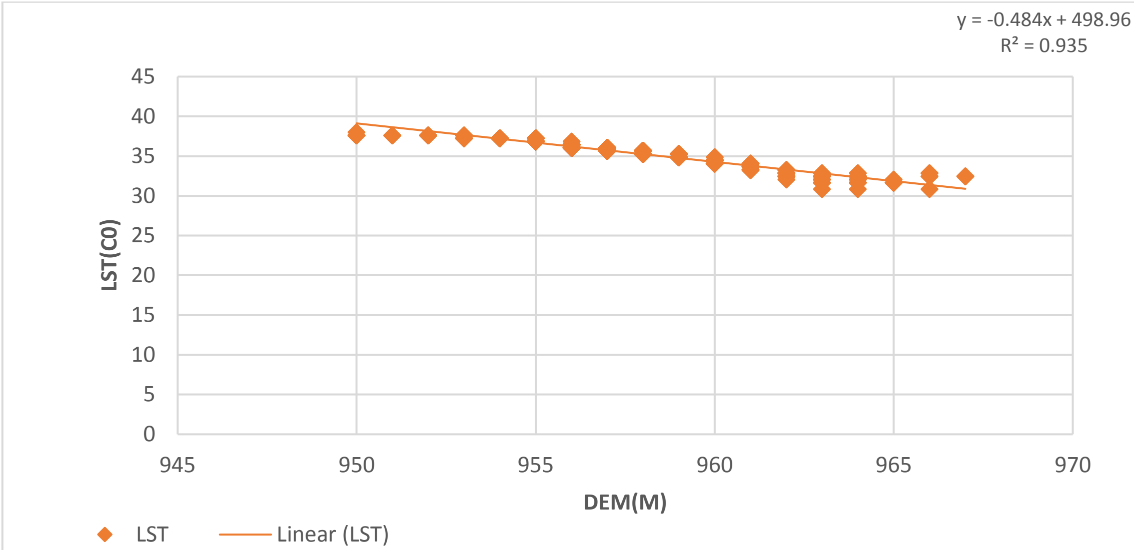

Figure 4. 26 : correlation between LST and elevation in 2010

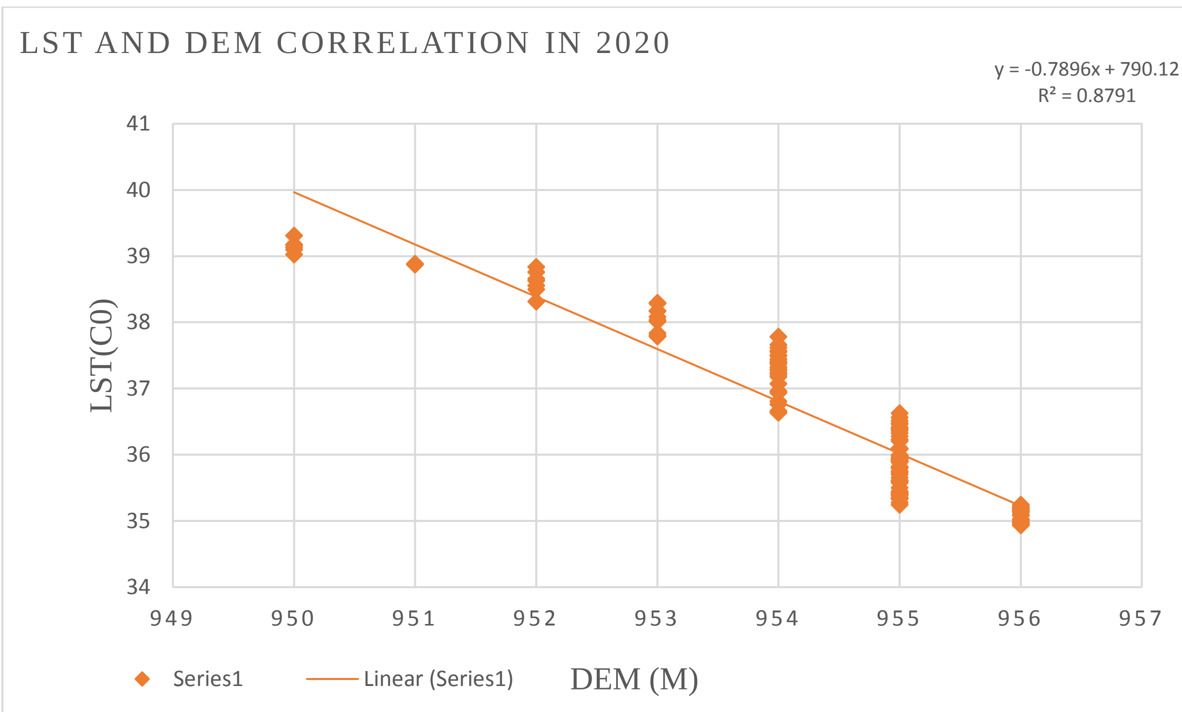

Figure 4. 27: correlation between LST and DEM in 2020

Chapter Five

5. Conclusion and Recommendation

5.1 Conclusion

This MSc thesis offers a comprehensive analysis of the intricate relationship between environmental factors, land surface temperature (LST) dynamics, and land use/land cover (LULC) changes in Metehara City, Ethiopia. The research examines LULC patterns and their effects on local climate dynamics by analyzing Landsat satellite images from 1999, 2010, and 2020, utilizing remote sensing and GIS techniques. The findings highlight significant urbanization trends in Metehara City, driven by economic development and population growth. Rapid urban expansion has led to substantial changes in LULC patterns, with built-up areas encroaching upon agricultural land and vegetation cover. This urban growth has resulted in the formation of urban heat islands (UHIs) and alterations in city temperature patterns, which have a notable impact on local climate dynamics.

The built-up area increased from 35.97 hectares in 1999 to 149.7 hectares in 2010, and further to 202.21 hectares in 2020. LST values ranged from 24.24°C to 32.95°C in 1999, 30.01°C to 38.387°C in 2010, and 22.4049°C to 39.39°C in 2020. The mean temperature differences were 0.77°C between 1999 and 2010, 0.75°C between 2010 and 2020, and 1.52°C from 1999 to 2020. The maximum temperatures recorded were 32.95°C, 38.887°C, and 39.4049°C for 1999, 2010, and 2020, respectively, indicating a warming trend over the study period. From 1999 to 2020, Metehara City experienced significant variations in LST across different LULC zones. Agriculture, in particular, exhibited notable changes in 1999 128.16 hectares, mean temperature 31.35°C in 2010 44.66 hectares, mean temperature 36.53°C and in 2020 113.85 hectares, mean temperature 36.12°C.

Correlation analyses reveal strong relationships between LST and LULC classes, showing that vegetated areas are cooler than built-up regions. The cooling effect of dense vegetation is evident, emphasizing the importance of green spaces in mitigating heat stress in urban settings. The study also highlights the influence of water bodies on LST, with areas lacking water features displaying higher surface temperatures. The research also explores the impact of topographical features, particularly elevation, on LST dynamics. Higher elevations were associated with lower temperatures, suggesting that topography influences local thermal dynamics. Consistent negative correlations between elevation and temperature were observed. The insights gained from this study enhance our understanding of the intricate interactions between LULC changes and LST dynamics in Metehara City. As urbanization continues, these findings are critical for climate resilience efforts, environmental conservation, and sustainable urban planning. The study provides valuable information for evidence-based decision-making to mitigate the negative effects of urbanization on regional climates by clarifying the impacts of land use changes on surface temperature.

5.2 Recommendation

These findings should be incorporated into urban planning and decision-making processes in Metehara City and other similar areas. Urban planners should prioritize sustainable development strategies, focusing on the protection of green spaces, promotion of vegetation cover, and implementation of heat mitigation techniques to counteract the negative effects of urban heat islands (UHIs). Local governments should invest in green infrastructure projects. Introducing green walls and roofs, planting trees, and establishing parks can make urban environments more livable and help mitigate the heat island effect.

Urban planners should minimize energy use, maximize natural ventilation, and reduce heat absorption in buildings and streetscapes. Implementing techniques like permeable pavements and cool roofing materials can enhance urban comfort and lower surface temperatures. Engaging residents through educational programs on sustainable land management, water conservation, and waste disposal can foster a sense of responsibility and ownership. This empowers the community to mitigate environmental degradation and promote resilience. A strong monitoring system supported by remote sensing technologies (such as Landsat 5 and Landsat 8) and on the ground observations should be established. This system will provide timely data to facilitate evidence based decision making and adaptive management strategies. In addition to Landsat 5 and Landsat 8, it is recommended to use high-resolution satellite imagery from sources like Sentinel-2, WorldView, and GeoEye. These high-resolution images can enhance the analysis of LULC changes and their impact on land surface temperature, allowing for more precise and effective urban planning and environmental management. Using data from Landsat 5, Landsat 8, and other high-resolution satellite images, urban planners and environmental managers should analyze the impacts of LULC changes on land surface temperature.

REFERENCE

Abrams, M., Crippen, R. and Fujisada, H., (2020). ASTER Global Digital Elevation Model (GDEM) and ASTER Global Water Body Dataset (ASTWBD) . *Remote Sensing*, Vol. 12(7). https://doi.org/10.3390/rs12071156.

Abel, B. 2018. Impacts of land use and land cover changes on land surface temperature distribution in Bahir Dar town and its surrounding using remote sensing. MSc. Thesis Addis Ababa University, Ethiopia.

Al Kafy, A.-, et al., 2021. Remote sensing approach to simulate the land use/land cover and seasonal land surface temperature change using machine learning algorithms in a fastest-growing megacity of Bangladesh. Remote Sens. Appl. Soc. Environ. 21, 100463. doi: 10.1016/j.rsase.2020.100463

Almazroui, M., Masshat, A., Assiri, M., & Butt, M. (2017). Application of landsat data for urban growth monitoring in Jeddah. *Earth System Environment*, *1*(2), 25. https:// doi.org/10.1007/s41748 017-0028-4

and West St Paul, Winnipeg, Manitoba, Canada. J. Environ. Manage. 66, 229.

Akram, A., Jamil, F., & Alvi, S. (2022). The effects of natural disasters on human development in developing and developed countries. *International Journal of Global Warming*, *27*(2), 155. https://doi.org/10.1504/ijgw.2022.123279

Aredehey, G., Mezgebu, A., & Girma, A. (2018). Land-use land-cover classification analysis of Giba catchment using hyper temporal MODIS NDVI satellite images. *International Journal of Remote Sensing*, *39*(3), 810–821. https://doi.org/10.1080/01431161.2017.1392639

Athick, A. A. S. M., & Shankar, K. (2019). Data on land use and land cover changes in Adama Wereda, Ethiopia, on ETM+, TM and OLI- TIRS landsat sensor using PCC and CDM techniques, *Data in Brief*, 24, 103880. https://doi. org/10.1016/j.dib.2019.103880

Ayele, G. T., Tebeje, A. K., Demissie, S. S., Belete, M. A., Jemberrie, M. A., Teshome, W. M., & Teshale, E. Z. (2018). Time series land cover mapping and change detection analysis using geographic information system and remote sensing, Northern Ethiopia. *Air, Soil and Water Research*, *11*, 1178622117751603. https://doi.org/ 10.1177/1178622117751603 .

Astuti, B., Mufrihah, A., & Alfiah, L. (2019, June 30). How School Climate Aspects Affect the Development of Adolescence's Psychological Well-being. *KnE Social Sciences*. https://doi.org/10.18502/kss.v3i17.4650

Ayanlade, A., & Howard, M. T. (2019, March). Land surface temperature and heat fluxes over three cities in Niger Delta. *Journal of African Earth Sciences*, *151*, 54–66. https://doi.org/10.1016/j.jafrearsci.2018.11.027

Bai, Y., Deng, X., Jiang, S., Zhang, Q., & Wang, Z. (2018). Exploring the relationship between urbanization and urban eco-efficiency: Evidence from prefecture-level cities in China. *Journal of Cleaner Production*, *195*, 1487–1496. https://doi.org/10.1016/j.jclepro.2017.11.115

Bangladesh: Using remote sensing to promote sustainable urbanization. *Applied Geography*, *29*(3), 390–401. https://doi.org/10.1016/j.apgeog.2008.12.005

Becker, F., & Li, Z. L. (1990, April). Temperature-independent spectral indices in thermal infrared bands. *Remote Sensing of Environment*, *32*(1), 17–33. https://doi.org/10.1016/0034-4257(90)90095-4

Benz, S.A., Bayer, P., Blum, P., 2017. Identifying anthropogenic anomalies in air, surface and groundwater temperatures in Germany. Sci. Total Environ. 584–585, 145–153. Chapman, S., Watson, J.E.M., Salazar, A., Thatcher, M., Mcalpine, C.A., 2017. The impact of urbanization and climate change on urban temperatures: a systematic review. Landsc. Ecol. 32, 1921–1935.

Bhagyanagar, R., Kawal, B. M., Dwarakish, G. S., & Surathkal, S. (2012). Land use/land cover change and urban expansion during 1983–2008 in the coastal area of Dakshina Kannada district, South India. *Journal of Applied Remote Sensing*, *6*(1), 063576. https://doi.org/10. 1117/1.JRS.6.063576

Blandford, T. R., Humes, K. S., Harshburger, B. J., Moore, B. C., Walden, V. P. & Ye, H. (2008). Seasonal and Synoptic Variations in Near-Surface Air Temperature LapseRates in a

Mountainous Basin. J. Appl. Meteor. Climatol., 47, 249–261. https://doi.org/10.1175/2007JAMC1565.1

Bokaie, M., Zarkesh, M. K., Arasteh, P. D., & Hosseini, A. (2016, May). Assessment of Urban Heat Island based on the relationship between land surface temperature and Land Use/ Land Cover in Tehran. *Sustainable Cities and Society*, *23*, 94–104. https://doi.org/10.1016/j.scs.2016.03.009

Brown, D. G., Pijanowski, B. C., & Duh, J. D. (2000). Modeling the relationships between land use and land cover on private lands in the Upper Midwest, USA. *Journal of Environmental Management, 59*(4), 247–263. https://doi.org/10.1006/jema.2000.0369.

Carter, J. G., Cavan, G., Connelly, A., Guy, S., Handley, J., & Kazmierczak, A. (2015, January). Climate change and the city: Building capacity for urban adaptation. Progress in Planning, 95, 1–66

Chao, Z., Wang, L., Che, M., & Hou, S. (2020, June 24). Effects of Different Urbanization Levels on Land Surface Temperature Change: Taking Tokyo and Shanghai for Example. *Remote Sensing*, *12*(12), 2022. https://doi.org/10.3390/rs12122022

Chew, C., Shah, R., Zuffada, C., Hajj, G., Masters, D., & Mannucci, A. J. (2016). Demonstrating soil moisture remote sensing with observations from the UK TechDemoSat-1 satellite mission. *Geophysical Research Letters*, *43*(7), 3317–3324. https://doi.org/10.1002/ 2016GL068189

Choudhury D. & Das Arijit Das, K., (2019), Assessment of land use land cover changes and its impact on variations of land surface temperature in Asansol-Durgapur Development Region, *The Egyptian Journal of Remote Sensing and Space Science*, 22, (2), 203-218

Choudhury, D., Das, K., Das, A., 2019. Assessment of land use land cover changes and its impact on variations of land surface temperature in Asansol-Durgapur Development Region, Egypt. J. Remote Sens. Sp. Sci. 22, 203–218. https://doi.org/10.1016/j.ejrs.2018.05.004.

Correction to Lancet Respir Med 2021; published online April 9. 2600(21)00160-0. (2021, June). *The Lancet Respiratory Medicine, 9*(6), e55. https://doi.org/10.1016/s2213-2600(21)00181-8.

Congalton, R. & Green, K. 2009. Thematic accuracy. *Assessing the Accuracy of Remotely Sensed Data: Principles and Practices***,** 55-61.

Das, S., & Sarkar, R. (2019). Predicting the land use and land cover change using Markov model: A catchment level analysis of the Bhagirathi-Hugli River. *Spatial Information Research*, *27*(4), 439–452. https://doi.org/10. 1007/s41324-019-00251-7

Dash, P., Göttsche, F. M., Olesen, F. S., & Fischer, H. (2002, January). Land surface temperature and emissivity estimation from passive sensor data: Theory and practice-current trends. *International Journal of Remote Sensing*, *23*(13), 2563–2594. https://doi.org/10.1080/01431160110115041

Deng Y, Wang S, Bai X, Tian Y,Wu L, Xiao J, et al. Relationship among land surface temperature and LUCC, NDVI in typical karst area. Sci Rep. 2018;8(1):641.

Dewan, A. M., & Yamaguchi, Y. (2009). Land use and land cover change in Greater Dhaka,

Duan, S.-B., Li, Z.-L., Li, H., Göttsche, F.-M., Wu, H., Zhao, W., Leng, P., Zhang, X., & Coll, C. (2019). Validation of Collection 6 MODIS land surface temperature product using in situ measurements. *Remote Sensing of Environment*, *225*, 16–29.

Ebrahimy, H., Aghighi, H., Azadbakht, M., Amani, M., Mahdavi, S., & Matkan, A. A. (2021). Downscaling MODIS land surface temperature product using an adaptive random forest regression method and google earth engine for a 19-years spatiotemporal trend analysis over Iran. *IEEE Journal of Selected Topics in Applied Earth Observations and Remote Sensing*, *14*(Ml), 2103–2112. https://doi.org/10.1109/

El Kenawy, A.; Lopez-Moreno, J.; Vicente-Serrano, S.; Mekled, M. Temperature trends in Libya over the second half of the 20th century. Theor. Appl. Climatol. 2009, 98, 1–8.

Environ. 89, 467–483. https://doi.org/10.1016/j.rse.2003.11.005.

Estoque, R. C., Murayama, Y., & Myint, S. W. (2017, January). Effects of landscape composition and pattern on land surface temperature: An urban heat island study in the megacities of Southeast Asia. *Science of the Total Environment*, *577*, 349–359. https://doi.org/10.1016/j.scitotenv.2016.10.195

Foley, J. A., et al. (2005). Global consequences of land use. *Science, 309*(5734), 570. https://doi.org/10.1126/science.1111772.

Frey, C. M., Kuenzer, C., & Dech, S. (2012, June 28). Quantitative comparison of the operational NOAA-AVHRR LST product of DLR and the MODIS LST product V005. *International Journal of Remote Sensing*, *33*(22), 7165–7183. https://doi.org/10.1080/01431161.2012.699693

Gallo, K.P., Mcnab, A.L., Karl, T.R., Brown, J.F., Hood, J.J., Tarpley, J.D., 1993. The use of

Gao, J. 2009. *Digital Analysis of Remotely Sensed Imagery: Multi-Temporal Image Analysis*, The McGraw-Hill Companies

Giorgi F, Hurrell JW, Marinucci MR, Beniston M (1997) Elevation dependency of the surface climate change signal: a model study. J Clim 10:288–296. https ://doi.org/10.1175/

Gogoi, P. P., Vinoj, V., Swain, D., Roberts, G., Dash, J., & Tripathy, S. (2019). Land use and land cover change effect on surface temperature over Eastern India. Scientific Reports, 9(1), 1–10. https://doi.org/10.1038/s41598-019-45213-z

Grover, A., & Singh, R. (2015, April 15). Analysis of Urban Heat Island (UHI) in Relation to Normalized Difference Vegetation Index (NDVI): A Comparative Study of Delhi and Mumbai. *Environments*, *2*(4), 125–138. https://doi.org/10.3390/environments2020125

Guha, S., Govil, H., Dey, A., & Gill, N. (2018). Analytical study of land surface temperature with NDVI and NDBI using landsat 8 OLI and TIRS data in florence and Naples city, Italy. *European Journal of Remote Sensing, 51*(1), 667–678. https://doi. org/10.1080/22797254.2018.1474494.

H., Mushore, T.D., 2018. Spatiotemporal analysis of land use/land cover and its effects on surface urban heat island using landsat data: a case study of metropolitan city Tehran (1988–2018). Sustainability 10 (4433), 2–25. https://doi.org/10.3390/su10124433

Haidu, I., Furtuna, P., Lebaut, S. (2019) Detection of old scattered windthrow using low cost resources. The case of Storm Xynthia in the Vosges Mountains, 28 February 2010, *Open Geosciences*, 11(1), 492–504, https://doi.org/10.1515/geo-2019-0040

Hathout, S., 2002. The use of GIS for monitoring and predicting urban growth in East

Hc, H., Srikanth, L., & Surendra, H. J. (2020). Prioritization of sub-watersheds of the Kanakapura watershed in the Arkavathi River Basin, Karnataka, India-using remote sensing and GIS. *Geology, Ecology, and Landscapes, 5* (2), 149–160.. https://doi.org/10.1080/24749508.2020. 1846841 heat island effect across biomes in the continental USA. Remote Sens. Environ.

Helmer, E. H., Brown, S., & Cohen, W. B. (2000). Mapping montane tropical forest successional stage and land use with multi-date Landsat imagery. *International Journal of Remote Sensing*, *21*(11), 2163–2183. https://doi.org/10.1080/01431160050029495.

Honnerová, P., Veselý, Z., & Honner, M. (2016, August). Experimental mathematical model as a generalization of sensitivity analysis of high temperature spectral emissivity measurement method. *Measurement*, *90*, 475–482. https://doi.org/10.1016/j.measurement.2016.04.070

Hu, Y., & Jia, G. (2009, July 28). Influence of land use change on urban heat island derived from multi-sensor data. International Journal of Climatology, 30(9), 1382–1395. https://doi.org/10.1002/joc.1984

Hussain, S. (2018). *Land use/land cover classification by using satellite NDVI tool for sustainable water and climate change in Southern Punjab* [MS thesis]. COMSATS University. https://doi.org/10.13140/RG.2.2.32363.69923 .

Igun, E. (2017). Analysis and Sustainable Management of Urban Growth's Impact on Land Surface Temperature in Lagos, Nigeria. Journal of Remote Sensing & GIS, 06(04). https://doi.org/10.4172/2469-4134.1000212

Imhoff, M.L., Zhang, P., Wolfe, R.E., Bounoua, L., 2010. Remote sensing of the urban in Australian rangelands. Int. J. Remote Sens. 9, 1815–1820.

Islam, S., Ma, M., 2018. Geospatial monitoring of land surface temperature effects on vegetation dynamics in the southeastern region of Bangladesh from 2001 to 2016. ISPRS Int. J. Geo-Inform. 7 (12), 486. doi: 10.3390/ijgi7120486

Jansen, L. J., & Di Gregorio, A. (2003, April). Land-use data collection using the "land cover classification system": results from a case study in Kenya. *Land Use Policy*, *20*(2), 131–148. https://doi.org/10.1016/s0264-8377(02)00081-9

Jensen, J. R. (2007). *Remote sensing of the environment* (2nd ed.). Upper Saddle River: Pearson Prentice Hall.

Jin, F. F., Boucharel, J., & Lin, I. I. (2015, October). Jin et al. reply. *Nature*, *526*(7575), E5–E6. https://doi.org/10.1038/nature15547

Junxiang, G., & Haiqing, D. (2011). Design of Greenhouse Surveillance System Based on Embedded Web Server Technology. Procedia Engineering, 23, 374–379. https://doi.org/10.1016/j.proeng.2011.11.2516

Khandelwal, S., Goyal, R., Kaul, N., & Mathew, A. (2018, April). Assessment of land surface temperature variation due to change in elevation of area surrounding Jaipur, India. *The Egyptian Journal of Remote Sensing and Space Science*, *21*(1), 87–94. https://doi.org/10.1016/j.ejrs.2017.01.005

Kopecká M, Nagendra H, Millington A. Urban land systems: an ecosystems perspective. Kumari, S., Gupta, M., & Kumar, M. (2012, March 1). Cryptanalysis and security enhancement of Chen et al.'s remote user authentication scheme using smart card. Open Computer Science, 2(1), 60–75. https://doi.org/10.2478/s13537-012-0003-y

Lambin, E. F., Turner, B. L., Geist, H. J., Agbola, S. B., Angelsen, A., Bruce, J. W., et al. (2001). The causes of land-use and land-cover change: Moving beyond the myths. *Global Environmental Change*, *11*(2), 261–269.

Lillesand, T., Kiefer, R. & Chipman, J. 2004. Remote sensing and image interpretation. *Remote sensing and image interpretation*

Li W, Cao Q, Lang K, Wu J. Linking potential heat source and sink to urban heat island: heterogeneous effects of landscape pattern on land surface temperature. Sci Total Environ.

Li, J., Song, C., Cao, L., Zhu, F., Meng, X., & Wu, J. (2011). Impacts of landscape structure on surface urban heat islands: A case study of Shanghai, China. *Remote Sensing of Environment, 115*(12), 3249–3263. https://doi.org/10.1016/J.RSE.2011.07.008

Li, M., Zang, S., Zhang, B., Li, S., & Wu, C. (2014). A review of remote sensing image classification techniques: The role of spatio-contextual information. *European Journal of Remote Sensing*, *47*(1), 389–411. https://doi.org/10.5721/EuJRS20144723.

Li, W., Cao, Q., Lang, K., & Wu, J. (2017, May). Linking potential heat source and sink to urban heat island: Heterogeneous effects of landscape pattern on land surface temperature. Science of the Total Environment, 586, 457–465. https://doi.org/10.1016/j .scitotenv.2017.01.191

Lo, C. P. (1986). *Applied remote sensing* (p. 227). New York: Longman Inc.

Lo, C. P., Quattrochi, D. A., & Luvall, J. C. (1997, January). Application of high-resolution thermal infrared remote sensing and GIS to assess the urban heat island effect. International Journal of Remote Sensing, 18(2), 287–304. https://doi.org/10.1080/014311697219079

Loveland T. R., & Acevedo W. (2006) *Land cover change in the Eastern United States, US Geological survey*. https://landcovertrends.usgs.gov/east/regionalSummary.html.

Mahmood, R., Pielke, R. A., Hubbard, K. G., Niyogi, D., Bonan, G., Lawrence, P., McNider, R., McAlpine, C., Etter, A., Gameda, S., Qian, B., Carleton, A., Beltran-Przekurat, A., Chase, T., Quintanar, A. I., Adegoke, J. O., Vezhapparambu, S., Conner, G., Asefi, S., . . . Syktus, J. (2010, January). Impacts of Land Use/Land Cover Change on Climate and Future Research Priorities. Bulletin of the American Meteorological Society, 91(1), 37–46. https://doi.org/10.1175/2009 bams2769.1

Malik, S. M., Arshad, S., Alam, K., & Bilal, O. (2020). Monitoring urban growth and land use changes using GIS and remote sensing: A case study of Tehsil Burewala. *Journal of Himalayan Earth Science*, *53*(1), 140

Malik, S., Pal, S. C., Sattar, A., Singh, S. K., Das, B., Chakrabortty, R., & Mohammad, P. (2020). Urban Climate Trend of extreme rainfall events using suitable Global Circulation Model to combat the water logging condition in Kolkata Metropolitan Area. *Urban Climate*, *32*, 100599. https://doi.org/10.1016/j.uclim.2020.100599

McDonald, R. I., Güneralp, B., Huang, C. W., Seto, K. C., & You, M. (2018, August). Conservation priorities to protect vertebrate endemics from global urban expansion. *Biological Conservation*, *224*, 290–299. https://doi.org/10.1016/j.biocon.2018.06.010

Minder JR, Letcher TW, Liu C (2018) The character and causes of elevation-dependent warming in high-resolution simulations of Rocky Mountain climate change. J Clim 31:2093–2113. https :// doi.org/10.1175/JCLI-D-17-0321.1

Mohammad, P., & Goswami, A. (2019). Temperature and precipitation trend over 139 major Indian cities: An assessment over a century. *Modeling Earth Systems and Environment*, *5*(4), 1481–1493. https://doi.org/10.1007/s40808-019-00642-7

Mohammad, P., Goswami, A., & Bonafoni, S. (2019). The impact of the land cover dynamics on surface urban heat island variations in semi-arid cities: A case study in Ahmedabad City, India, using multi-sensor/source data. *Sensors (Switzerland)*, *19*(17) 2 https://doi.org/10.3390/s19173701

Mohammed, A. A. A. S., Shankar, K., & Hasan, R. N. (2019). Data on time series analysis of land surface temperature variation in response to vegetation indices in twelve Wereda of Ethiopia using mono window, split window algorithm and spectral radiance model. *Data in Brief*, *27*, 104773. https://doi.org/10.1016/j.dib.2019.104773

NOAA AVHRR data for assessment of the urban heat island effect. J. Appl. Meteorol. 32 (5), 899–908. Gallo, K.P., Tarpley, J.D., 1996.

Olmanson, L. G., Brezonik, P. L., Finlay, J. C., & Bauer, M. E. (2016). Comparison of Landsat 8 and Landsat 7 for regional measurements of CDOM and water clarity in lakes. *Remote Sensing of Environment*, *185*, 119–128. http://dx.doi.org/10.1016/j.rse.2016.01.007

Osborne, P. E., & Alvares-Sanches, T. (2019, July). Quantifying how landscape composition and configuration affect urban land surface temperatures using machine learning and neutral landscapes. *Computers, Environment and Urban Systems*, *76*, 80–90. https://doi.org/10.1016/j.compenvurbsys.2019.04.003

Pal, S., Ziaul, S., 2017. Detection of land use and land cover change and land surface temperature in English Bazar urban centre. J. Remote Sens. Sp. Sci. 20, 125 145.https://doi.org/10.1016/j.ejrs.2016.11.003.

Palazzi E, Filippi L, von Hardenberg J (2017) Insights into elevationdependent warming in the Tibetan Plateau–Himalayas from CMIP5 model simulations. Clim Dyn 48(11–12):3991–4008. https ://doi.org/10.1007/s0038 2-016-3316-z

Peng, J., Xie, P., Liu, Y., Ma, J., 2016. Urban thermal environment dynamics and associated landscape pattern factors: a case study in the Beijing metropolitan region. Remote Sens. Environ. 173, 145–155.

Popp A, Calvin K, Fujimori S, Havlik P, Humpenöder F, Stehfest E, et al. Land-use futures in the shared socio-economic pathways. Glob Environ Chang. 2017;42:331–45.

Qin, Z., Dall'Olmo, G., Karnieli, A., & Berliner, P. (2001, October). Derivation of split window algorithm and its sensitivity analysis for retrieving land surface temperature from NOAA-advanced very high resolution radiometer data. *Journal of Geophysical Research: Atmospheres*, *106*(D19), 22655–22670. https://doi.org/10.1029/2000jd900452

Rajeshwari A. & Mani, N. (2014) Estimation of Land Surface Temperature of Dindigul district using Landsat 8 data, *International Journal of Research in Engineering and Technology*, 3(5), 122–126

Rangwala I, Miller JR (2012) Climate change in mountains: a review of elevation-dependent warming and its possible causes. Clim Chang 114:527–547. https ://doi.org/10.1007/s1058 4-012 0419-3

Reda, T. M., Gebrehiwot, W. Z., Jothimani, J. M., & Tirusew, S. Y. (2022, January 12). Assessing the effect of volcano-tectonic activity on the spatial distribution of surface temperature in the Main Ethiopian Rift, using integrated approach of remote sensing data. *European Journal of Remote Sensing*, *55*(1), 86–102. https://doi.org/10.1080/22797254.2021.2021555

Rimal, B., Keshtkar, H., Sharma, R., Stork, N., Rijal, S., & Kunwar, R. (2019, March 28). Simulating urban expansion in a rapidly changing landscape in eastern Tarai, Nepal. *Environmental Monitoring and Assessment*, *191*(4). https://doi.org/10.1007/s10661-019-7389-0

Rotem-Mindali, O., Michael, Y., Helman, D., & Lensky, I. M. (2015, January). The role of local land-use on the urban heat island effect of Tel Aviv as assessed from satellite remote sensing. Applied Geography, 56, 145–153. https://doi.org/10.1016/j.apgeog.2014.11.023

Rousta, I., Sarif, O., Gupta, R.V., Olafsson, H., Ranagalage, M., Murayama, Y., Zhang,

Roy, S., et al., 2020. Examining the nexus between land surface temperature and urban growth in Chattogram Metropolitan area of Bangladesh using long term Landsat series data. Urban Clim. 32, 100593. doi: 10.1016/j.uclim.2020.100593

Rozenstein, O., Qin, Z., Derimian, Y., & Karnieli, A. (2014, June 24). Correction: Rozenstein, O., et al. Derivation of Land Surface Temperature for Landsat-8 TIRS Using a Split Window Algorithm. Sensors 2014, 14, 5768–5780. *Sensors*, *14*(6), 11277–11277. https://doi.org/10.3390/s140611277

Sadiq Khan, M., Ullah, S., Sun, T., Rehman, A. U., & Chen, L. (2020). Land-use/land-cover changes and its contribution to urban heat island: A case study of Islamabad, Pakistan. *Sustainability*, *12*(9), 3861. https:// doi.org/10.3390/su12093861

Sahana, M., Ahmed, R., & Sajjad, H. (2016). Analyzing land surface temperature distribution in response to land use/ land cover change using split window algorithm and spectral radiance model in Sundarban Biosphere Reserve, India. *Modeling Earth Systems and Environment*, *2*(2), 81. https://doi.org/10.1007/s40808- 016-0135-5.

Sahana, M., Ahmed, R., & Sajjad, H. (2016, May 2). Analyzing land surface temperature distribution in response to land use/land cover change using split window algorithm and spectral radiance model in Sundarban Biosphere Reserve, India. Modeling Earth Systems and Environment, 2(2). https://doi.org/10.1007/s40808-016-0135-5

Sara Afrasiabi Gorgani 1, M. P. 2 and F. R. (2016). *The Relationship between NDVI and LST in the urban area of Mashhad, Iran. January 2013*.

Sobrino, J. A., & Raissouni, N. (2000, January). Toward remote sensing methods for land cover dynamic monitoring: Application to Morocco. *International Journal of Remote Sensing*, *21*(2), 353–366. https://doi.org/10.1080/014311600210876

Son, N. T., Chen, C. F., Chen, C. R., Thanh, B. X., & Vuong, T. H. (2017, April). Assessment of urbanization and urban heat islands in Ho Chi Minh City, Vietnam using Landsat data. *Sustainable Cities and Society*, *30*, 150–161. https://doi.org/10.1016/j.scs.2017.01.009

Song, J., Du, S., Feng, X., Guo, L., 2014. The relationships between landscape compositions and land surface temperature: quantifying their resolution sensitivity with spatial regression models. Landscape Urban Planning 123,

Souch, C., & Grimmond, S. (2006, April). Applied climatology: urban climate. *Progress in Physical Geography: Earth and Environment*, *30*(2), 270–279. https://doi.org/10.1191/0309133306pp484pr

Tomlinson, C. J., Chapman, L., Thornes, J. E., & Baker, C. (2011, August 22). Remote sensing land surface temperature for meteorology and climatology: a review. Meteorological Applications, 18(3), 296–306. https://doi.org/10.1002/met.287 (Tomlinson et al., 2011)

Ullah, S., et al., 2019. Remote sensing-based quantification of the relationships between land use land cover changes and surface temperature over the lower Himalayan re-gion. Sustainability 11 (19), 5492 .

Ullah, S., Tahir, A., Akbar, T., Hassan, Q., Dewan, A., Khan, A., & Khan, M. (2019). Remote sensing-based quantification of the relationships between land use land cover changes and surface temperature over the lower Himalayan region. *Sustainability*, *11*(19), 5492. https://doi.org/10.3390/su11195492

UN Department of Economic and Social Affairs, Population Division. (2018). World Urbanization Prospects: The 2018 Revision. Online Edition. Retrieved from https://population.un.org/wup/

UN DESA. Population Division. In World Urbanization Prospects: The 2018 Revision; UN DESA: New York,

Vani, V., & Venkata Ravibabu Mandla. (2017). Comparative Study of NDVI and SAVI Vegetation Indices in Anantapur District Semi-Arid Areas. *International Journal of Civil Engineering and Technology*, *8*(4), 559–566. Retrieved from

Walawender, J.P., Szymanowski, M., Hajto, M.J., Bokwa, A., 2014. Land surface temperature patterns in the urban agglomeration of Krakow (Poland) derived from Landsat-7/ETM+ data. Pure Appl. Geophys. 171 (6), 913–940.

Wang, W., Liang, S., & Meyers, T. (2008, March). Validating MODIS land surface temperature products using long-term nighttime ground measurements. Remote Sensing of Environment, 112(3), 623–635. https://doi.org/10.1016/j.rse.2007.05.024

Weng, Q., Lu, D., & Schubring, J. (2004, February). Estimation of land surface temperature–vegetation abundance relationship for urban heat island studies. *Remote Sensing of Environment*, *89*(4), 467–483. https://doi.org/10.1016/j.rse.2003.11.005

Weng, Q., Lu, D., Schubring, J., 2004. Estimation of land surface temperature vegetation abundance relationship for urban heat island studies.

Wolf, I. D., Sobhani, P., & Esmaeilzadeh, H. (2023, January 11). Assessing Changes in Land Use/Land Cover and Ecological Risk to Conserve Protected Areas in Urban–Rural Contexts. *Land*, *12*(1), 231. https://doi.org/10.3390/land12010231

Xie, M., Wang, Y., Chang, Q., Fu, M., & Ye, M. (2013, July 17). Assessment of landscape patterns affecting land surface temperature in different biophysical gradients in Shenzhen, China. Urban Ecosystems, 16(4), 871–886. https://doi.org/10.1007/s11252-013-0325-0

Yanev, I.; Filchev, L. A comparative analysis between MODIS LST level-3 product and in-situ temperature

Yang, C., He, X., Yan, F., Yu, L., Bu, K., Yang, J., Chang, L., Zhang, S., 2017. Mapping the influence of land use/land cover changes on the urban heat island effect—a case study of Changchun, China. Sustainability 9:312. https://doi.org/10.3390/su9020312.

You, Q.; Kang, S.; Pepin, N.; Yan, Y. Relationship between trends in temperature extremes and elevation in

Yuan, F., & Bauer, M. E. (2007, February). Comparison of impervious surface area and normalized difference vegetation index as indicators of surface urban heat island effects

Zhang, H., Qi, Z. F., Ye, X. Y., Cai, Y. B., Ma, W. C., & Chen, M. N. (2013). Analysis of land use/land cover change, population shift, and their effects on spatiotemporal patterns of urban heat islands in metropolitan Shanghai, China. *Applied Geography*, *44*, 121–133. https://doi.org/10.1016/J.APGEOG.2013.07.021

Zhang, X., Wang, D., Hao, H., Zhang, F., & Hu, Y. (2017). Effects of land use/cover changes and urban forest configuration on urban heat islands in a loess hilly region: case study based on Yan'an City, China. *International Journal of Environmental Research and Public Health, 14*(8). https://doi.org/10.3390/IJERPH14080840

Zhang, Z., Liu, S., Wei, J., Xu, J., Guo, W., Bao, W., Jiang, Z., & Zhu, L. (2016). Mass change of glaciers in Muztag Ata– Kongur Tagh, Eastern Pamir, China from 1971/76 to 2013/14 as derived from remote sensing data. *PloS One*, *11*(1), e0147327. http://dx.doi.org/10.1371/journal.pone. 0147327

Zhou, Q., Robson, M., Pilesjo, P., 1998. On the ground estimation of vegetation cover

Zhou,W., Pickett, S.T.A., Cadenasso,M.L., 2017a. Shifting concepts of urban spatial heterogeneity and their implications for sustainability. Landsc. Ecol. 32, 15–30.

APPENDICES

Ground points were used for accuracy assessment of LULC classification.

For 2020			
OID *	Name	Latitude	longitude
1	bare land	8° 53' 29.216" N	39° 55' 38.139" E
2	water body	8° 53' 33.559" N	39° 55' 4.645" E
3	bare land	8° 53' 37.607" N	39° 55' 31.750" E
4	bare land	8° 53' 41.770" N	39° 55' 39.282" E
5	bare land	8° 53' 41.960" N	39° 55' 23.541" E
9	water body	8° 53' 42.410" N	39° 54' 58.165" E
6	vegetation	8° 53' 42.474" N	39° 55' 36.680" E
7	vegetation	8° 53' 46.987" N	39° 55' 23.867" E
8	built up	8° 53' 48.367" N	39° 54' 59.512" E
9	water body	8° 53' 49.851" N	39° 54' 37.433" E
10	built up	8° 54' 1.316" N	39° 54' 56.903" E
11	vegetation	8° 54' 1.741" N	39° 54' 40.936" E
12	built up	8° 54' 11.255" N	39° 54' 51.120" E
13	built up	8° 54' 11.585" N	39° 55' 5.529" E
14	built up	8° 54' 13.029" N	39° 55' 3.480" E
15	built up	8° 54' 13.894" N	39° 55' 27.079" E
16	vegetation	8° 54' 15.100" N	39° 54' 54.836" E
17	built up	8° 54' 17.484" N	39° 55' 2.772" E
18	built up	8° 54' 20.012" N	39° 54' 59.533" E
19	vegetation	8° 54' 22.343" N	39° 55' 57.215" E
20	agriculture	8° 54' 26.181" N	39° 55' 56.563" E
21	agriculture	8° 54' 27.863" N	39° 55' 50.917" E
22	vegetation	8° 54' 3.068" N	39° 54' 33.772" E
23	agriculture	8° 54' 3.541" N	39° 54' 41.801" E
24	vegetation	8° 54' 31.097" N	39° 56' 11.463" E
25	agriculture	8° 54' 32.069" N	39° 55' 10.922" E

26	agriculture	8° 54' 34.548" N	39° 55' 24.242" E
27	agriculture	8° 54' 34.945" N	39° 56' 2.298" E
For 1999			
28	agriculture	8° 54' 38.040" N	39° 56' 6.778" E
29	built up	8° 54' 10.805" N	39° 55' 11.855" E
30	built up	8° 54' 10.062" N	39° 55' 8.553" E
31	bare land	8° 53' 58.856" N	39° 55' 37.018" E
32	bare land	8° 53' 53.698" N	39° 55' 36.164" E
33	bare land	8° 54' 3.130" N	39° 55' 34.721" E
34	bare land	8° 53' 59.883" N	39° 55' 30.513" E
35	bare land	8° 53' 58.550" N	39° 55' 24.724" E
36	bare land	8° 53' 45.131" N	39° 55' 38.407" E
37	bare lanad	8° 53' 43.795" N	39° 55' 29.777" E
38	vegetatation	8° 53' 13.194" N	39° 54' 36.073" E
39	vegetation	8° 53' 9.673" N	39° 54' 41.557" E
40	vegetation	8° 53' 7.068" N	39° 54' 37.352" E
41	vegetation	8° 53' 21.283" N	39° 54' 43.981" E
42	vegetation	8° 53' 15.588" N	39° 54' 55.740" E
43	vegetation	8° 53' 12.420" N	39° 55' 2.151" E
44	vegetation	8° 53' 43.546" N	8° 53' 43.546" N
45	vegetation	8° 53' 56.010" N	39° 54' 39.132" E
46	vegetation	8° 53' 50.724" N	39° 54' 36.481" E
47	vegetation	8° 53' 59.806" N	39° 54' 40.709" E
48	vegetation	8° 53' 25.112" N	39° 55' 33.327" E
49	vegetation	8° 53' 15.831" N	39° 55' 31.040" E
50	vegetation	8° 53' 27.858" N	39° 55' 28.553" E
51	vetation	8° 53' 16.724" N	39° 55' 25.137" E
52	built up	8° 54' 5.560" N	39° 55' 3.422" E
53	built up	8° 54' 6.685" N	39° 55' 13.950" E
54	built up	8° 54' 10.687" N	39° 54' 50.481" E
55	built up	8° 53' 57.055" N	39° 55' 3.990" E

56	built up	8° 54' 11.102" N	39° 55' 2.004" E
57	agriculture	8° 54' 31.974" N	39° 55' 11.013" E
58	agriculture	8° 54' 32.821" N	39° 55' 15.189" E
59	agriculture	8° 54' 32.831" N	39° 55' 25.980" E
60	agriculture	8° 54' 26.227" N	39° 55' 2.321" E
For 2010			
OID *	Name	latitude	longitude
1	vegetation	8° 53' 37.974" N	39° 54' 39.387" E
2	bare land	8° 53' 2.800" N	39° 54' 26.350" E
3	water body	8° 53' 10.408" N	39° 54' 37.447" E
4	water body	8° 53' 9.279" N	39° 54' 44.035" E
5	water body	8° 53' 17.664" N	39° 54' 48.454" E
6	water body	8° 53' 20.493" N	39° 54' 41.685" E
7	water body	8° 53' 30.528" N	39° 54' 44.547" E
8	water body	8° 53' 18.365" N	39° 54' 59.202" E
9	water body	8° 53' 7.016" N	39° 54' 45.570" E
10	water body	8° 53' 15.673" N	39° 54' 42.612" E
11	water body	8° 53' 13.805" N	39° 54' 50.220" E
12	built up	8° 53' 57.613" N	39° 55' 6.613" E
13	built up	8° 54' 9.385" N	39° 55' 19.199" E
14	built up	8° 53' 55.320" N	39° 55' 10.470" E
15	built up	8° 53' 56.219" N	39° 55' 1.479" E
16	built up	8° 54' 8.295" N	39° 55' 12.912" E

17	built up	8° 53' 50.413" N	39° 55' 9.370" E
18	built up	8° 54' 6.205" N	39° 54' 47.843" E
19	builtup	8° 54' 0.903" N	39° 54' 56.906" E
20	built up	8° 53' 41.969" N	39° 55' 5.172" E
21	built up	8° 53' 11.442" N	39° 55' 6.711" E
22	built up	8° 53' 27.168" N	39° 55' 5.661" E
23	built up	8° 54' 12.617" N	39° 55' 4.107" E
24	agirculture	8° 53' 48.638" N	39° 54' 40.649" E
25	agriculture	8° 53' 42.965" N	39° 54' 38.944" E
26	agriculture	8° 53' 58.686" N	39° 54' 45.538" E
27	agriculture	8° 54' 24.196" N	39° 55' 3.189" E
28	agriculture	8° 54' 20.938" N	39° 55' 16.115" E
29	agriculture	8° 54' 18.327" N	39° 55' 21.210" E
30	agriculture	8° 54' 16.651" N	39° 55' 26.640" E
31	agriculture	8° 54' 28.609" N	39° 55' 26.428" E
32	agriculture	8° 54' 17.575" N	39° 55' 31.397" E